4. SITE 546[1]

Shipboard Scientific Party[2, 3]

HOLE 546

Date occupied: 1 May 1981

Date departed: 3 May 1981

Time on hole: 1 day, 21 hr., 46 min.

Position: 33°46.71′N; 09°33.86′W

Water depth (sea level; corrected m, echo-sounding): 3958

Water depth (rig floor; corrected m, echo-sounding): 3968

Bottom felt (m, drill pipe): 4002 (beneath rig floor)

Penetration (m): 192

Number of cores: 21

Total length of cored section (m): 191

Total core recovered (m): 118.5

Core recovery (%): 61.7

Oldest sediment cored:
Depth sub-bottom (m): 155.5
Nature: Halite
Age: ?Rhaetian–Sinemurian
Measured velocity (km/s): 3.2

Basement: Not reached

HOLE 546A

Date occupied: 3 May 1981

Date departed: 3 May 1981

Time on hole: 8 hr., 39 min.

Position: 33°46.72′N; 09°33.8′W

Water depth (sea level; corrected m, echo-sounding): 3958

Water depth (rig floor; corrected m, echo-sounding): 3968

Bottom felt (m, drill pipe): 4002 (beneath rig floor)

Penetration (m): 50

Number of cores: 1 combined heat probe–*in situ* pore water sampler

Total length of cored section (m): 0

Total core recovered (m): 0

Core recovery (%): 0

Oldest sediment cored: N/A

Basement: N/A

Principal results: Site 546 discovered diapiric salt about 12 km west and seaward of the sialic block drilled at Site 544 (Fig. 1). The following section was drilled (Fig. 2).

0–125.7 m: Pleistocene to upper Miocene foraminiferal–nannofossil ooze. Rests unconformably on:

125.7–147 m: middle Miocene greenish, clayey, stiff nannofossil ooze and red brown clay. Common glauconite.

147–149 m: Greenish and grayish red sandy claystone with layers rich in gypsum crystals. Early Cretaceous and Late Jurassic radiolarians, Early Cretaceous foraminifers, nannofossils, and palynomorphs, mixed with middle Miocene radiolarians, foraminifers, and nannofossils in green layers.

149–155.5 m: Barren, grayish red, gypsiferous sandy claystone.

155.5–192 m: Halite banded with subhorizontal streaks of grayish red, grayish green, and gray clayey and minor potash salts, including carnallite, sylvite, and polyhalite. Some halite crystals 1 cm in diameter. Interstitial water salinity increased steadily from 34 to 217‰ in the section above halite, but no dissolved hydrocarbons could be detected.

BACKGROUND AND OBJECTIVES

A major structural unit of the Moroccan continental margin is a north-northeast–trending zone of diapirlike structures that starts southeast of Fuerteventura Island (Canary Island group) and continues to the north, perhaps beneath the pre-Rif Nappes (Fig. 3). On the land, the diapirs are known to be the result of salt rising through the overlying sediments, but offshore their nature had not been tested with the drill before Leg 79. The exact age of the salt was unknown: it could be as old as Triassic or as young as Lias/earliest Dogger. The western boundary of the diapiric province is sharp and locally fault controlled. It corresponds roughly to the eastern limit of clearly recognizable oceanic crust on seismic records. In the south, within the North Tarfaya segment, the diapiric zone is 10–45 km seaward of the Late Jurassic platform edge (Fig. 3). The zone broadens within the Tafelney Plateau and Essaouira segments and continues onshore into the southwest Moroccan coastal basin.

The western boundary of the Moroccan diapiric province fits well with the eastern boundary of a similar

---

[1] Hinz, K., Winterer, E. L., et al., *Init. Repts. DSDP*, 79: Washington (U.S. Govt. Printing Office).

[2] Karl Hinz (Co-Chief Scientist), Bundesanstalt für Geowissenschaften und Rohstoffe, 3 Hannover, Postfache 510153, Federal Republic of Germany; E. L. Winterer (Co-Chief Scientist), Geological Research Division, Scripps Institution of Oceanography, La Jolla, CA 92093; Peter O. Baumgartner, Geological Research Division, Scripps Institution of Oceanography, La Jolla, CA 92093 (present address: Escuela Centroamericana de Geologia, Apartado 35, Ciudad Universitaria Rodrigo Facio, San José, Costa Rica); Martin J. Bradshaw, Department of Geological Sciences, University of Aston, Birmingham B4 7ET, United Kingdom (present address: Shell International Petroleum Company, The Hague, The Netherlands); James E. T. Channell, Lamont-Doherty Geological Observatory, Columbia University, Palisades, New York (present address: Department of Geology, 1112 GPA Building, University of Florida, Gainesville, Florida 39611); Michel Jaffrezo, Département de Géotectonique, Université Pierre et Marie Curie, 4 place Jussieu, 75230 Paris Cedex 05, France; Lubomir F. Jansa, Geological Survey of Canada, Bedford Institute of Oceanography, Dartmouth, Nova Scotia, Canada; Robert Mark Leckie, Department of Geological Sciences, University of Colorado, Boulder, Colorado 80309 (present address: Department of Geology and Geography, University of Massachusetts, Amherst, Massachusetts 01003); Johnnie N. Moore, Department of Geology, University of Montana, Missoula, Montana 59812; Jürgen Rullkötter, Institut für Erdöl und Organische Geochemie, ICH-5, KFA Jülich, Postfach 1913, D-517 Jülich, Federal Republic of Germany; Carl H. Schaftenaar, Department of Geophysics, Texas A&M University, College Station, Texas 77843 (present address: Chevron, U.S.A., 700 S. Colorado Blvd., Denver, Colorado 80222); Torsten H. Steiger, Institut für Paläontologie und Historische Geologie, Universität München, Richard-Wagner-Strasse 10, D-800 München 2, Federal Republic of Germany; Vassil T. Vuchev, Kansas Geological Survey, University of Kansas, Lawrence, Kansas 66044 (present address: Geological Institute, Bulgarian Academy of Sciences, UL. Academy G. Bonchev, Block 2, 1113 Sofia, Bulgaria); and George E. Wiegand, Department of Geology, Florida State University, Tallahassee, Florida 32306.

[3] The descriptions of sites, cores, and data included in these site reports were completed within one year of the cruise, but many of the topical chapters that follow were completed at a later date. More data were acquired and authors' interpretations matured during this interval, so readers may find some discrepancies between site reports and topical papers. This is particularly true of biostratigraphic age assignments. The timely publication of the *Initial Reports* series, which is intended to report the early results of each leg, precludes incurring the delays that would allow the site reports to be revised at a later stage of production.

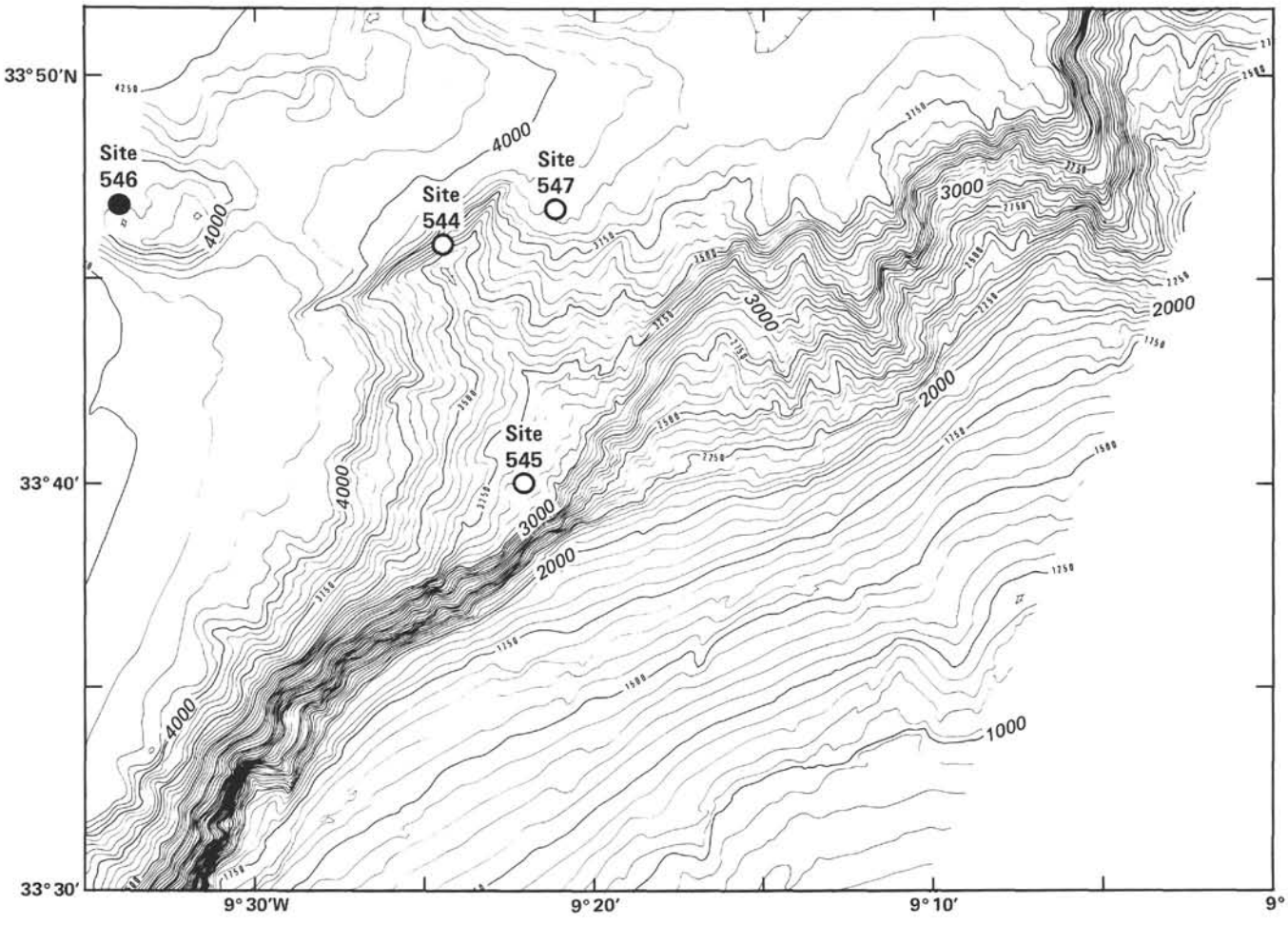

Figure 1. Bathymetry around Site 546, based on SEAZAGAN Seabeam map (Auzende et al., this volume).

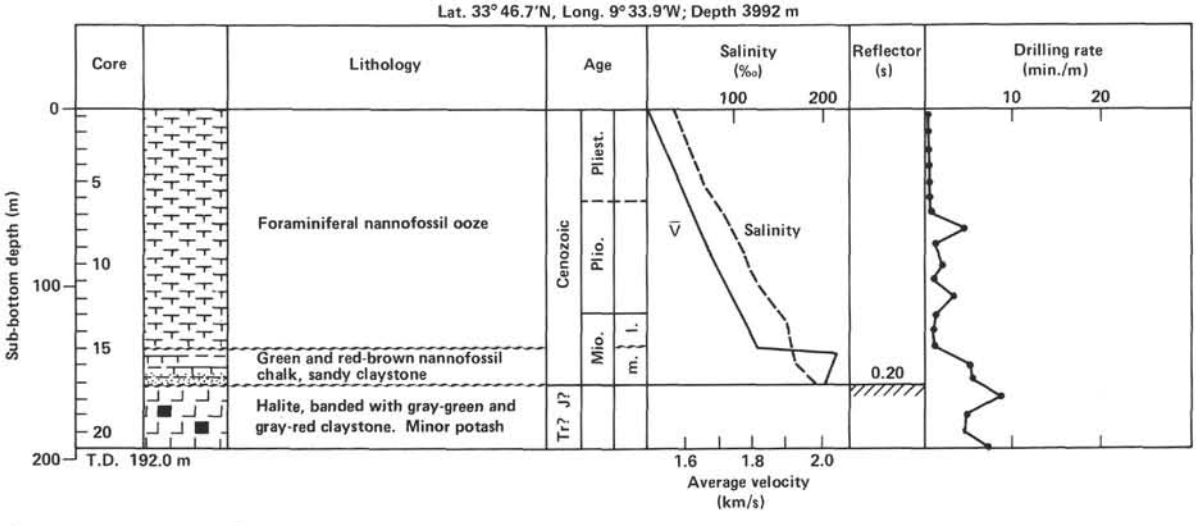

Figure 2. Summary graphic log of Site 546.

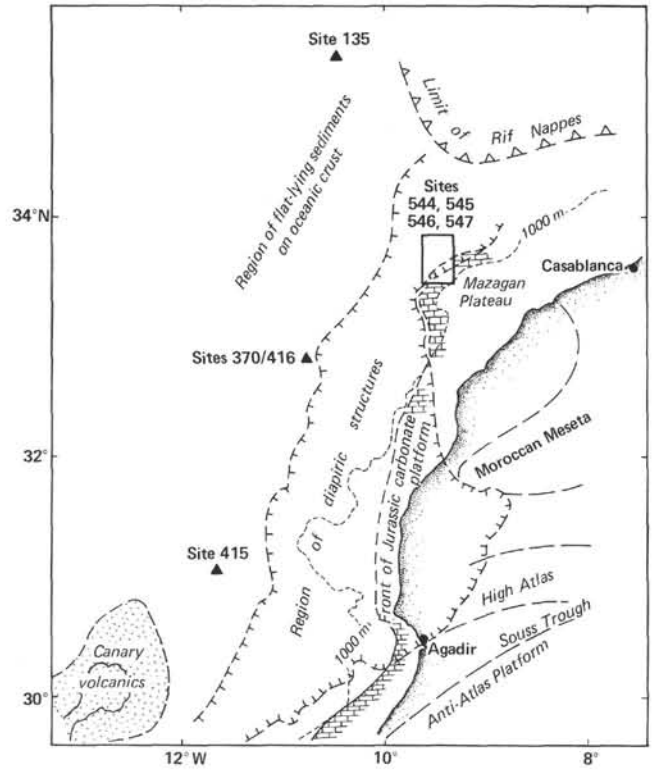

Figure 3. Map showing the regional setting of the Mazagan Plateau. The area inside the square is shown in greater detail in Figure 4.

diapiric province of Nova Scotia, Canada. If these are salt diapirs, this suggests that, before wide separation of the African and North American plates, a single evaporite basin developed and broadened during the early development of the margin, when the crust was being thinned. The distinct western boundary of the Moroccan diapiric province may thus mark the beginning of the actual separation of Morocco and Nova Scotia.

Objectives at Site 546

After drilling into gneissic basement at Site 544, we began a close study of the seismic profiler records over the many structural highs that lie seaward of the Site 544 fault block, with the possibility in mind that some of these might also be sialic blocks rather than diapiric structures. We still could not, however, distinguish between these two cases with certainty, and a test with the drill was necessary.

The implications of the two hypotheses are far-reaching. First, the sialic blocks indisputably belong to the African continent, whereas salt may have been deposited either on continental crust (perhaps thinned or "contaminated" by basic igneous rocks) or on oceanic crust: the occurrence of the Messinian salt in the Mediterranean oceanic basin is an example of the latter possibility. On the Moroccan side of the Atlantic the ocean/continent boundary is not unequivocally defined by geophysical data. The documenting of salt off Morocco would obviously affect interpretations of the geologic history of the conjugate Nova Scotian margin, with its implication for the generation, migration, and accumulation of hydrocarbons.

We therefore focused our efforts on searching for a structure that would be safe to drill, without risk of encountering hydrocarbons, and for a structure whose seismic signature resembled that at Site 544. We identified such a feature in the very next structural high seaward of Site 544 (Fig. 4). With the data at hand we inferred that this feature trends more or less parallel to the northeast-trending fault that bounds the 544 block. It appears to be ridgelike, with marked culminations along its trend. One culmination forms an oval-shaped topographic high on the seafloor about 10 km west of Site 544, now seen more clearly in multibeam data acquired after Leg 79 (Fig. 1). This feature is crossed by *Valdivia* 79-05 and *Meteor* 53-05 multichannel seismic lines (Figs. 5 and 6). These lines both show acoustic basement at a very shallow depth (0.2–0.3 s) beneath acoustically very transparent sediments. The *Valdivia* line further shows a very steep slope on the southwest side of the feature, and the record strongly suggests that the acoustic basement crops out there. At any event, the acoustic basement is well above the level of the adjacent seafloor, using plausible values for sound velocity in the transparent sediment. All in all, the resemblance to the picture at Site 544 is close, and the feature appeared safe to drill.

A brief seismic survey conducted with *Glomar Challenger* on the transit from Sites 544 to 545 (Figs. 5, 7, and 8) crossed the feature twice and gave results compatible with the *Meteor* and *Valdivia* lines. DSDP, after consultation with the Pollution Prevention and Safety

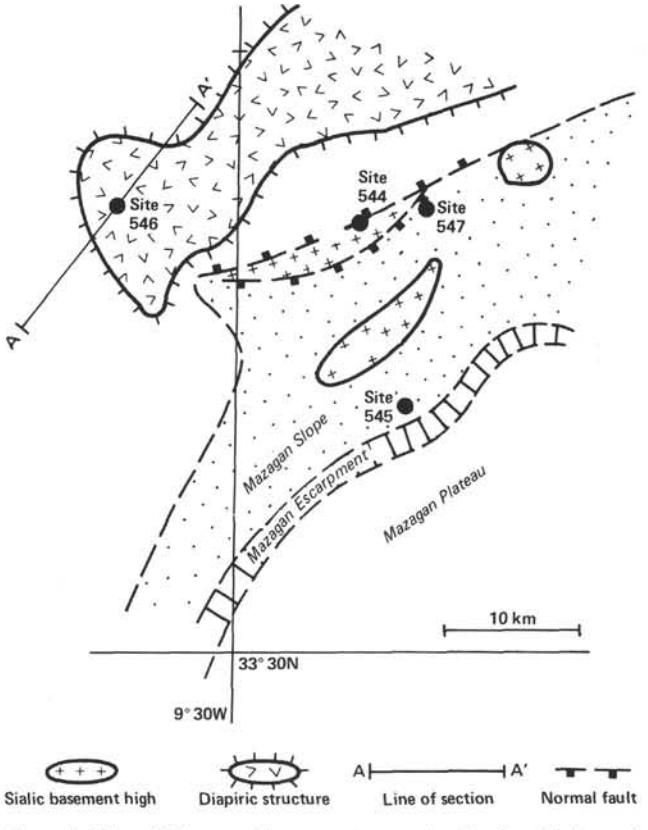

Figure 4. Map of Mazagan Escarpment area, showing Leg 79 sites and major geologic features. Line A–A′ is line of seismic reflection profile *Valdivia* 79-05.

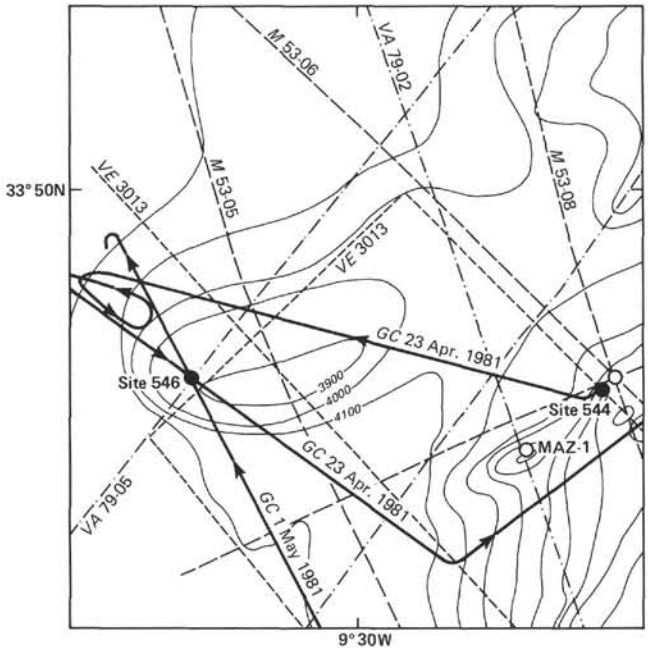

Figure 5. Approach and departure of *Glomar Challenger*, Site 546, showing seismic lines in vicinity and outlines of structurally high areas.

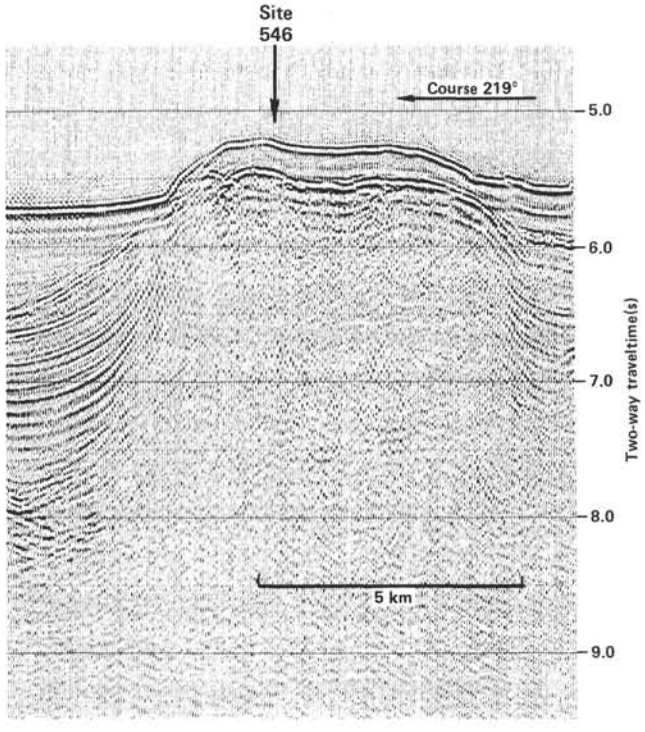

Figure 6. *Valdivia* 79-05 seismic profile over structural high drilled at Site 546.

Panels of JOIDES and SI0, radioed permission to drill the structure, provided we stayed above the level of the adjacent seafloor and monitored carefully for hydrocarbons.

We therefore prepared to drill at the crossing of the *Valdivia* line and the *Glomar Challenger* line, near the west end of the structure. We had as our main objective the discovery of the nature of the acoustic basement: salt or granite?

OPERATIONS

Approach

From Site 545, *Glomar Challenger* followed a dogleg course to Site 546, to obtain a seismic tie line between *Meteor* multichannel lines *M* 53-08 and *M* 53-05 by traversing parallel to and just seaward of the foot of Mazagan Escarpment (Fig. 5). Seeing that conditions at the structural high were as anticipated from our study of previously taken seismic profiles (Fig. 8), we dropped the acoustic beacon at 0217 GMT on 1 May 1981, at a position very close to the intersection of *Valdivia* 79-05 and *Glomar Challenger* 23 April lines, at the desired position. The site is just west of a narrow depression on the top of the structural high shown on seismic lines.

Echo sounding gave a corrected seafloor depth from the derrick floor of 3968 m, and the pipe was thus lowered to 3963 m and cores taken until, in the interval 3994.5–4004 m, the core barrel recovered 1.8 m of sediment. On this basis the seafloor depth was established as 4002.0 m below the derrick floor (3992 m below sea level).

Coring proceeded continuously from the seafloor to the total depth of 192 m BSF. Immediately after each core was retrieved on deck, samples were taken for analysis of dissolved hydrocarbons and for interstitial water salinity. No dissolved hydrocarbons were detected in any sample, but the salinity of the interstitial water increased progressively from the seafloor downward, reaching a value of 217 ppt in Core 17, at a depth of 154 m BSF, just above the halite.

We also kept a sharp lookout in the cores for any mineralogy or texture resembling caprock. Gypsum crystals occur in weakly consolidated red nannofossil claystone in Cores 17 and the top of 18, but this is not like typical caprock.

The bit entered layered halite at 155.5 m BSF and recovery was excellent, averaging about 70% over the 36.5 m of salt cored. The salt was cored at a speed of about 5 min./m, and the cores are for the most part only a little dissolved. Most gratifying of all was the fact that considerable lengths of core, as much as a meter at a time, are perfectly intact, with no drilling break.

Before *Glomar Challenger* left the site, the bit was pulled back above the seafloor and washed in again to a depth of 50 m below the seafloor, in Hole 546A. A combination heat probe and *in situ* pore water sampler was lowered. The pore water sampler obtained a good sample, but the heat probe behaved erratically, and the data could not be used.

At 1048 GMT on 3 May 1981, the ship departed Site 546, toward Site 547.

A summary of the coring operations at Site 546, giving core numbers and depths, is shown in Table 1.

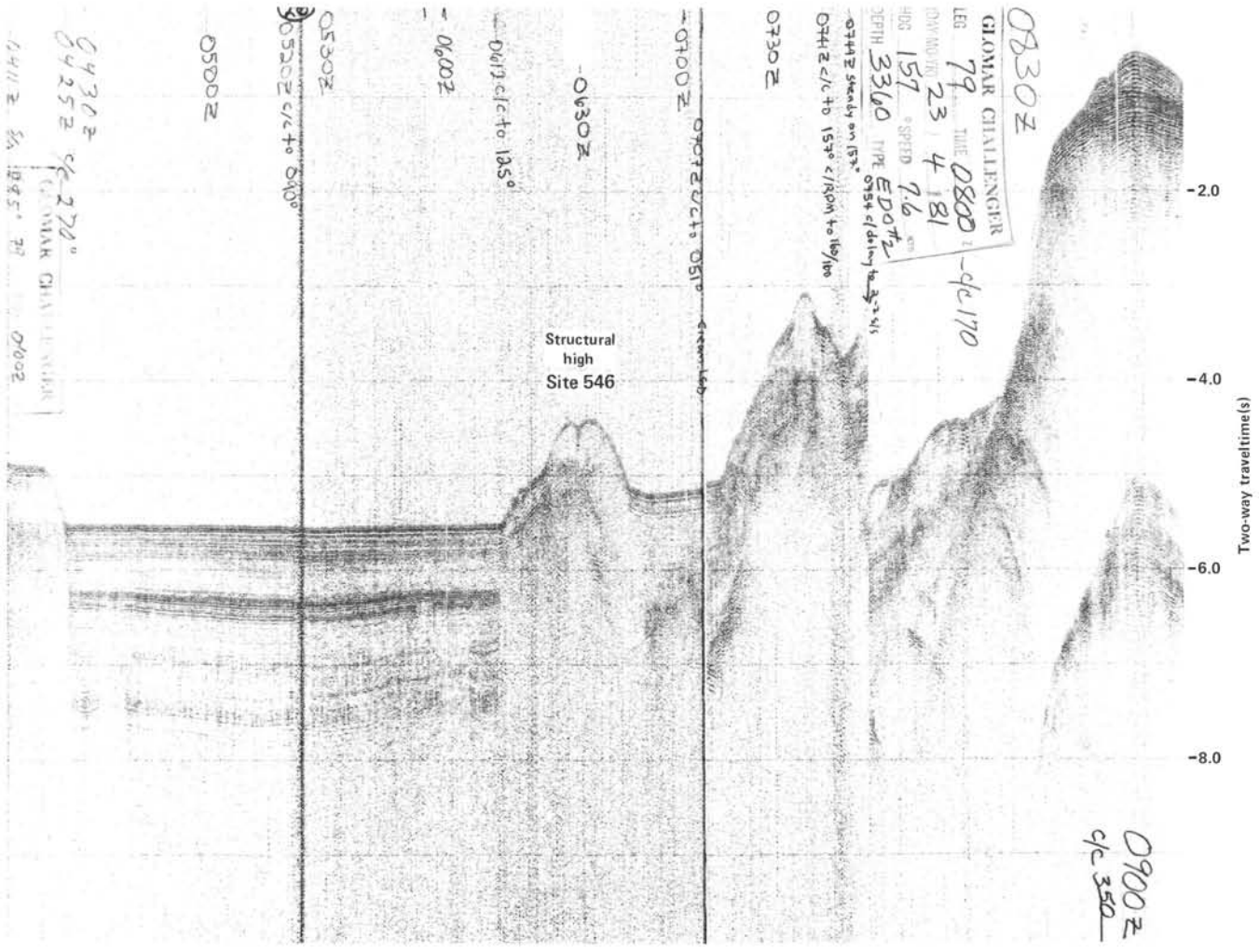

Figure 7. Seismic reflection profile record made from *Glomar Challenger* across structural high at potential Site 546.

SEDIMENT LITHOLOGY

Strata drilled at Site 546 are divided into three lithological units. The first unit consists of brownish pelagic and hemipelagic nannofossil ooze of Pleistocene to late Miocene age. The second unit is characterized by a complex interlayering of red claystone and greenish nannofossil ooze. In this unit, of mid-Miocene age, reworked microfossils of Early Cretaceous age occur. The third unit consists of halite. A detailed log of the lithology and biostratigraphic succession at Site 546 is shown at the end of this chapter, in Figure 28.

Unit I (0–125.7 m; Core 1 to 546-15-1, 20 cm)

Unit I has a total thickness of 125.7 m and consists of pale yellowish brown (10YR 6/2), light olive gray (5YR 6/1), light yellowish olive gray (5Y 7/1), and grayish orange pink (5YR 7/2, lower cores) slightly clayey nannofossil ooze (63%) and foraminiferal nannofossil ooze (37%) of Pleistocene to late Miocene age. Owing to disturbance from drilling, the first cores are partly structureless and watery and partly highly disturbed, with strong alteration of the original sedimentary fabric. In this zone the sediment is intensely oxidized. The first recognizable sedimentary structures occur in Core 2 as a faint lamination of greenish and dark brownish colors with minor thin interlayers rich in black ferrous sulfide. Scarce pyritized blebs point to the presence of burrows. From Section 546-2-1 down to the base of Unit I, the sediment generally shows changes of color at a scale of 60–100 cm, but these color units are commonly intercalated with thin zones in which these change on millimeter scale (for example, 546-8-4, 50–60 cm; 546-8-5, 30–50 cm). Bioturbation first becomes especially apparent in Cores 6 and 7, where there is less drilling disturbance, and from Core 9 downward it is common (546-9-5, 0–60 cm; 546-9-6, 0-40 cm). It appears as a slight mottling of pale yellowish brown and grayish orange pink or as burrow fills (tubes 1 cm in diameter) which are darker or lighter than the surrounding sediment.

Unit II (125.7–155.5 m; 546-15-1, 20 cm to 546-18-1, 145 cm)

At 546-15-1, 20 cm, a smeared but distinct contact separates the brownish sediments of Unit I from greenish sediments assigned to Unit II (Fig. 9). Unit II is 29.8 m thick and is characterized by interlayering of greenish and reddish brown calcareous sediments and grayish red

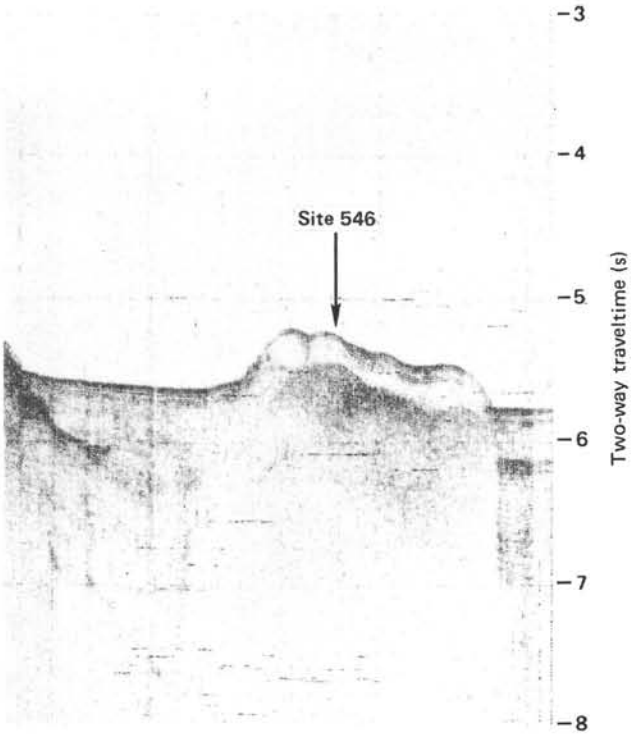

Figure 8. Seismic reflection profile record made from *Glomar Challenger* during approach to Site 546.

Table 1. Coring summary, Site 546.

Core no.	Date (May 1981)	Time	Depth from drill floor (m) Top Bottom	Depth below seafloor (m) Top Bottom	Length cored (m)	Length recovered (m)	Percentage recovered
Hole 546							
1	1	1713	4002.0–4004.0	0.0–2.0	2.0	1.8	90
2	1	1817	4004.0–4013.5	2.0–11.5	9.5	4.3	45
3	1	1927	4013.5–4023.0	11.5–21.0	9.5	6.2	65
4	1	2037	4023.0–4032.5	21.0–30.5	9.5	5.3	56
5	1	2147	4032.5–4042.0	30.5–40.0	9.5	0.0	0
6	1	2254	4042.0–4051.5	40.0–49.5	9.5	8.1	85
7	2	0006	4051.5–4061.0	49.5–59.0	9.5	8.7	92
8	2	0200	4061.0–4070.5	59.0–68.5	9.5	9.5	100
9	2	0307	4070.5–4080.0	68.5–78.0	9.5	8.8	93
10	2	0428	4080.0–4089.5	78.0–87.5	9.5	7.8	82
11	2	0546	4089.5–4099.0	87.5–97.0	9.5	6.1	64
12	2	0712	4099.0–4108.5	97.0–106.5	9.5	6.9	73
13	2	0828	4108.5–4118.0	106.5–116.0	9.5	5.0	53
14	2	0945	4118.0–4127.5	116.0–125.5	9.5	5.0	53
15	2	1103	4127.5–4137.0	125.5–135.0	9.5	1.1	12
16	2	1440	4137.0–4146.5	135.0–144.5	9.5	2.1	22
17	2	1652	4146.5–4156.0	144.5–154.0	9.5	5.3	56
18	2	1959	4156.0–4165.5	154.0–163.5	9.5	8.1	85
19	2	2151	4165.5–4175.0	163.5–173.0	9.5	4.5	47
20	2	2351	4175.0–4184.5	173.0–182.5	9.5	7.1	75
21	3	0211	4184.5–4194.0	182.5–192.0	9.5	6.8	72
					192.0	118.5	62
Hole 546A							
Downhole measurements only; no cores attempted.							

claystone. No major lithologic change is associated with the color change between Units I and II; the sediment is still clayey nannofossil ooze. The main difference is a higher degree of bioturbation: the sediments in Unit II are more mottled in color and include common blebs rich in pyrite. Different shades of green (greenish gray, 5GY 6/1, 68%; light olive gray, 5Y 6/1, 2%; dark greenish gray, 5G 4/1, 2%) grading into pale yellowish brown

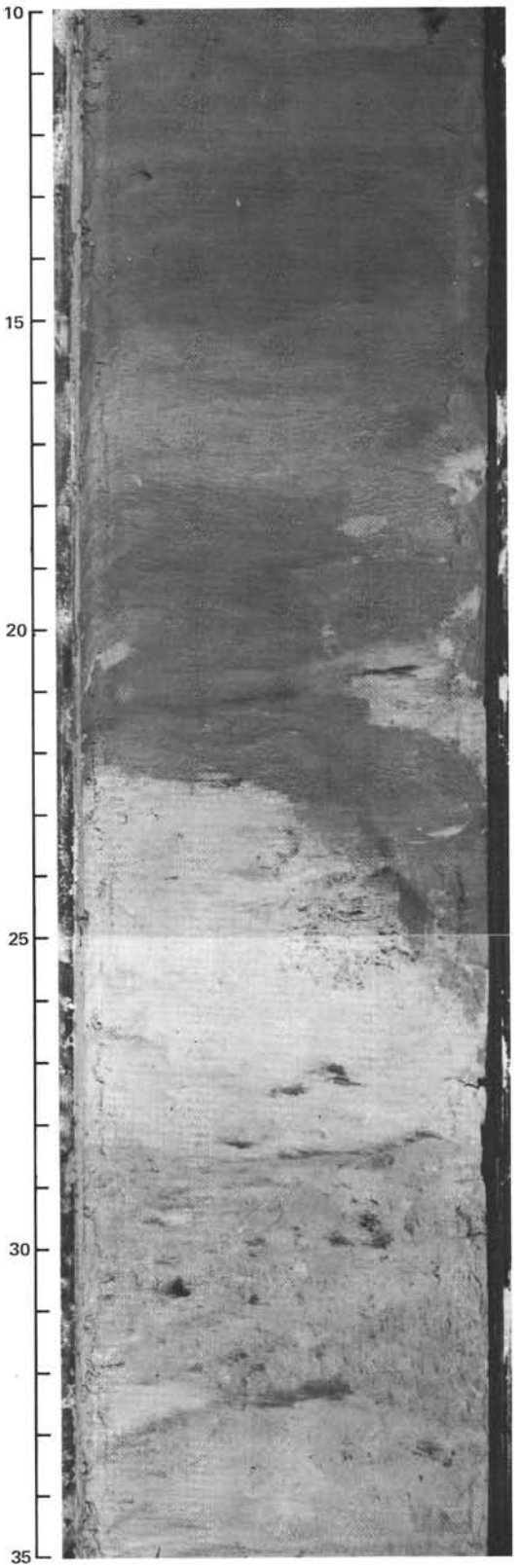

Figure 9. Boundary between Unit I and Unit II, at 546-15-1, 20 cm. Sediment above the boundary is moderate brown (5YR 4/4) clayey nannofossil ooze; below, the sediment is greenish gray (5GY 6/1) clayey nannofossil ooze with black FeS-rich blebs. The contact, which is bioturbated, marks a hiatus of some 5–8 m.y. between middle and late Miocene.

(10YR 6/2, 15%) are visible in the major portion of the core. They are here and there interrupted by thin layers of light green gray (5GY 8/1).

Sediments of the same lithology continue through 546-16-2, 37 cm, where they are interlayered with medium dark gray (N4) nannofossil ooze with some red laminae. Grayish red (10R 4/2), light gray (N7), and pale green (5G 4/2) calcareous claystone of variable firmness is interlayered in intervals 3–10 cm thick, suggesting a complex mixing of sediments having different histories. This is supported by the occurrence in Section 546-16-2 of two subangular limestone clasts of peloidal grainstone containing a few small indeterminate foraminifers, echinoderms, and superficial ooids in a sparry calcite cement (Fig. 10). Shipboard X-ray diffractograms show strong halite peaks. Halite probably crystallized from highly saline pore water during preparation of these samples. Both the mixed sequence and the remaining 37 cm of greenish gray (5GY 6/1) and grayish red (10R 4/2) mottled, clayey nannofossil ooze of Core 16 contain soft nodules of microcrystalline carbonate and gypsum.

Core 17 consists mainly of two alternating types of sediment: Section 546-17-1 through 546-17-2, 32 cm and 546-17-2, 135 cm through 546-17-3, 73 cm are composed of pale green (5G 7/2) nannofossil ooze with pale red (10R 6/2) and olive gray (5Y 4/1) interbeds; this part of the core also contains intervals about 10 cm thick of nannofossil-bearing calcareous chalk. In the interval 546-17-2, 32–135 cm, grayish red (10R 4/2) claystone dominates. A layer of medium bluish gray (5B 5/1), silty dolomite, 15 cm thick, occurs 7 cm below the top of the claystone (Fig. 11). Below a sharp boundary at 546-17-3, 75 cm, the rest of Core 17 contains grayish red (5Y 4/2) to dusky brown (5YR 2/2) claystone. The higher content of soft carbonate nodules and of soft white nodules of gypsum or anhydrite in this unit contrasts with the red claystone above. The claystone is composed of iron-stained clay and 20% quartz silt, with traces of zeolite(?) and minor amounts of halite crystals. As low as 546-17-3, 100 cm, mixed Tertiary and Cretaceous microfaunas (see section on biostratigraphy, this chapter) indicate complex structural mixing of stratigraphic units. Only sediment from below 546-17-3, 100 cm to the top of the salt (a section of 7.1 m) could represent residual muds from solution of the salt. In Section 546-18-1 a layer of coarsely crystalline gypsum, 4 cm thick, is intercalated within the clay. Several millimeter-sized crystals of gypsum are also scattered through the clay. Rounded quartz sand grains and hematite crystals are rare in the clay. Core 18 is barren of fossils.

Discussion of Units I and II: The units are separated by a distinct color change at the same level as a biostratigraphic gap embracing foraminiferal Zones N13–N17 (late Miocene; see section on biostratigraphy, this chapter). Another significant lithological change takes place at 546-16-2, 37 cm, the transition from nannofossil ooze to calcareous claystone. Figure 12 shows the composition of the cores according to smear-slide estimations and carbonate-bomb data.

In the uppermost cores, of Pleistocene age, a high terrigenous influx (40%) consisting of quartz, feldspars, mica, and clay is recorded. It decreases downward to the

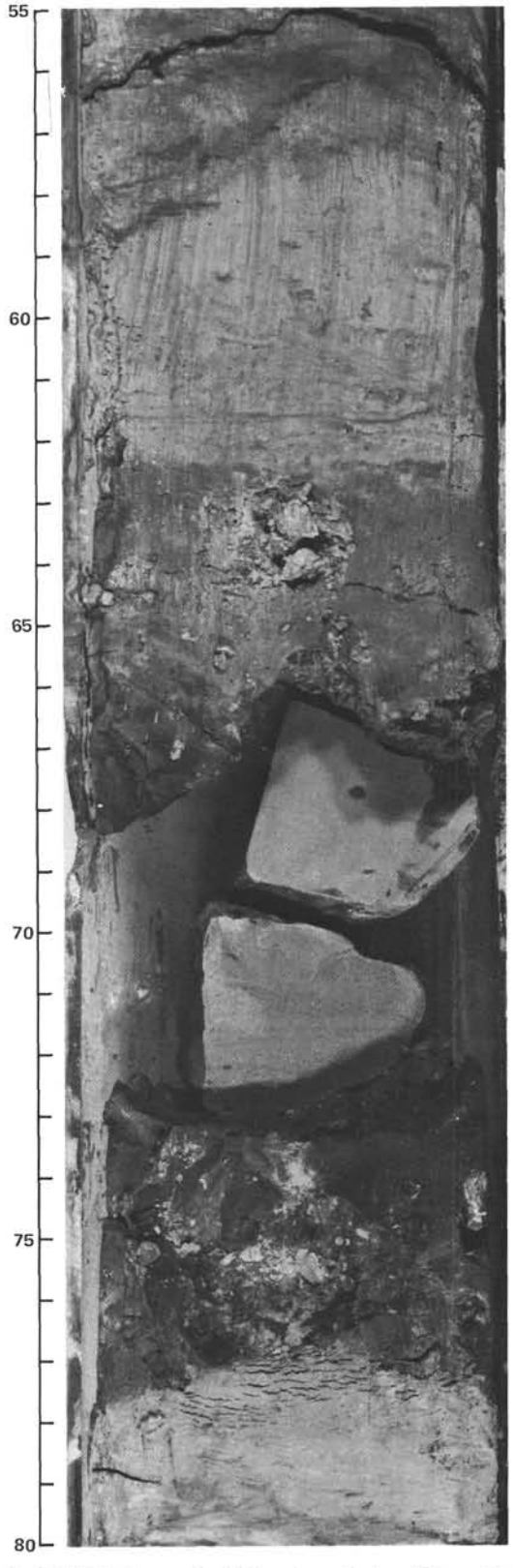

Figure 10. Peloidal (fine-grained) limestone clasts within a mixed series of grayish red (10R 4/2) and pale green (5G 4/2) calcareous claystones, Sample 546-16-2, 55–80 cm. The lower pebble is bioturbated; the upper pebble is laminated, slightly cross-bedded, and shows small-scale convolute bedding or a slump structure (not visible in photograph).

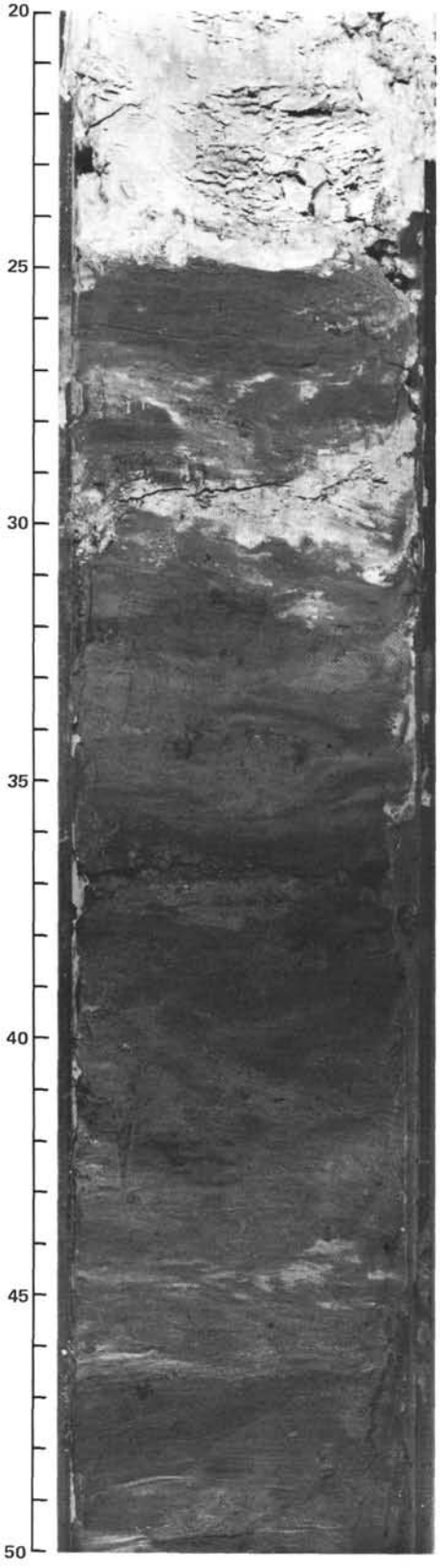

Figure 11. Lithologic change in 546-17-2, 20–25 cm: (a) pale green (5G 7/2) nannofossil ooze (20–25 cm); (b) pale reddish brown (10R 5/4) and pale green (5G 7/2) irregular interlayering of nannofossil ooze (25–35 cm); (c) medium bluish gray (5B 5/1) layer of silty dolomite (35–36 cm); (d) grayish red (10R 4/2) sandy claystone (36–50 cm).

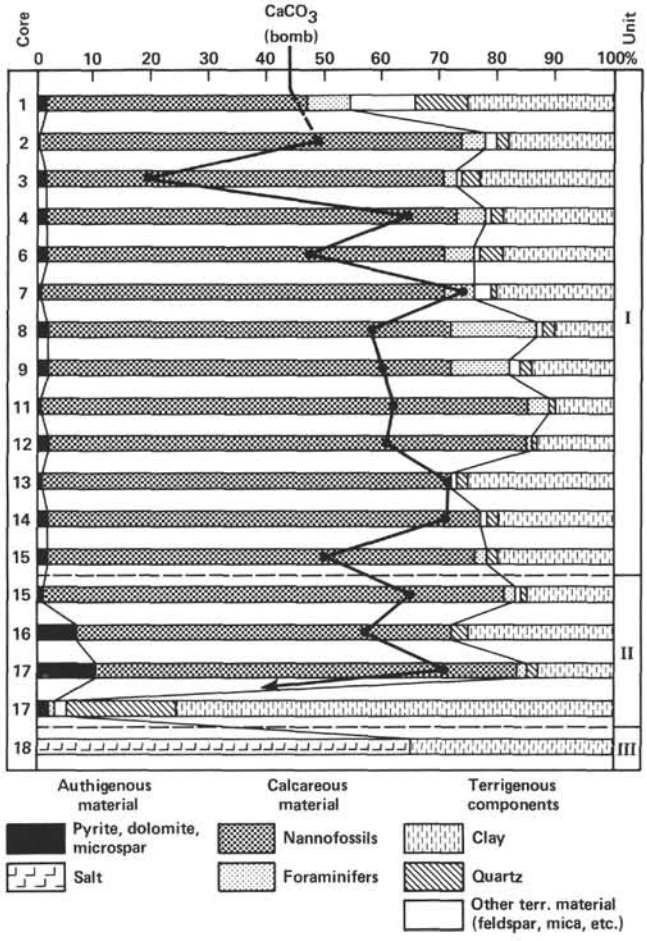

Figure 12. Pattern of the lithologic composition through the sequence of cores of Site 546, according to smear-slide estimations and carbonate-bomb data.

base of the Pleistocene (Core 6), remains relatively constant through the Pliocene (about 15%) and slightly increases again in the upper Miocene (about 20%). Among the calcareous particles, foraminifers seem to have a maximum in the upper Pliocene. The content of authigenic material like pyrite and dolomite is constant down to Core 15 (1–2%). Downward through Cores 16 and 17 clay content increases. In this interval, the percentage of authigenic minerals (dolomite, gypsum, anhydrite, and microspar) increases. The presence of these authigenic minerals can be explained by diagenesis in highly saline pore water derived from the underlying salt.

Mixed assemblages of Jurasssic, Cretaceous, and Miocene microfossils in Core 16 through Section 546-17-3 seem to be a consequence of the mixing of various lithologies. Although no direct correlation between particular lithologies and fossil ages could be established, these observations suggest that this sequence may have formed when sediment overlying the salt dome collapsed as salt dissolved, or may represent Lower Cretaceous material resedimented during the middle Miocene.

Unit III (155.5–192 m T.D.; 546-18-2 to 546-21-5)

This unit is a 36.5-m section of layered salt rock, dominantly halite, which from geophysical evidence rep-

resents a small sample from the top of an evaporitic diapir that probably contains hundreds of meters of section. An age of Rhaetian–Hettangian is suggested by palynology (J. Fenton, this volume), concordant with a maximum Hettangian–Sinemurian age for the oldest marine sediments of the area (described in the Site 547 site chapter).

The evaporite core is described in detail in Holser et al., this volume, and summarized in Figure 13. This description is based mainly on a detailed examination done at Lamont-Doherty Geological Laboratory by W. T. Holser in October 1981 (Holser et al., this volume), but incorporates more limited observations done on shipboard, and also some preliminary X-ray diffraction determinations by Martin Bradshaw and W. T. Holser.

The salt rock of the unit exposed in these cores is color banded on a scale of 0.5 to 3 cm, with colors ranging from translucent to varying shades of reddish brown ("redbeds") in about half of the section, and to gray green in other parts of the section (Fig. 14). The reddish and orange colors are for the most part caused by hematite-stained silt and clay included in the dominant halite mineralogy. Alternations of the red to brown oxidized sediments with the gray to green, more reduced sections are on a scale of 5 to 200 cm.

Both red orange and gray green beds represent rock that is dominantly halite but is colored by hematite and also contains quartz, clay, anhydrite, and dolomite, all ranging up to 30% in some parts of the section but averaging perhaps 5%. These impurities are concentrated in bands several centimeters thick, where they occur as centimeter-scale fragments that seem to be boudins in the more plastic halite (e.g., at 127 cm in Fig. 14). Much of the dark (red or gray green) material is also present as disseminations in the halite. Millimeter-scale anhydrite laminae that are common in many other evaporite sections are present at only a few places in this core.

Preliminary X-ray diffractometry of the red beds shows dominant quartz-rich silt, with a clay-sized fraction of illite, kaolinite, and mixed-layer illite–smectite. Ankerite was also detected by X-ray diffraction in a sample from Core 18. In contrast, the gray green to white intercalations within the halite contain much anhydrite (up to 5%), with considerable quartz and even feldspar. X-ray diffraction of the clay-sized fraction of this material shows well-ordered, mixed-layer illite–smectite, with illite and kaolinite. Anhydrite is also disseminated (1%) in the halite itself.

Potash-facies mineral deposition is prominent in the cored section (Fig. 15). Potash mineralization is most evident on the core surface through prevalent solution pitting. The solution pits are commonly plastered with bright copper-colored encrustations, which are hematite-stained sylvite consequent upon the incongruent dissolution of primary ferroan carnallite by the seawater-rich drilling mud. Carnallite was independently identified as yellowish deliquescent crystals in interior broken surfaces of the core. Some of the pitting is not carnallite but rock sylvite, identified in amounts up to 6% by X-ray diffraction. An additional indicator of potash-facies mineralization is the presence of halite that is colored deep blue by radiation. Some disseminations of orange red aggregates in halite suggest the presence of polyhalite. Other potash-facies minerals were not identified in the preliminary studies. In particular, no evidence was found for the occurrence of the residual minerals tachyhydrite and bischofite. The proportions of the potash minerals were not determined by the preliminary studies.

A prominent feature of the salt rock is its cataclastic texture (Fig. 16). This is most clearly expressed in the finer-grained halite, occurring as lenticular grains averaging perhaps 1 mm, the boundaries of which are outlined by secondary fluid inclusions, and which are elongate parallel to bedding.

The finer-grained cataclastic halite contrasts clearly with augen of clear halite 1 to 3 cm in diameter. The finer material bends around these augen in a schistose pattern, and the exposed corners of the larger single-crystal augen are crushed, as shown in Figure 17. These halite crystals commonly exhibit birefringent deformation lamellae. A puzzling feature of the cataclastic texture is that the large halite augen are much clearer and purer. Impurities of clay, silt, and hematite seem to be predominantly concentrated in the finer cataclastic material.

Clay–halite bedding and cataclastic lenticularity are concurrently and predominantly subhorizontal (Figs. 14 and 16). Local deviations of dip, in a few places up to 60°, occur in potash-rich beds, which are already known to be much less competent than pure halite.

Study of raw and polished core surfaces by eye and hand lens did not reveal any clear examples of primary halite growth textures such as cubes, hoppers, or chevrons.

The evaporite section sampled at Hole 546 did not display any evident regular sequences of evaporite facies. However, there seems to be some tendency for potash mineralization to accompany the gray green rather than the red-bed facies of the evaporite section.

Discussion of Unit III: A few provisional generalizations can be made concerning the evaporites in this interval.

1. Much of the evaporite deposition and/or diagenesis is generally in a red-bed facies, with abundant oxidized sediments of which some at least are detrital. This might suggest a somewhat shallow or even intermittently exposed regime of sedimentation of the evaporites. Jansa et al. (1980) suggested from a study of a salt sequence in the western North Atlantic that evaporites with red clays were deposited in a basin with a brine layer not deeper than 30 m, to allow oxygenation of the bottom of the basin. However, much of the potash deposition, which might have been supposed to occur in an even more highly evaporated shallow brine, is associated with green, olive, or black clays.

2. Banding of the clay and/or anhydrite is rather irregular and broken; this may have resulted from deformation into a boudinage-type texture. There were no examples of specific textures related to intertidal or supratidal exposed conditions, such as mud cracks, ripple

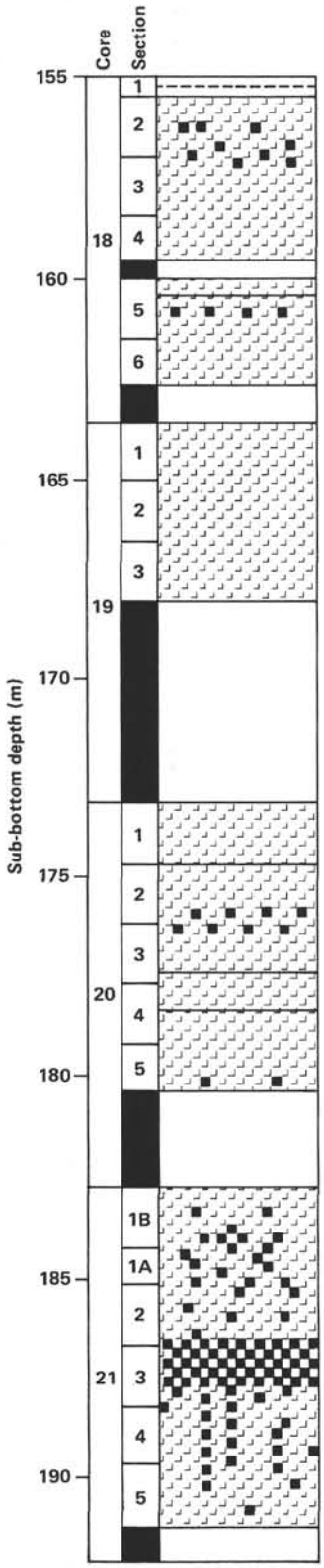

Section 1 is grayish red sandy claystone.

At top of Section 2, contact with salt rock, light gray to pink 3 mm halite of schistose texture, with 2 to 5 mm laminae of dark gray to moderate red anhydritic mudstone spaced 1 to 6 cm, dip 0 to 10°. Occasional 1 mm laminae or disseminations of potash minerals (sylvite, carnallite); surface of core pitted and coated with coppery secondary sylvite, some with selvages of blue halite. Rare dark gray 2 to 5 mm wispy laminae of anhydrite.

Below 35 cm in Section 5 and continuing through all of Core 19, red and brown colors begin to dominate over gray and green; increasing 1 to 3 cm metacrysts of clear halite in schistose halite bands; potash absent. Red and brown colors are in part a mixture of layers or wispy fragments of mudstone, and in part a paler pink disseminated coloration in some halite layers.

Salt rock, olive to yellowish gray, with 1 to 2 cm alternating darker and lighter bands, more and less rich in clay.

In Sections 2 and 3, reddish and brown colors again begin to dominate.

At base Section 3 there begins 1 m of laminae and disseminations, and one 6 cm concentration of potash.

Salt rock, pale to dark reddish brown from admixtures of claystone; halite has 3 mm schistose texture, enclosing 5 to 1 mm metacrysts of clearer halite.

Beginning at base of Section 5, and continuing to bottom of hole, with a maximum in Sections 1A, 2, and 3 of Core 21, potash is very common in beds and disseminations; some parts of core are nearly destroyed by solution pitting. The dominant colors in this zone are pinks and browns, but dark green mudstone is common, particularly in association with potash beds. Local plastic deformation, resulting in dips to 60° and cross-cutting relationships, as at 546-21-2, 105 cm, is confined to potash beds.

Figure 13. Summary log of the salt core at Site 546.

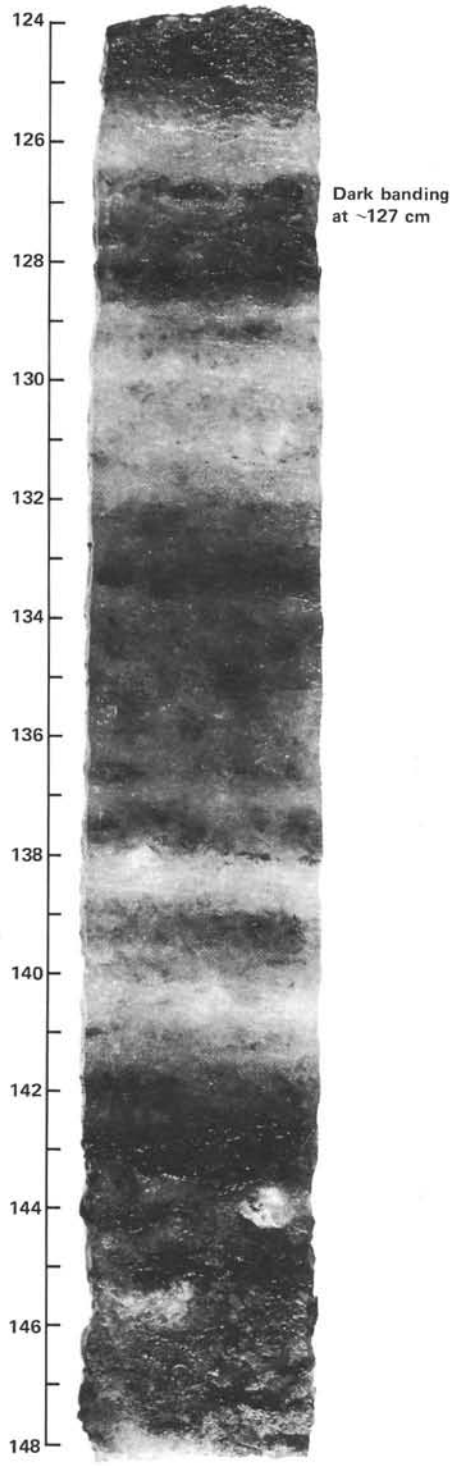

Figure 14. Typical banding in salt rock, in Sample 546-20-1, 124–148 cm. In this section the rock is typically yellowish-gray, with 1- to 2-cm alternations of nearly clear halite and olive gray bands. Some gray bands have a few flecks of brown clay. Halite crystal size increases toward the bottom of the photograph, where a few 5-mm clear halite augen may be seen, in a section richer in dark clay.

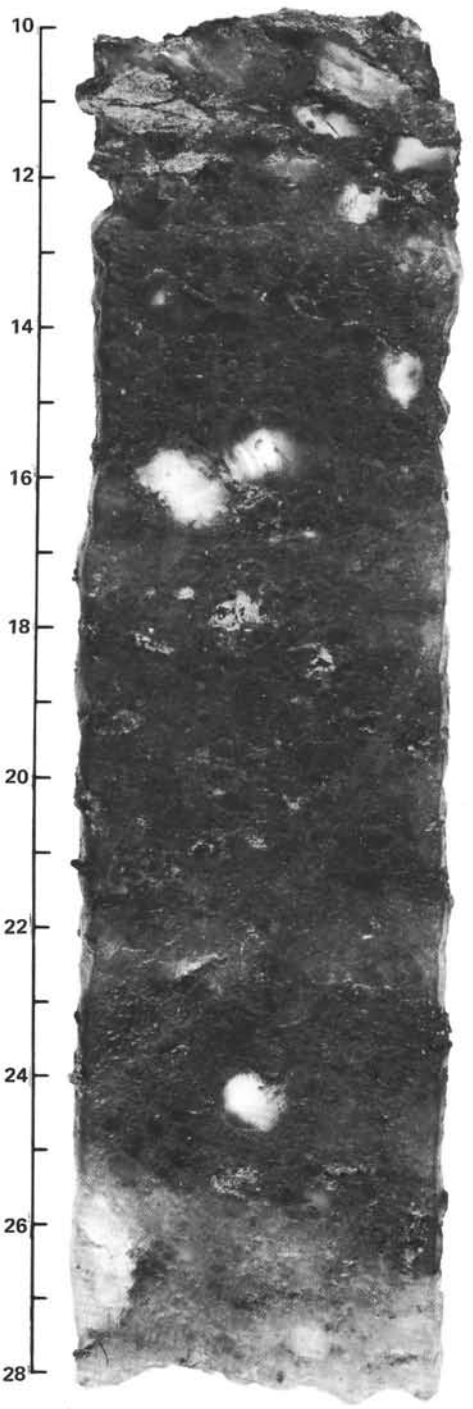

Figure 15. Potash mineralization in Sample 546-20-4, 10–28 cm. Rock rich in pale yellow carnallite (with sylvite?) is dark gray in the photograph. Much of the section is moderate red, with augen of halite (some of which are stained blue by radiation damage); some of these augen may be seen at the base of this section.

marks, erosion surfaces, or stromatolites. Only one doubtful case of nodular or flaser texture was seen, but little anhydrite is present to generate the latter textures.

3. Much of the interval is in the potash facies. Although the detailed mineralogy is yet to be determined, a high stage of evaporation is clear. There is no evidence of final dessication, but such a condition, if present, would probably have been redissolved. Clearly defined cycles of halite and potash facies are not in evidence.

4. Interbeds of the carbonate and $CaSO_4$ facies of the type common in marine evaporites are absent from this interval. In fact, very little anhydrite was found. Furthermore, the section that overlies the salt rock (base of

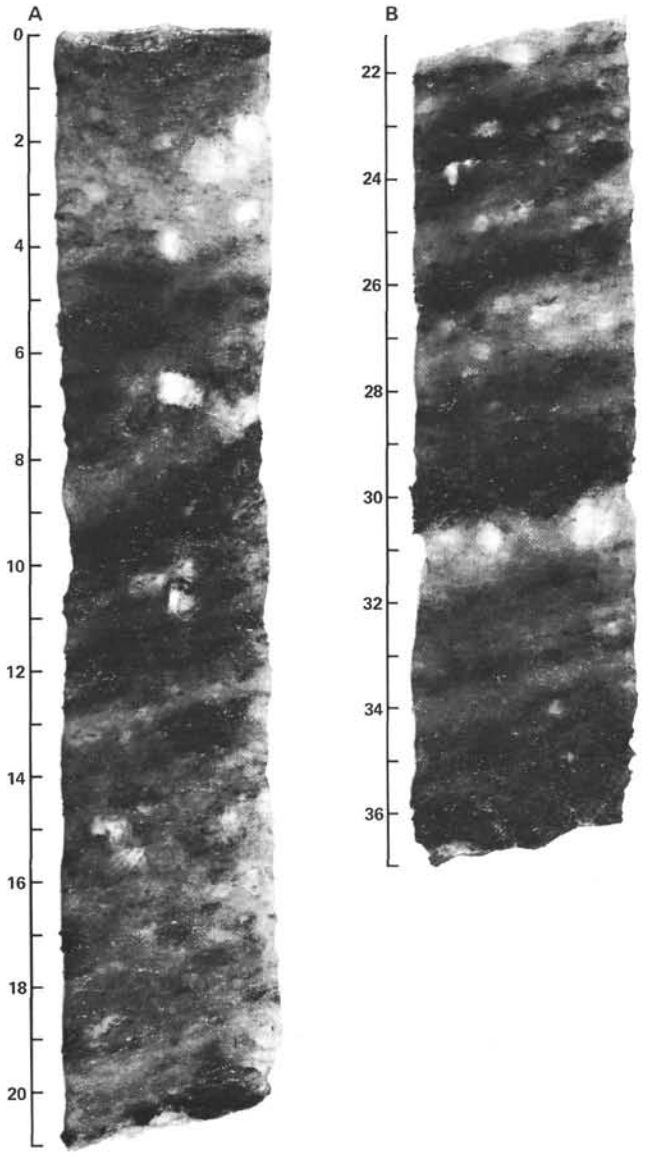

Figure 16. Cataclastic texture in Sample 546-21-4, 0–35 cm. The salt rock is greenish gray in the first 20 cm (A), and a darker grayish red in the next 8 cm (B). Prominent 0.3- to 1-cm augen are moulded by finer cataclastic halite (0.5 to 1 mm), and their prominent corners are snubbed by cataclasis. Banding has been somewhat obscured by deformation but may still be clearly seen. Several thin seams of potash mineralization are present but not clear in the photograph.

Core 17 to top of Core 18) and that is presumably residual to solution of the salt has only a very little (1%?) gypsum or anhydrite, in contrast to the usual tens or hundreds of meters of caprock composed exclusively of anhydrite, gypsum, and derivative calcite. This anomalous condition is also seen offshore Canada (Jansa et al., 1980).

5. The banding in this interval is almost universally subhorizontal. The few strong divergences (and discordances) found in Section 546-21-2, for example, are in potash-rich rocks. This facies is generally much less competent than the halite facies, and commonly displays flow textures even when the section is still structurally in its original horizontal aspect, with no diapirism whatever (e.g., Zechstein Z1 in the Werra Basin, Germany). The horizontally banded Zechstein interval lies immediately under a nearly flat top of the salt dome that has presumably been leveled by salt solution. Domes are always necessarily a product of sharp upward flowage that deforms a major fraction of the bedding into "handkerchief" folds with very steep dips and repetitive stratigraphy. The section cored in Hole 546 shows neither dips nor repetitions. The best guess is that this is pure coincidence, and that the horizontal placement of the site just happened to be in one of the dome's limited areas of horizontal dip.

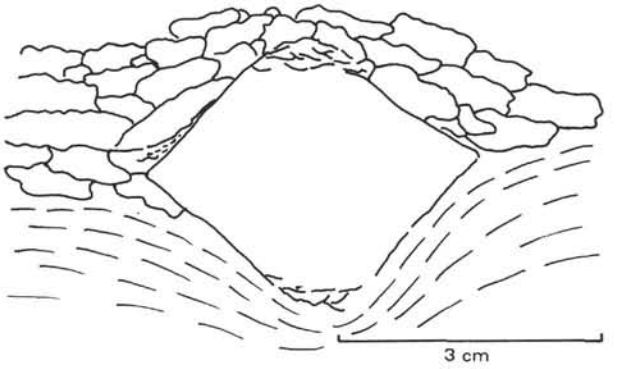

Figure 17. Typical cataclastic texture in salt rock. Clear halite augen are molded by smaller lenticular crystals of impure halite; the exposed corners of the large augen are also rounded by fracturing.

6. The proximity of the offshore diapir field to the onshore Donkkala and pre-Rif evaporite basins (Salvan, 1974) suggests that the offshore basin may be a continuation of either of the onshore basins. Such a relation is also suggested by the fact that both of these onshore basins also have potash-facies evaporites.

BIOSTRATIGRAPHY

Biostratigraphic Summary and Synthesis

A nearly continuous Pleistocene through uppermost Miocene succession of foraminiferal nannofossil oozes and nannofossil oozes (Unit I) was recovered in Core 1 through 546-15-1, 20 cm (125.7 m subbottom). This sequence yielded rich nannofossil and foraminiferal assemblages with rare radiolarians and ostracodes.

A late to middle Miocene hiatus is represented by a marked lithostratigraphic and biostratigraphic break at 546-15-1, 20 cm. Unit II consists of clayey nannofossil oozes, calcareous claystones, nannofossil-bearing calcareous chalk, silty dolomite, and sandy claystone. This sequence overlies salt at the top of Section 546-18-2 (155.5 m sub-bottom). The red silty dolomite and sandy claystone intervals which characterize the lower sections of Core 17 and Section 546-18-1 appear to be barren of fossils. The greenish and grayish nannofossil oozes and chalks of Core 17 contain both nannofossil and foraminifer assemblages of middle Miocene age and reworked specimens of Early Cretaceous age (and Late Jurassic radiolarians). Some intervals contain mixed middle Miocene and Early Cretaceous flora and fauna, whereas other intervals are strictly one age or the other. There

appears to be some relationship between the sediment color and age. A variety of soft Lower Cretaceous (and Jurassic) sediments, possibly exposed by salt tectonics, may have been a source for reworked clasts and microfossils in the middle Miocene sequence.

Nannofossils

Core 1 appears to be in the *Emiliania huxleyi* Zone (NN21) (Gartner, 1977) of late Pleistocene age. Because only a limited amount of time was spent using scanning electron microscope, *E. huxleyi* was recognized only in Core 1. A typical assemblage is *E. huxleyi, Calcidiscus macintyrei, Gephyrocapsa oceanica, G. caribbeanica*, and *G.* sp.

The appearance of *C. macintyrei* in the late Pleistocene appears to be caused by reworking, and Core 2 through 546-6-5, 10 cm have been temporarily assigned a Pleistocene age until this section can be resolved. The assemblage consists of *C. macintyrei, Discolithina viginitiforata, Helicosphaera sellei, H.* sp., *Pseudoemiliania lacunosa*, and *G. caribbeanica*. Nannofossils of this assemblage, as well as the others throughout this Pleistocene section, are in a state of moderate to good preservation and are common.

The interval from 546-6-6, 21 cm through Core 9 is placed within the *Discoaster brouweri* Zone (NN18–NN16) (Okada and Bukry, 1980); this zone ranges from late to middle Pliocene in age. A representative assemblage consists of *D. brouweri, C. macintyrei, P. lacunosa, Discolithina viginitiforata, Coccosphaera leptopora, Discoaster surculus*, and *D. tamalis*. Preservation is moderate to good and nannofossils are common.

The calcareous nannofossils of Core 10 are placed in the *Reticulofenestra pseudoumbilica* Zone (NN15) (Okada and Bukry, 1980) of middle Pliocene age. Cores 11–12 cannot be placed within zones, but are early Pliocene in age. The assemblage, in part, consists of *R. pseudoumbilica, D. brouweri, Amaurolithus tricorniculatus, A. primus, A. delicatus, D. surculus*, and *D. variabilis*; preservation within these cores is good, and nannofossils are common.

Core 13 is placed within the *A. tricorniculatus* Zone, *Triquetrorhabdulus rugosus* Subzone (bottom half of NN12) (Okada and Bukry, 1980), which is latest Miocene in age. The assemblage is essentially the same as Cores 11–12 with the addition of *T. rugosus*. Core 14 is assigned to the *D. quinqueramus* Zone (NN11) (Okada and Bukry, 1980) and is of late Miocene age. The assemblage is as above except for the inclusion of *D. quinqueramus*; preservation is good and nannofossils are few to common.

The nannofossils of Core 15 to 546-17-1, 127–130 cm are of early middle Miocene age; this interval cannot be placed within a precise zone. The assemblage, in part, consists of *Cyclicargolithus floridanus, Calcidiscus macintyrei, C. leptopora, R. pseudoumbilica*, and *D. variabilis*, along with some reworked Early Cretaceous nannofossils. Nannofossils are few to common, preservation moderate.

The lithologies in Core 17 vary from greenish nannofossil oozes to red claystones. Samples taken from the red claystones are barren of calcareous nannofossils; Sample 546-17-3, 41–43 cm there is a Cretaceous assemblage with some Cenozoic nannofossils mixed in. The assemblage consists of mostly background fossils except for *Cruciellipsis cuvillieri* which, according to Thierstein (1976), places it from the Berriasian to mid-Hauterivian. At 546-17-3, 70 cm, is an assemblage with several Early Cretaceous fossils: *Micrantholithus hoschulzii, Nannoconus steinmanii, C. cuvillieri*, and *Conusphaera mexicana* also suggest a Berriasian to mid-Hauterivian age. The background nannofossils common to both intervals are *Cretarhabdus angustiforata, Parhabdolithus embergeri, Lithraphidites carniolensis*, and *Vagalapilla stradneri*. These Cretaceous assemblages are poorly to moderately preserved and are few to common in abundance. No lithology break corresponds to the rapid change in assemblages, but diapiric structural influences may have been at least part of the cause.

In Core 18 is a small interval of red claystone and beneath this is salt; no nannofossils were found.

Neogene Foraminifers

The Neogene of Site 546 (Cores 1 through 16) is typical of this area. It ranges in age from Pleistocene through middle Miocene and contains a late (N17) to middle Miocene (N10–N13) hiatus greater than that found at Holes 544A and 545, also between late and middle Miocene. The late Miocene rests upon an interval of (?)mixed middle Miocene and Lower Cretaceous sediments (Core 17), red gypsiferous clays, and finally salt at the top of Section 546-18-2.

Core-catcher samples have revealed a complete sequence from Core 1 through 546-15-1, 23 cm, where there lies a marked biostratigraphic and lithostratigraphic hiatus between the late and middle Miocene. The Recent is not clearly distinguished, but the *Globorotalia truncatulinoides* Zone (Pleistocene), *Pulleniatina obliquiloculata* Zone (late Pliocene), *Globorotalia margaritae* Zone (early to middle Pliocene), and the upper part of the *Globorotalia acostaensis* Zone (late Miocene) are present in this interval.

The middle Miocene (N10–N13) extends from 546-15-1, 23 cm through 546-16; it is unzoned. Sample 546-16,CC contains a diverse assemblage of debris including glauconite, pyrite, dolomite rhombs, euhedral quartz crystals, pyritized foraminifers and radiolarians, glauconitized foraminifers, fish debris, and reworked, Early Cretaceous, primitive, arenaceous foraminifers.

Core 17 is a variegated, clayey nannofossil ooze that contains middle Miocene planktonic and Early Cretaceous benthic assemblages. Some intervals contain both ages, whereas others are either middle Miocene or Early Cretaceous.

Radiolarians

The Cenozoic section drilled at Site 546 contains only rare siliceous forms throughout. However, Sample 546-

1,CC contains a well-preserved but highly diluted radiolarian assemblage.

Cores 2 through 4 did not yield significant amounts of radiolarians. Core 14, still in the same well-oxygenated facies, is also barren of radiolarians.

At 546-15-1, 20 cm (125.7 m sub-bottom), the contact between red (Unit I) and greenish, variegated, stiff oozes (Unit II) occurs. In the green and gray lithologies, Mesozoic microfossils were found mixed with middle Miocene assemblages. Sample 546-15,CC contains rare pyritized diatoms, Miocene radiolarians, and reworked Late (or Middle?) Jurassic radiolarian species: *Hsuum* sp. aff. *H. maxwelli, Acanthocircus suboblongus, Angulobracchia* sp.

Sample 546-16-1, 22–24 cm contains dominantly pyritized diatoms and rare pyritized Cenozoic radiolarians. Sample 546-16,CC contains rare pyritized diatoms, Cenozoic radiolarians, and a reworked but reasonably well preserved assemblage of Early Cretaceous (Valanginian to Barremian) age, including *Thanarla pulchra, Pantanellium* sp. aff. *P. corriganensis (Sphaerostylus lanceola* group), *Archaeodictymoitra apiara, A. vulgaris, Hemicryptocapsa* sp., and *Holocryptocanium* sp.

Core 17 has not yielded any determinable radiolarians, and Core 18 is massive halite overlain by a barren sandy claystone.

Age of Salt

J. Fenton (this volume) examined palynomorphs from clay layers in the salt. The occurrence of *Perinopollenites elatoides* means that the salt is no older than Rhaetian, and an abundance of *Corollina meyeriana*, by comparison with offshore eastern Canada, suggests Rhaetian–Hettangian.

DEPTH VERSUS AGE CURVE

A 155.5-m-thick sequence of middle Miocene to late Pleistocene–Recent age overlies diapiric salt at Site 546. The sedimentary cover is subdivided by an unconformity into an upper unit consisting of brownish pelagic and hemipelagic nannofossil ooze and a lower unit consisting of a complex interlayering of red claystone and greenish nannofossil ooze.

The average sedimentation rate of the upper unit, ranging in age from late Pleistocene or Recent to late Miocene (Fig. 18), is about 22 m/m.y. For the lower middle Miocene unit lying beneath a late to middle Miocene hiatus (7 to 10 m.y.), a sedimentation rate of about 25 m/m.y. can be estimated.

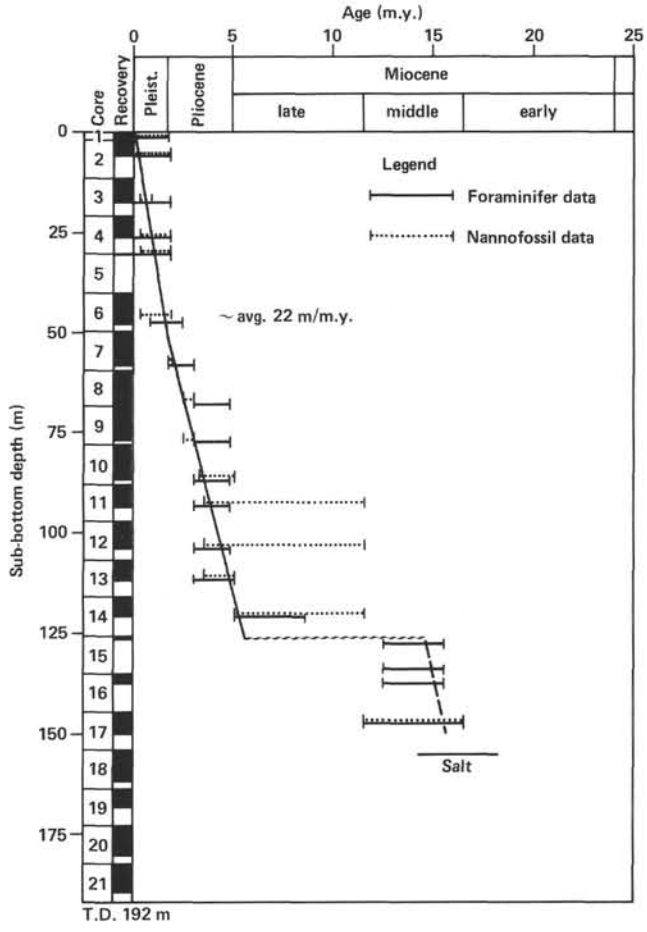

Figure 18. Depth versus age, Site 546.

ORGANIC GEOCHEMISTRY

Carbon and Nitrogen Contents

All sediments recovered from Hole 546 are lean in organic matter (Table 2) with a mean of 0.17% C_{org} and very low N_{org} values in the partly clayey foraminiferal–nannofossil oozes of Lithologic Unit I. The carbonate content is fairly uniform in this unit but slightly increases toward Unit II. A sample of the sediment directly overlying the halite shows the highest organic carbon value (0.51%). A positive correlation exists between the proportion of noncarbonate material in the sediments and the organic carbon contents, as is indicated by the correlation coefficient $r = 0.83$ ($r_{05;15} = 0.497$). Additional results of statistical treatment of carbonate, organic carbon, and nitrogen data are summarized in Table 3.

Table 2. Carbon and nitrogen contents, Hole 546.

Core-Section (interval in cm)	Sub-bottom depth (m)	Lithologic unit	Age	C_{org} (%)	$CaCO_3$ (%)	N_{org} (%)
2-1, 144–150[a]	3.5			0.27	35.3	0.05
2-2, 118–120	4.7			0.37	48.7	0.05
2-3, 0–2	5.0		Pleistocene	0.30	44.7	0.04
6-3, 140–150[a]	44.5			0.14	58.6	0.03
6-4, 118–120	45.7			0.16	56.1	0.03
6-5, 0–2	46.0			0.24	40.8	0.05
8-4, 144–150	65.0	I		0.12	63.0	0.03
9-4, 118–120	74.2			0.12	61.5	0.03
9-5, 0–2	74.5			0.15	59.5	0.03
10-4, 144–150[a]	84.0		Pliocene	0.11	59.5	0.03
12-3, 118–120	101.2			0.16	58.1	0.03
12-4, 0–2	101.5			0.13	63.5	0.03
12-4, 140–150[a]	103.0			0.13	65.0	0.03
14-3, 140–150[a]	120.5					
			Miocene–	0.07	70.9	0.02
16-1, 57–58	135.6			0.10	72.4	0.02
18-1, 29–30	154.3	II	?	0.51	8.7	0.04

[a] Residues from interstitial water analysis.

Gas Chromatography of Light Hydrocarbons

No free hydrocarbon gases were observed in the sediments at Site 546. Carrier gas stripping gas chromatography was performed for three samples from the Mio-

Table 3. Statistical characteristics of $CaCO_3$, C_{org}, and N_{org} contents in sediments from Hole 546.

Lithologic unit	Age	N	$CaCO_3$ (%) Range	Mean	Variance	S.D.	C_{org} (%) Range	Mean	Variance	S.D.	N_{org} (%) Range	Mean	Variance	S.D.
I	Pleistocene–Miocene	14	35.3–70.9	56.1	93.90	10.06	0.07–0.37	0.17	7×10^{-3}	0.085	0.02–0.05	0.03	8×10^{-5}	0.009
II	Miocene–?	1		72.4				0.10				0.02		
		1		8.7				0.15				0.04		
	Total	16												

Note: Mean $= \bar{y} = \frac{1}{N}\sum_{i=1}^{N} y_i$; variance $= \frac{1}{N}\sum_{i=1}^{N} y_i^2 - \left(\frac{1}{N}\sum_{i=1} y_i\right)^2$; S.D. $= \sqrt{\text{var}\,\frac{N}{N-1}}$.

cene–Pliocene section (Table 4). The absolute hydrocarbon concentrations are very low in Sections 546-8-4 and 546-12-4. Normalized to the low amount of organic carbon present in these sediments, these concentrations are relatively high, indicating that part of the hydrocarbons may not be indigenous. No hydrocarbons at all could be detected in Section 546-16-1. There was no indication of major hydrocarbon generation associated with the salt diapir below.

INORGANIC GEOCHEMISTRY

A summary of the inorganic geochemistry data for Site 546 is given in Table 5 and in Figures 19 and 20.

PHYSICAL PROPERTIES

Physical properties measured at Site 546 include compressional wave velocity, wet-bulk density, porosity, water content, and shear strength. These measurements are summarized in Tables 6 and 7. Variations of velocity, density, porosity, water content, and computed acoustic impedance with depth are shown in Figure 21.

Unit I (0–125.7 m) consists of slightly clayey nannofossil ooze and foraminiferal–nannofossil ooze. In this unit, velocity increases from ~1.5 km/s near the sediment surface to 1.81 km/s at a depth of 120 m. Density increases from 1.65 to 1.92 g/cm³ at the base of the unit. Shear strength increases with depth to nearly 70 kPa (Table 7).

Unit II (125.7–155.5 m) is an interlayered clayey nannofossil ooze and grayish red claystone in which the nearly equal vertical and horizontal velocities increase from 1.84 to more than 2.0 km/s. In this interval, density increases to 2.14 g/cm³.

Unit III (155.5–192 m) consists of coarsely crystalline, thinly layered, reddish brown and clear halite. An attempt was made to measure the compressional wave velocity in the salt rock, but only a very weak signal could be transmitted through a thin slab (1 cm) of this material. The measured velocity of 3.2 km/s should therefore be regarded only as an estimate. GRAPE measurements on the halite sample indicate a density of 2.03 g/cm³.

Water content and porosity were determined gravimetrically on all samples except the halite. Because interstitial water salinity increases to nearly 200 ppt, salt corrections were made on the water content (Boyce, 1976). The salinity at the depth where gravimetric samples were

Table 4. Light hydrocarbon values (nl/g sediment) detected in Hole 546 sediments by carrier gas stripping gas chromatography.

Core-Section (interval in cm)	Sub-bottom depth (m)	C_2	C_3	i-C_4	n-C_4	i-C_5	n-C_5	Total HC	Total HC (nl/g C_{org})
8-4, 0–1	65.0	3.6	5.2	0.9	1.4	tr	tr	11.1	9,250
12-4, 0–2	103.0	3.5	3.0	1.6	1.0	tr	tr	9.1	7,000
16-1, 57–58	135.6	—	—	—	—	—	—	—	—

Note: tr = trace; — = not detected.

Table 5. Summary of shipboard inorganic geochemical data, Hole 546.

Core-Section (interval in cm)	Sub-bottom depth (m)	pH	Alkalinity (meq/l)	Salinity (‰)	Calcium (mmoles/l)	Magnesium (mmoles/l)	Chlorinity (‰)
IAPSO standard		7.66	2.44	35.2	10.55	64.54	19.378
2-1, 144–150	3.44–3.50	7.22	4.12	39.7	10.33	52.11	22.36
4-3, 92–96	24.96			57.5			
6-3, 144–150	44.44–44.50	7.19	3.71	71.5	14.58	47.56	43.00
6-6, 148–150	49.0			78.4			
In situ water sample 1	50.0	7.98	4.26	78.1	13.92	49.30	50.61
7,CC	59.0			85.3			
8-4, 144–150	64.94–65.00	7.03	3.13	92.4	15.20	46.64	56.30
8,CC	68.5			97.9			
9,CC	78.0			105.0			
10-4, 144–150	83.94–84.00	7.15	2.33	111.9	17.39	43.37	70.71
10,CC	87.5			110.6			
11,CC	97.0			126.0			
12-4, 140–150	102.90–103.00	7.11	1.74	138.6	21.06	38.68	88.88
12,CC	106.5			139.7			
13,CC	116.0			151.3			
14-3, 140–150	120.40–120.50	6.91	1.61	162.0	24.82	34.50	106.81
14,CC	125.5			161.7			
15,CC	135.0			152.9			
16,CC	144.5			177.2			
17-3, 120–130	148.70–148.80	6.79	1.22	198.0	33.93	27.61	134.07
17,CC	154.0			174.9			
18-1, 30–40	154.30–154.40	6.97	0.580	193.6	39.30	25.90	127.22
18,CC	163.5			216.7			

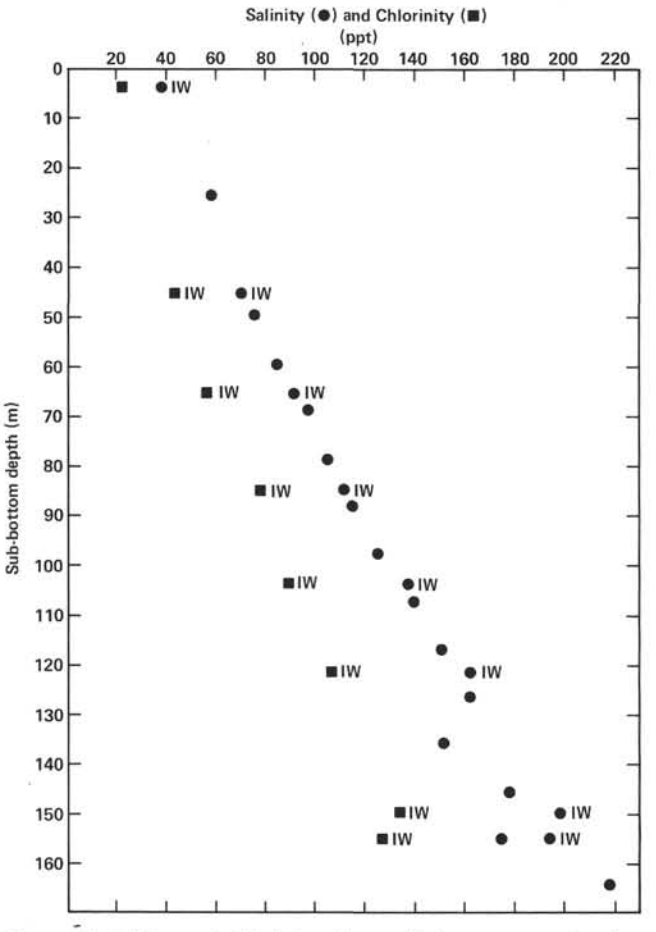

Figure 19. Salinity and chlorinity of interstitial water versus depth at Site 546. IW = interstitial water sample (other salinities from squeezed core-catcher samples).

taken was estimated by linear interpolation from measured salinity values. Table 6 and Figure 21 show that salt-corrected values of water content decrease from approximately 40% near the sediment surface to about 14% near the contact with Unit III. No salt corrections were made to the porosity values shown, and consequently the presented values are slightly less than the *in situ* values. In order to estimate the GRAPE porosity of the halite sample a grain density of 2.16 g/cm^3 was assumed, but no correction was made for increased pore fluid density.

The relatively rapid velocity increase observed in the sediments of Units I and II contrasts with the slight increases observed at the previous sites. Measured velocities at both Sites 544 and 545 are generally less than 1.6 km/s in the upper 120 m of sediments, whereas velocities at Site 546 are greater than 1.6 km/s at 20 to 40 m sub-bottom depth.

SEISMIC STRATIGRAPHY

Introduction

The reason for drilling Site 546 was to determine the nature of the structural high beneath this site. In the seismic sections it looks very similar to numerous diapiric structures, interpreted as salt domes and mapped seismically within a zone off Morocco that is from 30 to about 100 km wide. The zone can be traced over a distance of about 700 km from east of Fuerteventura Island, Canary Islands, to latitude 34°N. The somewhat similar structural high at Site 544 was shown by drilling to be underlain by gneissic rocks at shallow depths.

From the seismic data it appears that the western boundary of this Moroccan diapiric province fits well with the eastern boundary of the diapiric zone of Nova Scotia (Fig. 22). From this finding, and under the assumption that these seismically diapirlike structures con-

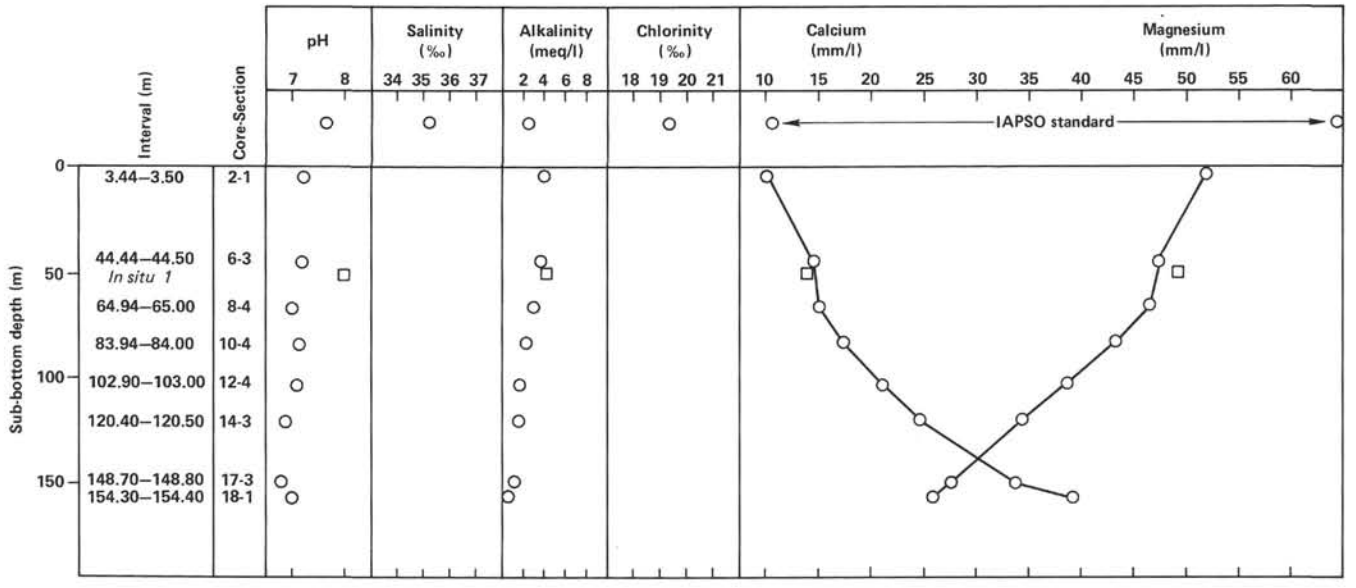

Figure 20. Inorganic geochemistry, Site 546.

Table 6. Summary of physical properties, Hole 546.

Core-Section (interval in cm)	Sub-bottom depth (m)	Velocity Horizontal (km/s)	Velocity Vertical (km/s)	GRAPE Density (g/cm^3)	GRAPE Porosity (%)	Density (g/cm^3)	Porosity (%)	Water content (%)	Acoustic impedance ($10^5 g \cdot cm^{-2} s^{-1}$)
2-3, 98-100	6.0	1.51				1.65	63.0	39.9	2.49[a]
3-4, 118-120	17.2	1.55				1.69	60.8	37.9	2.61[a]
4-3, 134-136	25.4	1.60				1.72	59.6	36.8	2.75[a]
6-4, 101-103	45.5	1.63				1.78	55.6	33.8	2.90[a]
7-5, 84-86	56.4	1.65				1.86	49.7	29.1	3.07[a]
8-5, 124-126	66.3	1.66				1.81	53.5	32.6	3.00[a]
9-3, 113-115	72.6	1.68				1.82	52.7	32.3	3.06[a]
10-4, 101-103	83.5	1.69				1.80	50.0	31.2	3.05[a]
11-3, 116-118	91.7	1.74				1.84	44.8	27.6	3.20[a]
12-4, 108-110	102.6	1.75				1.91	38.0	23.1	3.35[a]
13-3, 127-129	110.8	1.77				1.90	37.9	23.4	3.36[a]
14-3, 114-116	120.2	1.81				1.92	37.4	23.3	3.47[a]
15-1, 68-70	126.2	1.85	1.84			1.95	36.4	22.2	3.59
16-2, 85-87	136.1	2.09	2.07			2.14	28.4	15.6	4.42
17-3, 95-97	148.5	2.03	2.04			2.14	23.7	13.8	4.36
18-4, 13-15	158.6		3.22	2.03	11.5				

[a] Value computed using horizontal velocity.

Table 7. Shear strength of sediments, Hole 546.

Core-Section (interval in cm)	Depth (m)	Shear strength (kPa)
2-3, 107-109	6.1	21
3-4, 122-124	17.2	21
4-3, 138-140	25.4	20
6-4, 105-107	45.6	25
7-5, 91-93	56.4	26
8-5, 129-131	66.3	29
9-3, 118-120	72.7	34
10-4, 106-108	83.6	53
11-3, 122-124	91.7	43
12-4, 113-115	102.6	67
13-3, 131-133	110.8	66
14-3, 118-120	120.2	68

sist of salt, we believed that before or during the earliest stage of opening of the central North Atlantic, there existed a single evaporite basin the two halves of which were separated by later seafloor spreading and are now preserved in the southwestern Moroccan Basin and beneath the Nova Scotia shelf. Under one hypothesis, this basin would have been enlarged by subcrustal processes preceding the drift phase, for example, by stretching and extension of the continental crust, upwelling of hot asthenosphere, and then subsidence as a result of lithospheric cooling. For space reasons (Sleep, 1971; McKenzie, 1978), thinning of the continental crust by extensive erosion or by crustal extension is necessary to produce deeply subsided basins. Listric faults (de Chapral et al., 1978) could account for the large extension required. Movements along listric faults can produce rotational blocks, either with the basement involved, as in the structure at Site 544, or without the basement. Both types of rotational structures might resemble diapirs in seismic sections. To understand the evolution of the central North Altantic, it is very important to investigate the nature of these diapirlike seismic structures to learn whether they are continental basement blocks gliding along listric faults, rotational sedimentary blocks, or salt domes.

For Site 546, a structure was selected which lies directly next to the structure at Site 544 (Fig. 23).

Location of Site 546, Bathymetry, and Seismic Coverage

Site 546 lies within the western part of the top of a domelike structure, in 3958 m water depth (Fig. 1). At Site 546, the relatively flat and gently northwest dipping top of the dome is 5 to about 8 km wide and as much as about 300 m above the adjacent seafloor. A narrow east-trending depression crosses the top of the ridge. The shortest distance between Site 546 and the steep Mazagan Escarpment is about 22 km. The distance to Site 544 is about 15 km.

Seismic coverage near Site 546 is good and includes single-channel reflection seismic lines of *Vema* cruise 3013 and multichannel seismic lines (Fig. 24). In addition, a brief site survey was carried out by *Glomar Challenger* on 23 April 1981 and during the approach from Site 545 to Site 546 on 1 May 1981. After carefully studying the seismic records, we located Site 546 at about the crossing of line *VA* 79-05 and a *Glomar Challenger* line, where the acoustic basement lies well above the adjacent seafloor.

Seismic Sequences and Their Correlation with the Drilling Results

The following seismostratigraphic discussion is abased upon Line *VA* 79-05 (Figs. 25 and 26). For a general description of seismic sequences in the Mazagan region, see the regional synthesis chapter by Winterer and Hinz, this volume.

At Site 546 there is one recognizable depositional sequence overlying the acoustic basement. The sequence is acoustically transparent and is 0.2 s (2-way traveltime) thick at Site 546. The acoustic basement is a reflectionless or an opaque zone with a strong top reflector. The weaker reflectors running parallel to and beneath the strong top reflector are thought to be internal multiples.

For a correlation of the seismic data with the drilling results the reflection time for the boundaries of the biostratigraphically and lithostratigraphically identified units was calculated by using sonic velocities approximated by

$$V_Z = 1515 + 2.16\,Z,$$

where 1525 (m/s) is the velocity at the seafloor, V_Z (m/s) is the velocity at a depth Z (m) below the seafloor, and 2.16 (s^{-1}) is the velocity gradient.

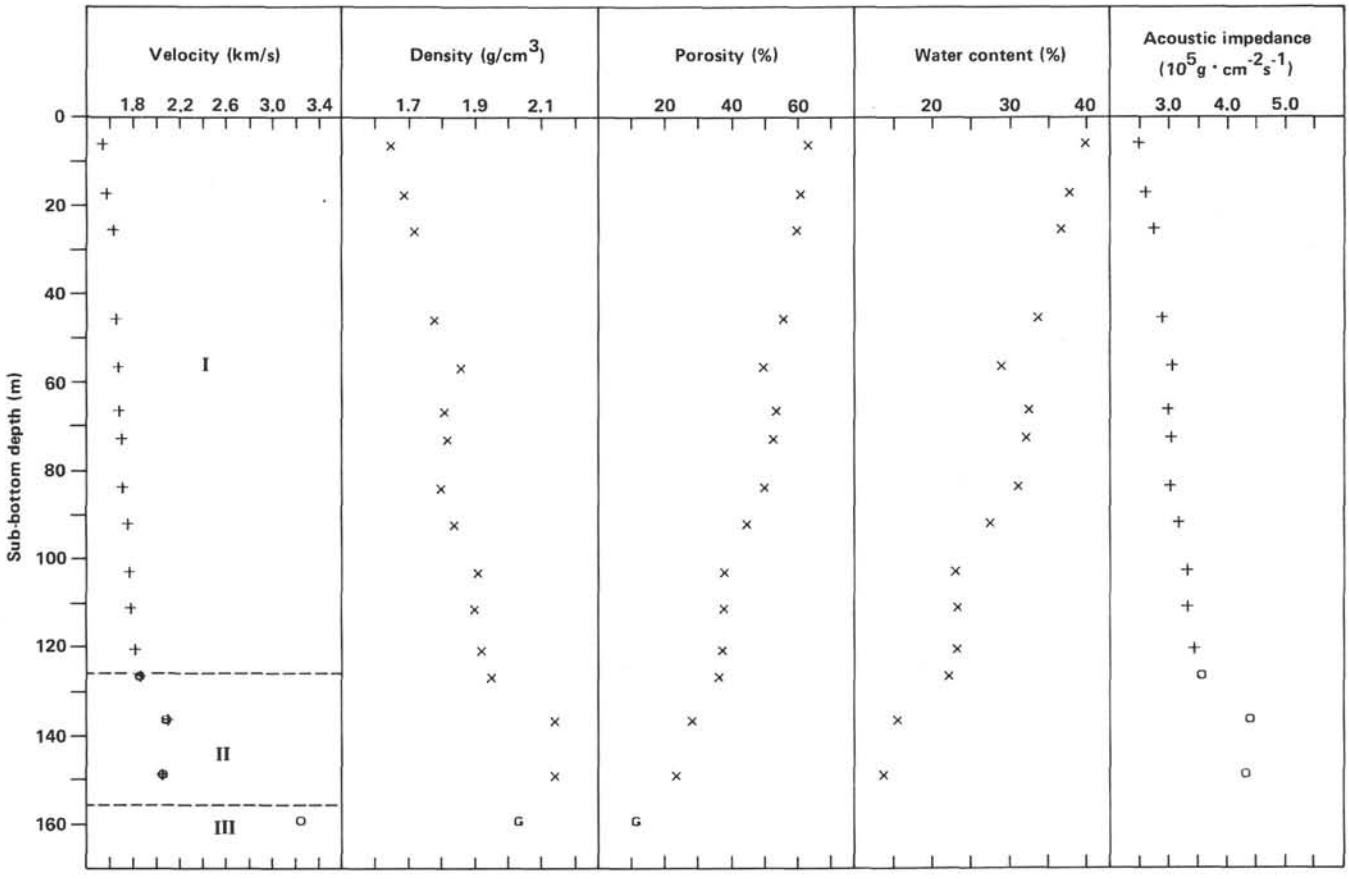

Figure 21. Physical properties versus depth, Hole 546. +,o represent horizontal and vertical values, respectively. X,G represent gravimetric (immersion) and GRAPE values, respectively.

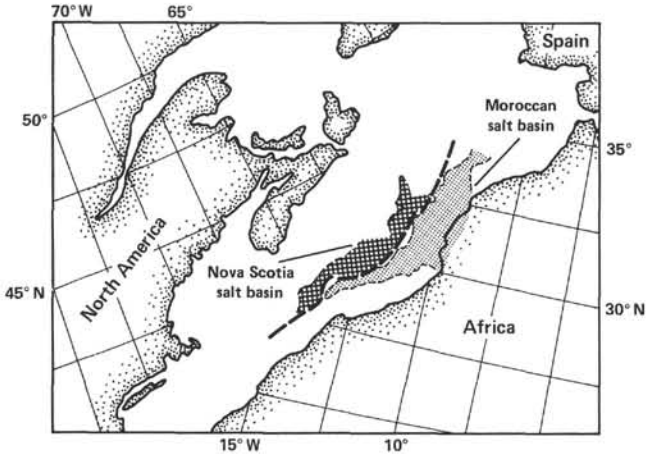

Figure 22. Inferred extent of diapiric salt (Triassic–Early Jurassic) provinces of Morocco Northwest Africa) and Nova Scotia (eastern America).

The strong reflector lying 0.2 s beneath the seafloor very probably represents the top of the salt, drilled to a depth of 156.5 m. This correlation implies an average velocity of 1565 m/s for the interval from the seafloor to the top of the salt. The calculated interval velocity is remarkably smaller than the measured horizontal sonic velocities, ranging from 1540 (Core 3) to 2060 m/s (Core 16). A plausible explanation for this strange difference would be that the beacon landed a little off the seismic line at a place where the thickness of the Neogene sediments overlying the salt is only 0.18 to 0.19 s (two-way traveltime) instead of 0.2 s. This would result in an average velocity of 1710 to 1620 m/s. The marked increase of the horizontal velocities with depth correlates with the measured increase of salinity with depth.

In the region away from the proven salt diapir, the following seismic sequences have been identified (Fig. 25, southwest flank):

Beneath the seafloor lies the transparent Sequence Ma 1.3, about 0.4 s thick, which according to the drilling results is interpreted to consist of upper Miocene to Pliocene–Pleistocene ooze.

The underlying Sequence Ma 1.2 shows a parallel reflection pattern. Sequence Ma 1.2 is about 0.4 s thick and is thought to consist of clay and chalk of early and middle Miocene age drilled at Site 545. Both Sequences Ma 1.3 and Ma 1.2 thin toward the flank of the salt dome, which in our opinion indicates that the salt diapir has been rising at a more or less uniform rate from the early Miocene to the present time. The lower boundary of Sequence Ma 1.2 forms a distinct erosional unconformity, probably shaped during the Oligocene.

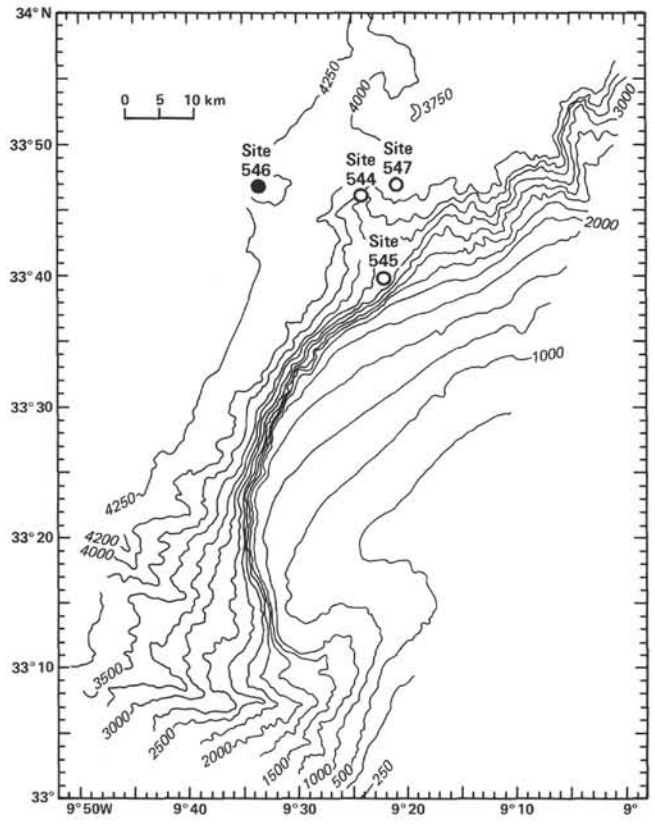

Figure 23. Bathymetric map of the Mazagan continental margin segment, from echo soundings of *Meteor* cruises 9/1967, 39/1975, 53/1980, the *Valdivia* West Africa cruise 1979, and the SEAZAGAN seabeam survey of *Jean Charcot* (Auzende et al., this volume). Depths in m.

According to the results of Site 547, Sequence Ma 1.1 probably represents intercalated claystone and chalk of Paleogene age, here preserved in a rim syncline that probably originated during a stage when salt was rapidly rising in the Paleogene. Outside the rim syncline, the thickness of Ma 1.1 is strongly reduced by the overlying erosional unconformity.

Reflector Red (marker R in Fig. 25) separates Cenozoic from Cretaceous strata and defines the top of Sequence Ma 2.3, which thickens toward the flank of the salt diapir. Extrapolating the results of Sites 545 and 547, Sequence Ma 2.3 presumably consists of Aptian to Cenomanian clay, claystone, and chalk. The underlying Sequence Ma 2.2 is interpreted as Valanginian–Hauterivian to Aptian. Its upper boundary is interpreted as an erosional unconformity.

In contrast to Sequence Ma 2.3, the thickness of Sequence Ma 2.2 decreases towards the flank of the salt dome. This shape, known as primary rim syncline, indicates (Trusheim, 1957) a pillow stage of a salt structure, whereas an increase of thickness toward the flanks, known as secondary rim syncline, indicates a piercement stage. Under this line of reasoning, a salt pillow developed at Site 546 in the Early Cretaceous, followed by periods when salt rapidly rose in the early Late Cretaceous (lower half of Sequence Ma 2.3) and in the Paleogene (Sequence Ma 1.1).

Reflector Blue (marked B in Fig. 25) is interpreted as the top of the Jurassic carbonates. The flat-lying reflection element at about 8.2–8.3 s is thought to represent the base of the salt. The estimated total thickness of sediments above the interpreted base of the salt amounts to about 3500 m, assuming interval velocities of 2000 m/s for Sequences Ma 1.1, 1.2, and 1.3; 2500 m/s for Sequence Ma 2.3; 3500 m/s for Sequence Ma 2.2; and 4500 m/s for Sequence Ma 3.

SUMMARY AND CONCLUSIONS

The main result of drilling at Site 546 was the discovery of diapiric salt, lying beneath a relatively thin cover of Neogene pelagic sediments. This result confirms the inference drawn from the study of seismic records across this same structure, and allows us more confidently to place the diapiric label on the many other structures in the region that show the same seismic characteristics.

Neogene Sediments

The Neogene sediments at Site 546 are 155.5 m thick and consist of two lithologic and biostratigraphic units separated by an unconformity. The upper unit, about 125.7 m thick, consists of slightly clayey nannofossil ooze and foraminiferal nannofossil ooze, ranging in age from late Pleistocene or Recent at the top to late Miocene (foraminiferal Zone N17) at the base. Terrigenous quartz, feldspar, mica, and clay constitute nearly 50% of the material in cores from the upper Pleistocene, but drop to 15 or 20% in the Pliocene and Miocene. The rate of accumulation was about from 20–30 m/m.y., which is about 2 g/cm^2 per 10^3 yr. when the thickness values are corrected for density and porosity.

The unconformity separating Unit I from Unit II is most likely at a depth of about 125.7 m, judging from the sudden decrease in drilling rate at this level. Core 15, from 125.5–135.0 m, recovered only 1.1 m of material, and the lithologic–biostratigraphic contact between the brownish sediments of Unit I and the greenish sediments of Unit II occurs at 546-15-1, 20 cm. The conventional scheme of assigning all recovered material to the upper part of the cored interval when recovery is incomplete would be misleading here, in light of the drilling-rate data. The unconformity separates ooze containing foraminifers of Zone N17 from chalk containing faunas from Zones N13 to N10. The estimated amount of lost record (Figure 18) is about 6 m.y., and the hiatus corresponds fairly closely to that crossed at Sites 544 and 545. More detailed study of the fossils is required to pin down precisely the paleontological zones bracketing this regional hiatus.

Beneath the hiatus there is greenish clayey nannofossil chalk for the first 5 m, but in the lowest part of the recovered material in Core 16, reddish brown nannofossil clay, stained with Fe-Mn, makes its appearance. This is underlain (Core 17) by a confusing sequence of alternating irregular layers of greenish nannofossil chalk and claystone, grayish red sandy mudstone containing gypsum and anhydrite crystals, and silty dolomite. Middle Miocene fossils occur in some of the layers, whereas others contain a mixture of middle Miocene and Early

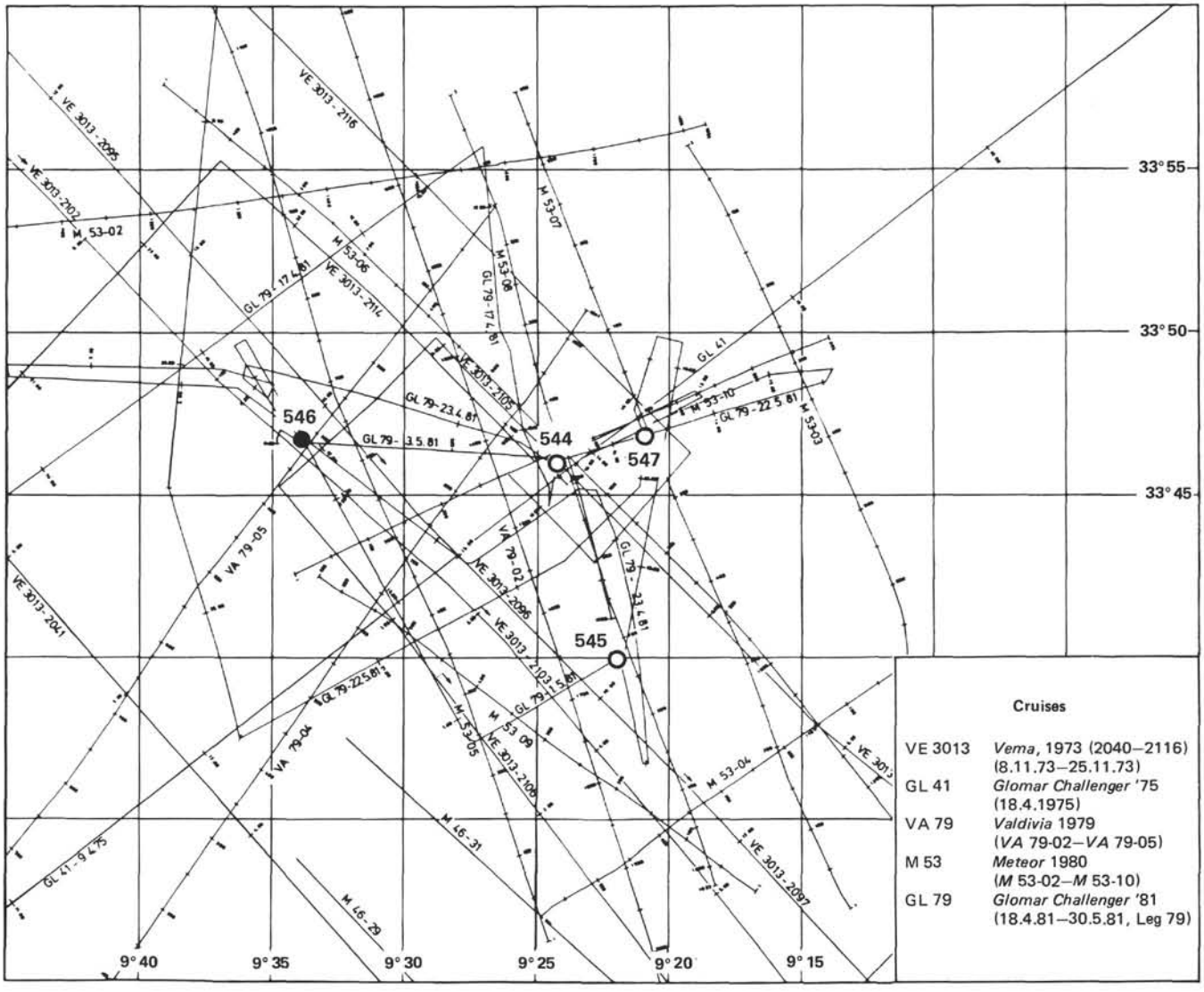

Figure 24. Location of seismic profiles around Site 546.

Cretaceous nannofossils and Jurassic radiolarians. The presumably reworked Mesozoic biota occurs in both the greenish and reddish layers. In Core 18, immediately above the salt, only barren, reddish, sandy claystone and a 4-cm layer of coarsely crsytalline anhydrite were recovered.

The steady increase in the salinity of pore waters with increasing depth (Fig. 19) gave us a clue that salt lay below. Thus we gave special attention to the possibility of an accumulation of hydrocarbons, but none could be detected in any sample analyzed. This evidence, combined with the strong evidence for upward diffusion of salty water, made it appear unlikely that any hydrocarbons lay below. The reddish sandy clay in Cores 16 and 17 was studied carefully for signs of characteristic caprock mineralogy and texture, but none of the special features of diagenesis of petroleum-associated caprock (i.e., the formation of calcite and sulfur) were seen. Instead, only relatively small amounts of anhydrite and its hydration product, gypsum, were seen as evidence of dissolution residues from the salt.

The reworked Cretaceous fossils suggested that we might in fact be dealing instead with the deposits of a solution valley or sink. The seismic profile (Fig. 25) shows what appears to be a broad, shallow depression. Dissolution of salt that included smears of Cretaceous strata carried upward during diapirism and transport of clay flukes and fossils from these layers into the shallow sink would account for the interlayering of "normal" Miocene chalk with reworked Cretaceous material.

The salt, which was cored to a depth of 36.5 m below the Neogene unconformity, consists mainly of coarsely crystalline, thinly layered, reddish brown and clear translucent halite. The color bands, in shades of brown, red, and greenish gray, are generally 2 to 3 cm wide and dip at angles ranging from about 10 to 45°, in some places changing dip over this full range within a single unbroken core. The color bands are mainly concentrations of illite, kaolinite, and mixed-layer clay minerals, stained red in some layers from hematite. Reddish and relatively clear zones alternate on a scale of about a meter, and the wavy anastomosing pattern suggests cataclasis; it is

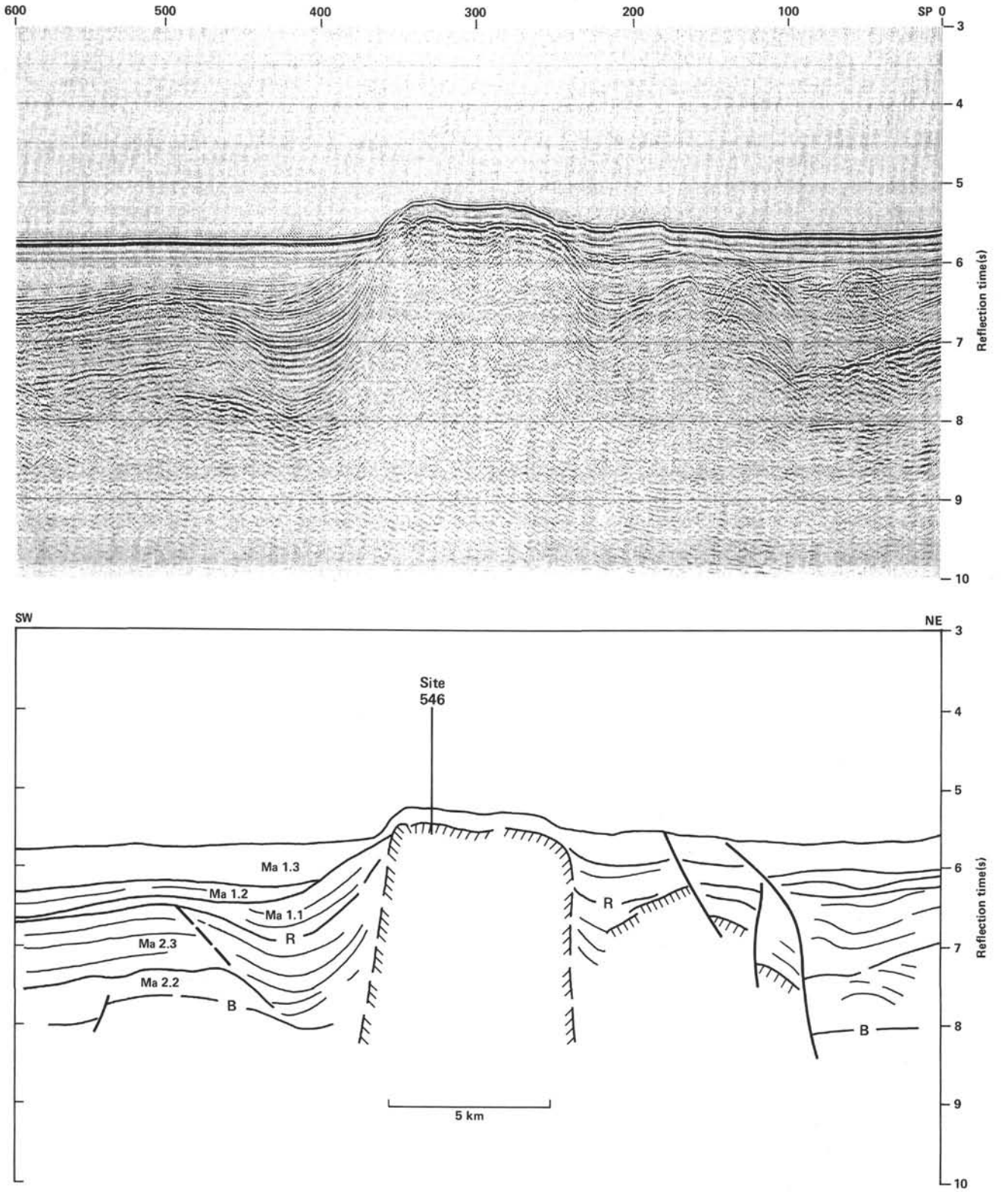

Figure 25. Seismic record of *Valdivia* line *VA* 79-05 and line drawing with identified seismic sequences and reflectors. Location of the profile is indicated in Figure 24. B., Blue reflector; R, Red reflector.

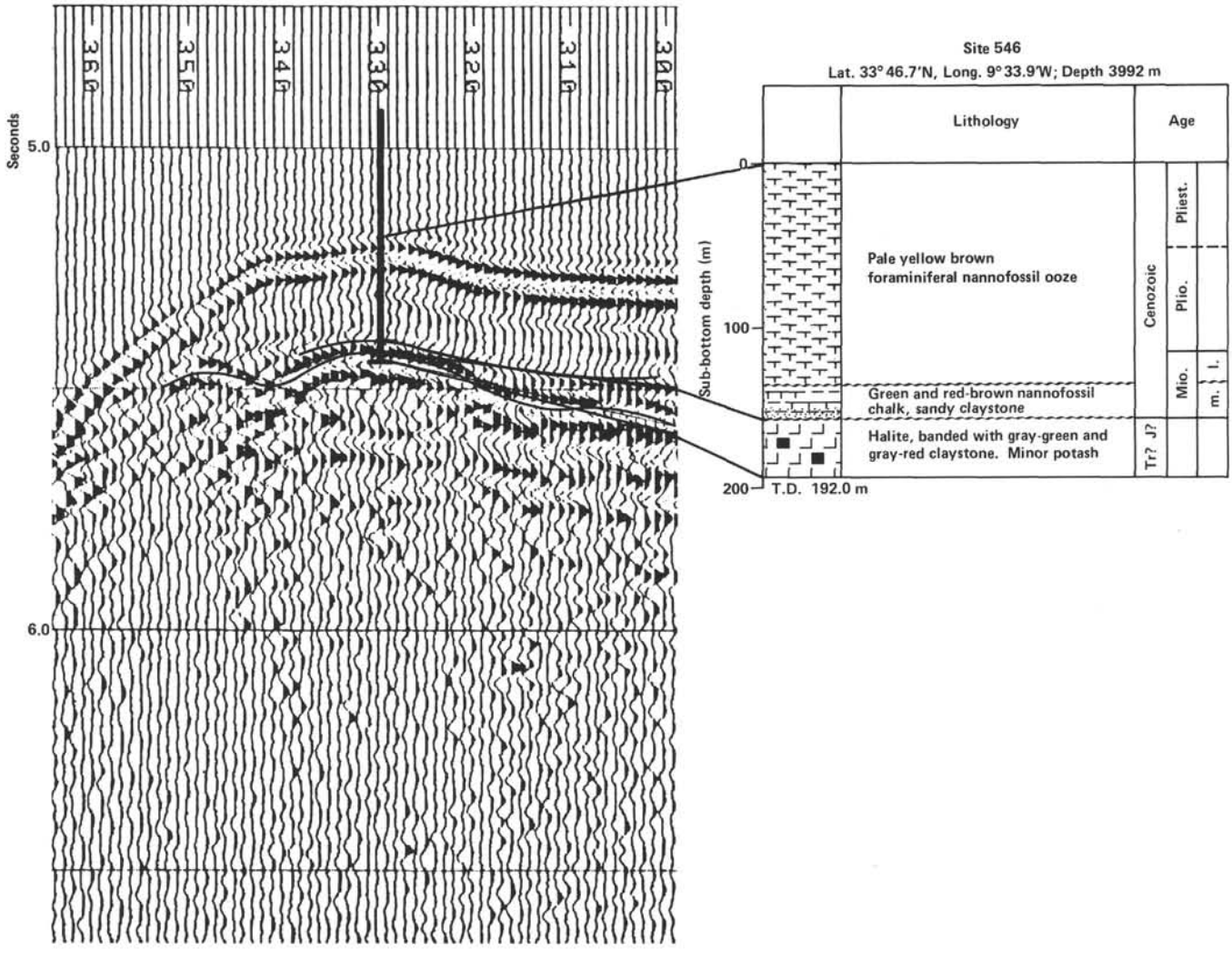

Figure 26. Correlation of seismic sequences and reflectors with the drilling results of Site 546.

certainly not a primary depositional fabric. Finely crystalline anhydrite occurs in gray clayey seams, and small amounts of dolomite occur with the anhydrite. Sylvite occurs in minute amounts as reddish specks. Large solution cavities (2–3 cm) filled with clear halite are conspicuous, and do not appear to be affected by cataclasis.

The salt is certainly diapiric: there is a good rim syncline, and there is seismic stratigraphic evidence for a multistage rise. The cataclastic textures and variable dip of the foliation also support diapirism.

A cross section (Fig. 27), constructed along the line of *Valdivia* profile 79-05, shows the diapir and its accompanying flank structures, corrected for sound velocities and with no vertical exaggeration.

A detailed summary of the lithologic and biostratigraphic successions at Site 546 is shown in Figure 28.

The age of the salt, according to Fenton's study of palynomorphs (this volume), is Rhaetian to Early Jurassic. Holser et al. (this volume) argue that sulfur isotope ratios in the anhydrite associated with the salt are more compatible with a Permian or Early Triassic than with a Late Triassic or Early Jurassic age. Chemical and mineralogical studies by Holser et al. (this volume) show that the salt is of marine origin, and was deposited from brine in a relatively shallow basin which was not intermittently desiccated.

The regional significance of the salt is that we now have material confirmation of diapirs, and that other structures of a similar kind in the region seaward of the Mazagan Plateau can be more safely interpreted as salt structures. Great care must be exercised in this seismic interpretation, especially when working with profiles having a large vertical exaggeration. Most *Vema* and *Challenger* seismic profiles are of this kind, and it is virtually impossible to discriminate between sialic blocks and salt diapirs on these records. High-quality migrated multichannel records, in contrast, can show the characteristic rim syncline and pillow stage thinning of diapirs. The normal depositional and compactional draping of sediments over structural highs and their synclinal drape in structural lows cannot by themselves be used to distinguish basement blocks from diapirs.

There is no *a priori* reason to assume that salt diapirs and tilted basement blocks cannot occur together, and the region seaward of Mazagan, out to the limit of the structural highs and the beginning of unambiguous oce-

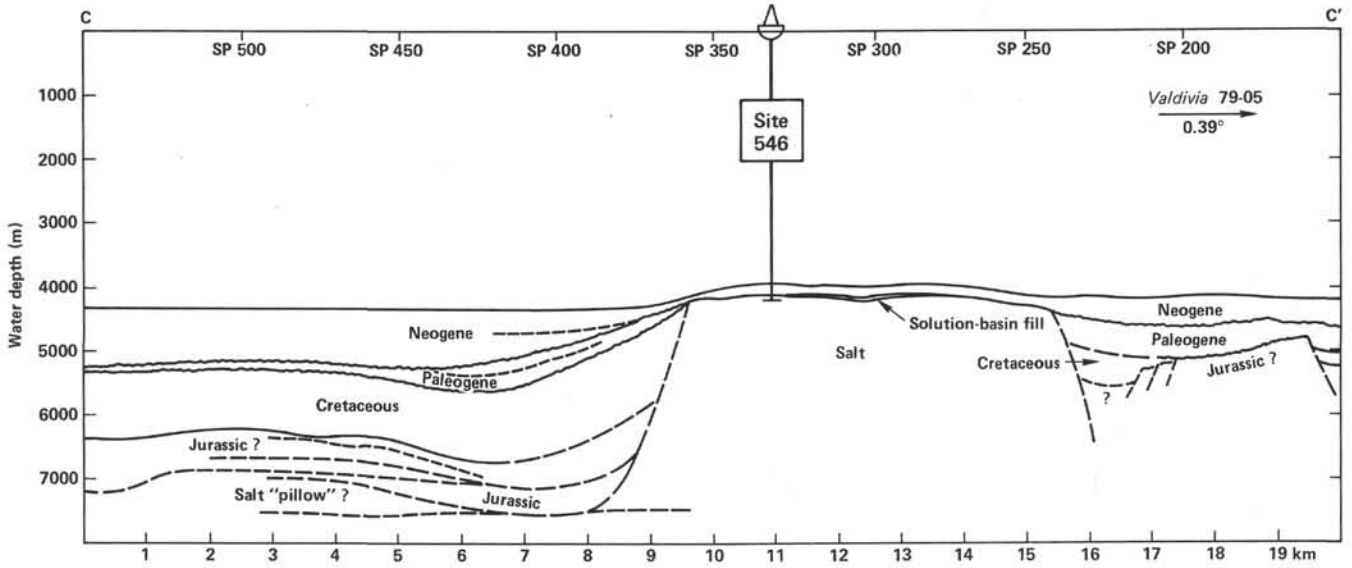

Figure 27. Geologic cross section through Site 546, along *Valdivia* seismic line 79-05 (Line A–A′ of Fig. 4).

anic crust, must be thoroughly studied to map the seaward limit of sialic blocks, if we are to understand the nature of the thin edge of the continent and how the African and North American margins were joined before the opening of the Atlantic.

REFERENCES

Boyce, R. E., 1976. Definitions and laboratory techniques of compressional sound velocity parameters and wet-water content, wet-bulk density, and porosity parameters by gravimetric and gamma ray attenuation techniques. *In* Schlanger, S., Jackson, E. D., et al., *Init. Repts. DSDP*, 33: Washington (U.S. Govt. Printing Office), 931–957.

de Chapral, G. O., Guennoc, P., Montadert, L., and Roberts, D. G., 1978. Rifting, crustal attenuation and subsidence in the Bay of Biscay. *Nature*, 275:706–711.

Gartner, S., 1977. Calcareous nannofossil biostratigraphy and revised zonation of the Pleistocene. *Mar. Micropaleontol.*, 2:1–25.

Jansa, L. F., Bujak, J. P., and Williams, G. L., 1980. Upper Triassic salt deposits of the western North Atlantic. *Can. J. Earth Sci.*, 17: 547–559.

McKenzie, D., 1978. Some remarks on the development of sedimentary basins. *Earth Planet. Sci. Lett.*, 40:25–32.

Okada, H., and Bukry, D., 1980. Supplementary modification and introduction of code numbers to the low-latitude coccolith biostratigraphic zonation (Bukry, 1973; 1975). *Mar. Micropaleontol.*, 5: 321–325.

Salvan, H. M., 1974. Le séries salifères du Trias marocain: caractères généraux et possibilités d'interprétation. *Bull. Soc. Geol. Fr.*, 16: 724–731.

Sleep, N. H., 1971. Thermal effects on the formation of Atlantic continental margins by continental breakup. *Geophys. F. R. Astron. Soc.*, 24:325–350.

Thierstein, H. R., 1976. Mesozoic calcareous nannoplankton biostratigraphy of marine sediments. *Mar. Micropaleontol.*, 1:325–362.

Trusheim, F., 1957. Uber Halokinese und ihre Bedeutung für die strukturelle Entwicklung Norddeutschlands. *Z. Deut. Geol. Ges.*, 109: 111–151.

Date of Acceptance: November 7, 1983

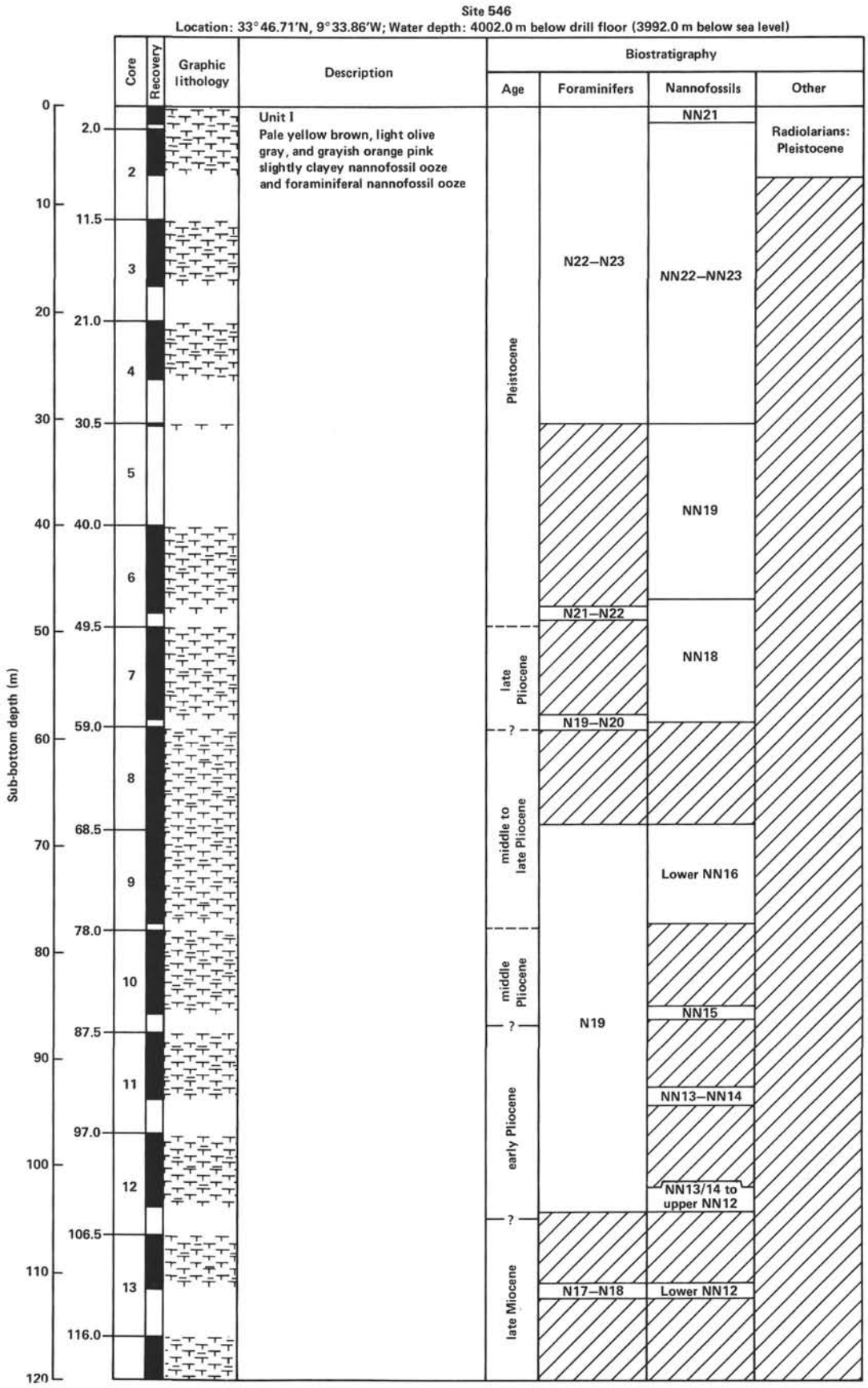

Figure 28. Detailed graphic log of Hole 546.

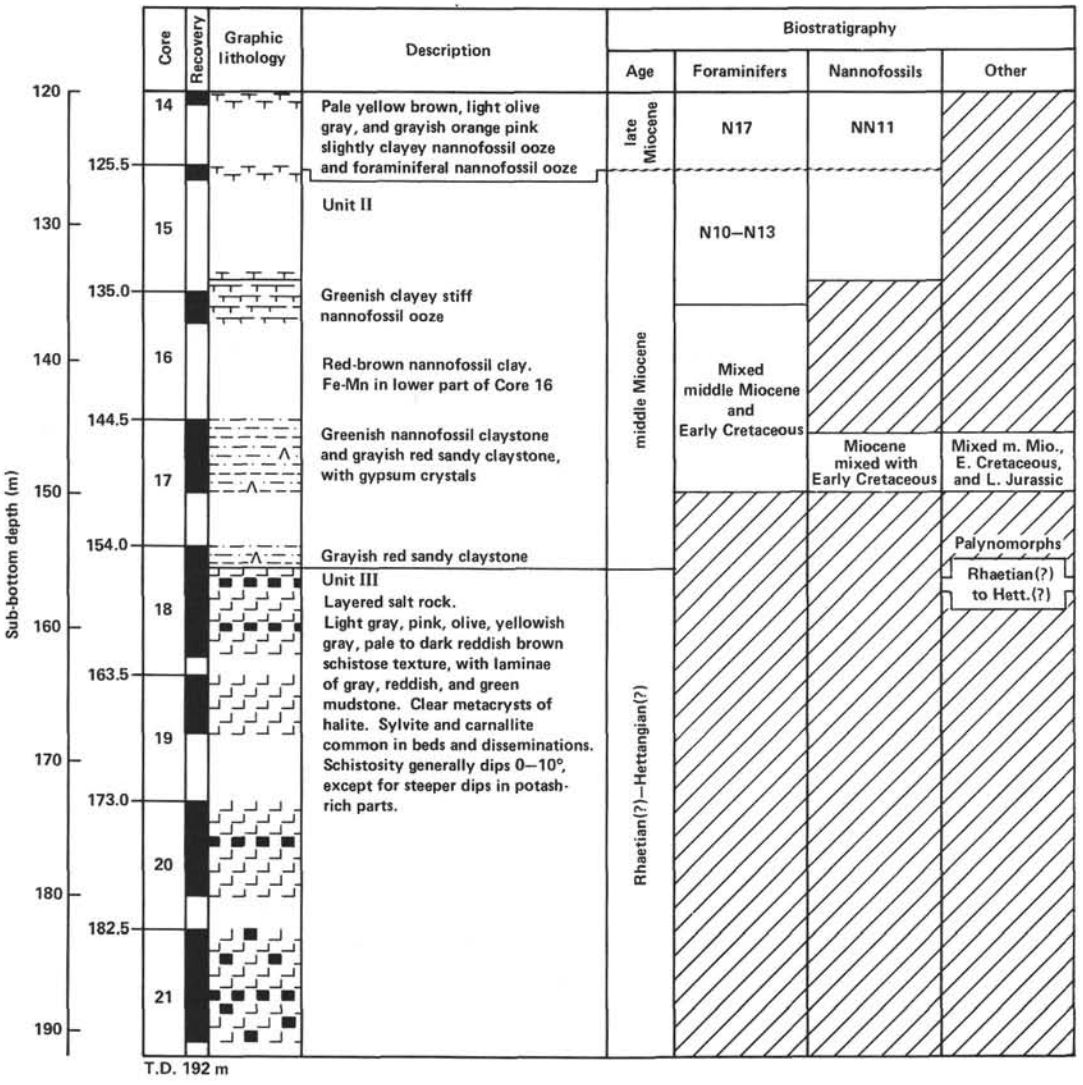

Figure 28. (Continued).

SITE 546 HOLE CORE 1 CORED INTERVAL 0.0–2.0 m sub-bottom

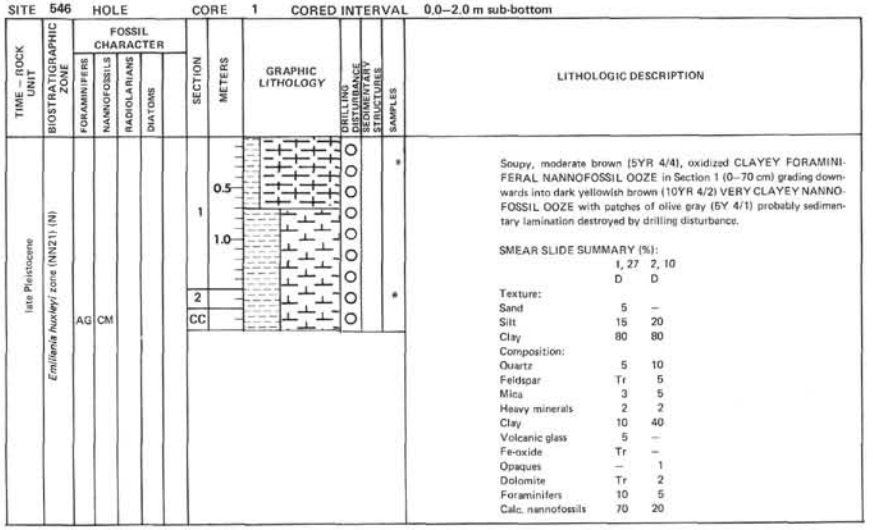

Soupy, moderate brown (5YR 4/4), oxidized CLAYEY FORAMINIFERAL NANNOFOSSIL OOZE in Section 1 (0–70 cm) grading downwards into dark yellowish brown (10YR 4/2) VERY CLAYEY NANNOFOSSIL OOZE with patches of olive gray (5Y 4/1) probably sedimentary lamination destroyed by drilling disturbance.

SMEAR SLIDE SUMMARY (%):

	1, 27 D	2, 10 D
Texture:		
Sand	5	–
Silt	15	20
Clay	80	80
Composition:		
Quartz	5	10
Feldspar	Tr	5
Mica	3	5
Heavy minerals	2	2
Clay	10	40
Volcanic glass	5	–
Fe-oxide	Tr	–
Opaques	–	1
Dolomite	Tr	2
Foraminifers	10	5
Calc. nannofossils	70	20

SITE 546 HOLE CORE 2 CORED INTERVAL 2.0–11.5 m sub-bottom

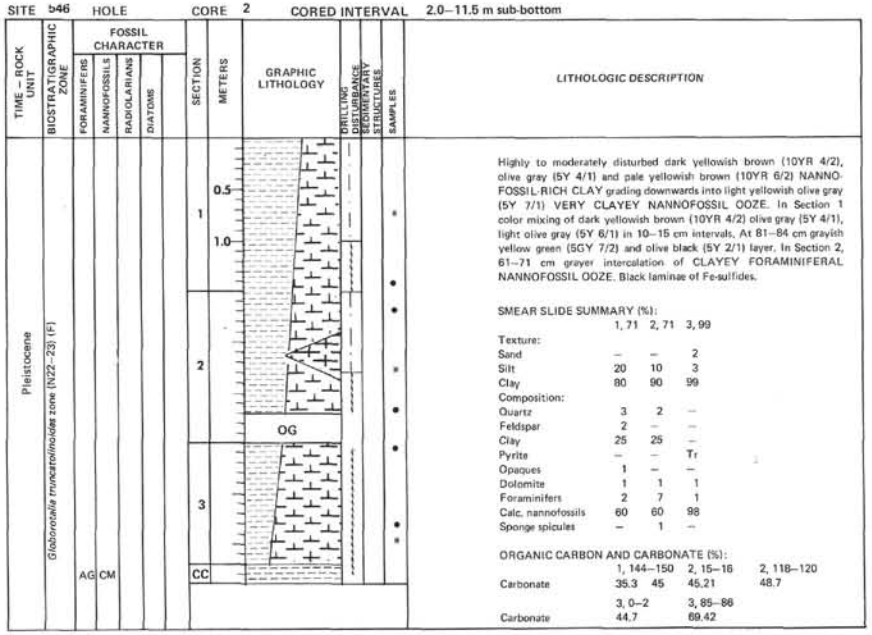

Highly to moderately disturbed dark yellowish brown (10YR 4/2), olive gray (5Y 4/1) and pale yellowish brown (10YR 6/2) NANNOFOSSIL-RICH CLAY grading downwards into light yellowish olive gray (5Y 7/1) VERY CLAYEY NANNOFOSSIL OOZE. In Section 1 color mixing of dark yellowish brown (10YR 4/2) olive gray (5Y 4/1), light olive gray (5Y 6/1) in 10–15 cm intervals. At 81–84 cm grayish yellow green (5GY 7/2) and olive black (5Y 2/1) layer. In Section 2, 61–71 cm greyer intercalation of CLAYEY FORAMINIFERAL NANNOFOSSIL OOZE. Black laminae of Fe-sulfides.

SMEAR SLIDE SUMMARY (%):

	1, 71	2, 71	3, 99
Texture:			
Sand	–	–	2
Silt	20	10	3
Clay	80	90	99
Composition:			
Quartz	3	2	–
Feldspar	2	–	–
Clay	25	25	–
Pyrite	–	–	Tr
Opaques	1	–	–
Dolomite	1	1	1
Foraminifers	2	7	1
Calc. nannofossils	60	60	98
Sponge spicules	–	1	–

ORGANIC CARBON AND CARBONATE (%):

	1, 144–150	2, 15–16	2, 118–120
Carbonate	35.3	45.21	48.7
	3, 0–2	3, 85–86	
Carbonate	44.7	69.42	

SITE 546 HOLE CORE 3 CORED INTERVAL 11.5–21.0 m sub-bottom

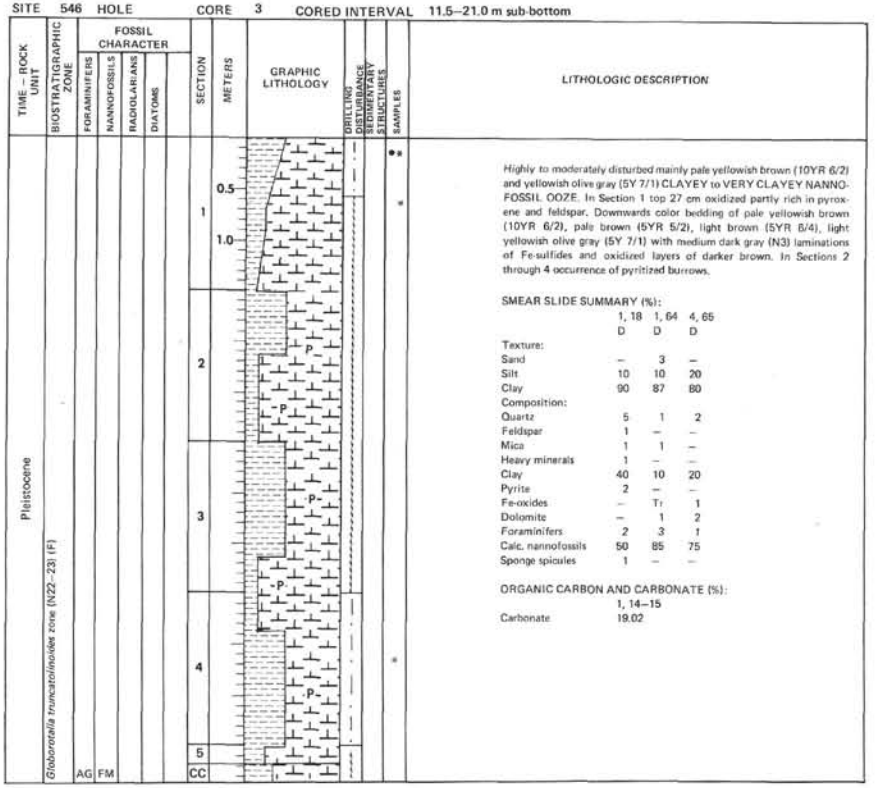

Highly to moderately disturbed mainly pale yellowish brown (10YR 6/2) and yellowish olive gray (5Y 7/1) CLAYEY to VERY CLAYEY NANNOFOSSIL OOZE. In Section 1 top 27 cm oxidized partly rich in pyroxene and feldspar. Downwards color bedding of pale yellowish brown (10YR 6/2), pale brown (5YR 5/2), light brown (5YR 6/4), light yellowish olive gray (5Y 7/1) with medium dark gray (N3) laminations of Fe-sulfides and oxidized layers of darker brown. In Sections 2 through 4 occurrence of pyritized burrows.

SMEAR SLIDE SUMMARY (%):

	1, 18 D	1, 64 D	4, 65 D
Texture:			
Sand	–	3	–
Silt	10	10	20
Clay	90	87	80
Composition:			
Quartz	5	1	2
Feldspar	1	–	–
Mica	1	1	–
Heavy minerals	1	–	–
Clay	40	10	20
Pyrite	2	–	–
Fe-oxides	–	Tr	1
Dolomite	–	1	2
Foraminifers	*2*	*3*	*1*
Calc. nannofossils	50	85	75
Sponge spicules	1	–	–

ORGANIC CARBON AND CARBONATE (%):

	1, 14–15
Carbonate	19.02

SITE 546 HOLE CORE 4 CORED INTERVAL 21.0–30.5 m sub-bottom

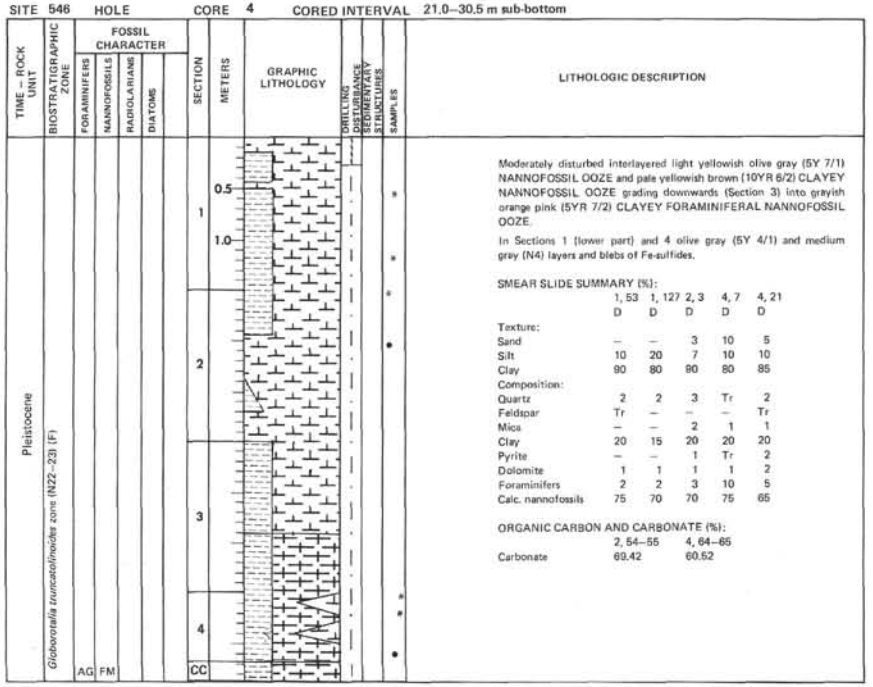

LITHOLOGIC DESCRIPTION

Moderately disturbed interlayered light yellowish olive gray (5Y 7/1) NANNOFOSSIL OOZE and pale yellowish brown (10YR 6/2) CLAYEY NANNOFOSSIL OOZE grading downwards (Section 3) into grayish orange pink (5YR 7/2) CLAYEY FORAMINIFERAL NANNOFOSSIL OOZE.

In Sections 1 (lower part) and 4 olive gray (5Y 4/1) and medium gray (N4) layers and blebs of Fe-sulfides.

SMEAR SLIDE SUMMARY (%):

	1, 53 D	1, 127 D	2, 3 D	4, 7 D	4, 21 D
Texture:					
Sand	–	–	3	10	5
Silt	10	20	7	10	10
Clay	90	80	90	80	85
Composition:					
Quartz	2	2	3	Tr	2
Feldspar	Tr	–	–	–	Tr
Mica	–	–	2	1	1
Clay	20	15	20	20	20
Pyrite	–	–	1	Tr	2
Dolomite	1	1	1	1	2
Foraminifers	2	2	3	10	5
Calc. nannofossils	75	70	70	75	65

ORGANIC CARBON AND CARBONATE (%):

	2, 54–55	4, 64–65
Carbonate	69.42	60.52

SITE 546 HOLE CORE 5 CORED INTERVAL 30.5–40.0 m sub-bottom

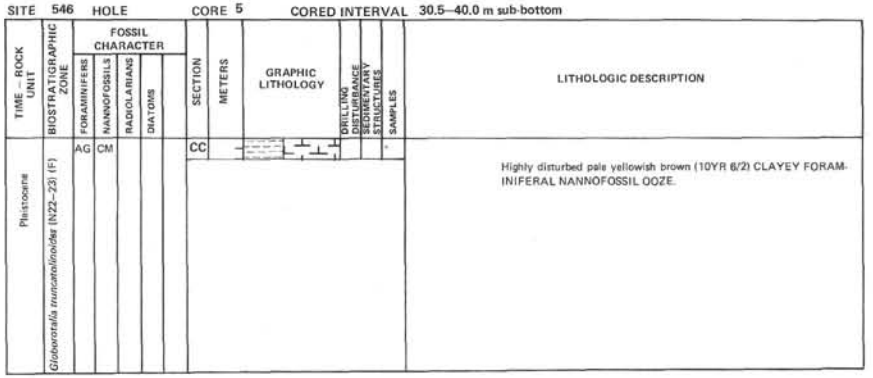

LITHOLOGIC DESCRIPTION

Highly disturbed pale yellowish brown (10YR 6/2) CLAYEY FORAMINIFERAL NANNOFOSSIL OOZE.

SITE 546 HOLE CORE 6 CORED INTERVAL 40.0–49.5 m sub-bottom

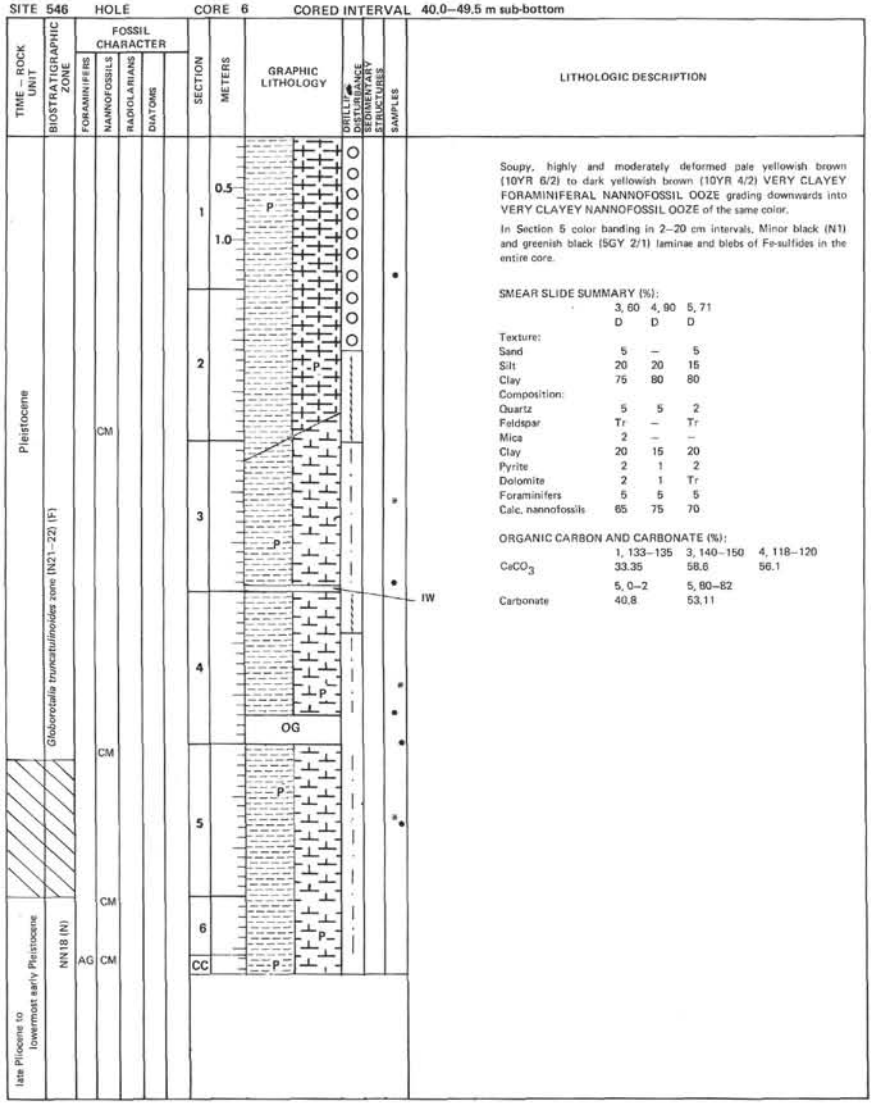

LITHOLOGIC DESCRIPTION

Soupy, highly and moderately deformed pale yellowish brown (10YR 6/2) to dark yellowish brown (10YR 4/2) VERY CLAYEY FORAMINIFERAL NANNOFOSSIL OOZE grading downwards into VERY CLAYEY NANNOFOSSIL OOZE of the same color.

In Section 5 color banding in 2–20 cm intervals. Minor black (N1) and greenish black (5GY 2/1) laminae and blebs of Fe-sulfides in the entire core.

SMEAR SLIDE SUMMARY (%):

	3, 60 D	4, 90 D	5, 71 D
Texture:			
Sand	5	–	5
Silt	20	20	15
Clay	75	80	80
Composition:			
Quartz	5	5	2
Feldspar	Tr	–	Tr
Mica	2	–	–
Clay	20	15	20
Pyrite	2	1	2
Dolomite	2	1	Tr
Foraminifers	5	5	5
Calc. nannofossils	65	75	70

ORGANIC CARBON AND CARBONATE (%):

	1, 133–135	3, 140–150	4, 118–120
$CaCO_3$	33.35	58.6	56.1
	5, 0–2	5, 80–82	
Carbonate	40.8	53.11	

SITE 546 HOLE CORE 7 CORED INTERVAL 49.5–59.0 m sub-bottom

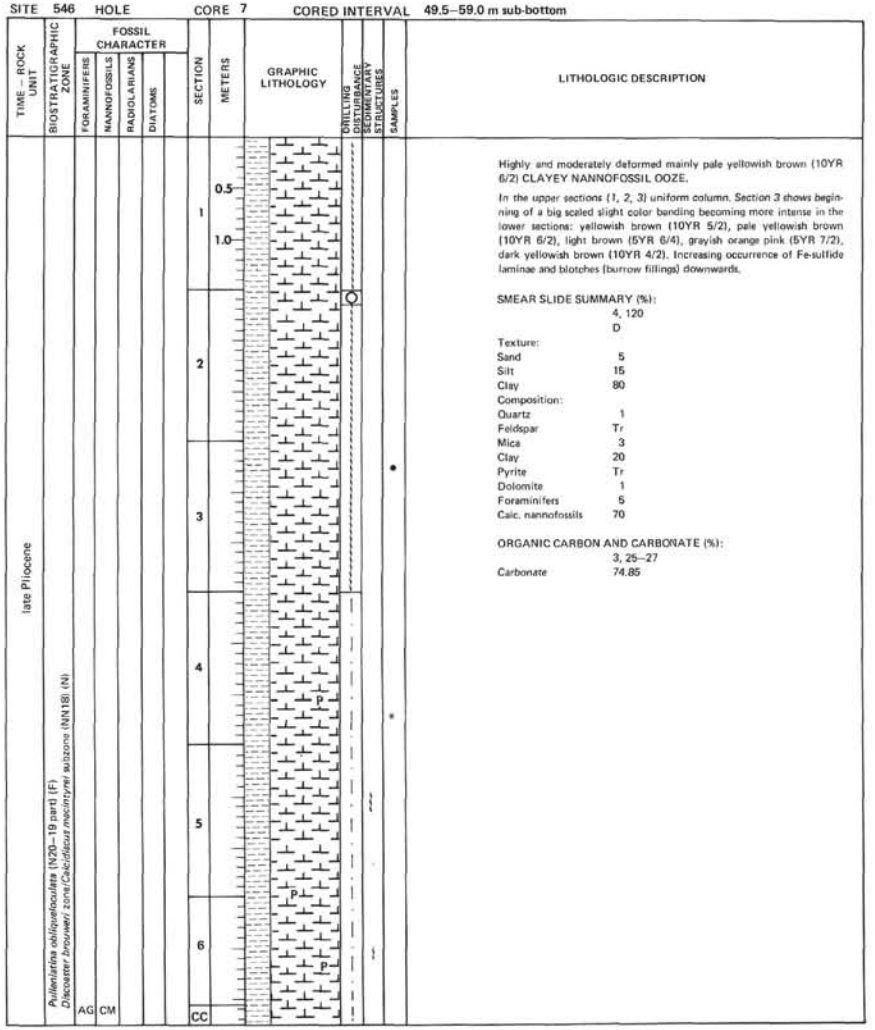

LITHOLOGIC DESCRIPTION

Highly and moderately deformed mainly pale yellowish brown (10YR 6/2) CLAYEY NANNOFOSSIL OOZE.

In the upper sections (1, 2, 3) uniform column. Section 3 shows beginning of a big scaled slight color banding becoming more intense in the lower sections: yellowish brown (10YR 5/2), pale yellowish brown (10YR 6/2), light brown (5YR 6/4), grayish orange pink (5YR 7/2), dark yellowish brown (10YR 4/2). Increasing occurrence of Fe-sulfide laminae and blotches (burrow fillings) downwards.

SMEAR SLIDE SUMMARY (%):

	4, 120 D
Texture:	
Sand	5
Silt	15
Clay	80
Composition:	
Quartz	1
Feldspar	Tr
Mica	3
Clay	20
Pyrite	Tr
Dolomite	1
Foraminifers	5
Calc. nannofossils	70

ORGANIC CARBON AND CARBONATE (%):

	3, 25–27
Carbonate	74.85

SITE 546 HOLE CORE 8 CORED INTERVAL 59.0–68.5 m sub-bottom

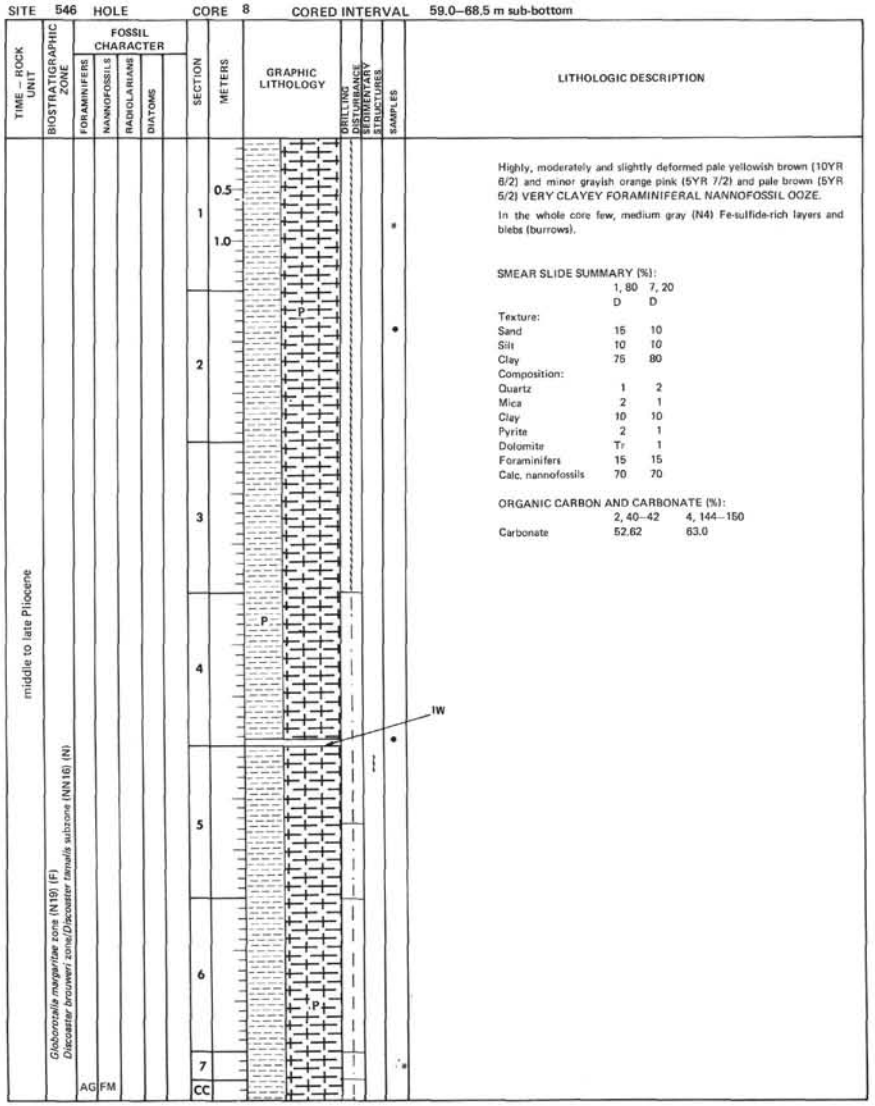

LITHOLOGIC DESCRIPTION

Highly, moderately and slightly deformed pale yellowish brown (10YR 6/2) and minor grayish orange pink (5YR 7/2) and pale brown (5YR 5/2) VERY CLAYEY FORAMINIFERAL NANNOFOSSIL OOZE.

In the whole core few, medium gray (N4) Fe-sulfide-rich layers and blebs (burrows).

SMEAR SLIDE SUMMARY (%):

	1, 80 D	7, 20 D
Texture:		
Sand	15	10
Silt	10	10
Clay	75	80
Composition:		
Quartz	1	2
Mica	2	1
Clay	10	10
Pyrite	2	1
Dolomite	Tr	1
Foraminifers	15	15
Calc. nannofossils	70	70

ORGANIC CARBON AND CARBONATE (%):

	2, 40–42	4, 144–150
Carbonate	52.62	63.0

SITE 546 HOLE CORE 9 CORED INTERVAL 68.5–78.0 m sub-bottom

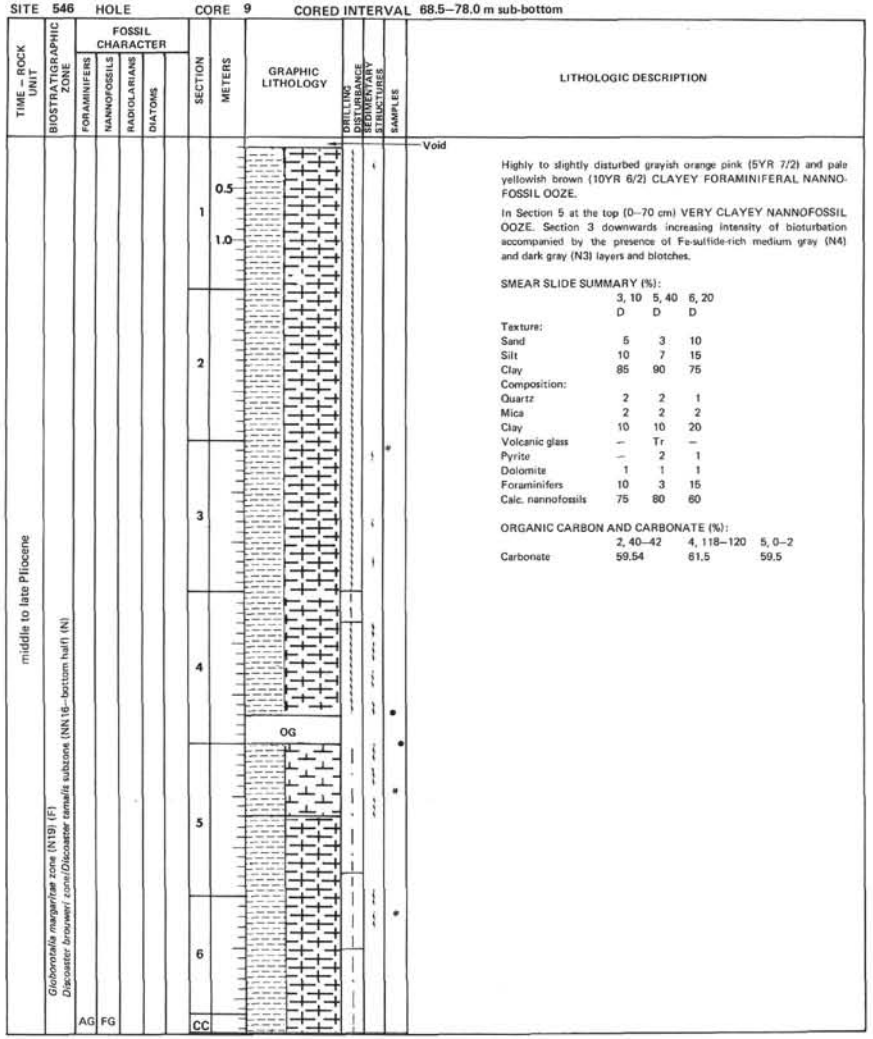

Highly to slightly disturbed grayish orange pink (5YR 7/2) and pale yellowish brown (10YR 6/2) CLAYEY FORAMINIFERAL NANNOFOSSIL OOZE.

In Section 5 at the top (0–70 cm) VERY CLAYEY NANNOFOSSIL OOZE. Section 3 downwards increasing intensity of bioturbation accompanied by the presence of Fe-sulfide-rich medium gray (N4) and dark gray (N3) layers and blotches.

SMEAR SLIDE SUMMARY (%):

	3, 10 D	5, 40 D	6, 20 D
Texture:			
Sand	5	3	10
Silt	10	7	15
Clay	85	90	75
Composition:			
Quartz	2	2	1
Mica	2	2	2
Clay	10	10	20
Volcanic glass	–	Tr	–
Pyrite	–	2	1
Dolomite	1	1	1
Foraminifers	10	3	15
Calc. nannofossils	75	80	60

ORGANIC CARBON AND CARBONATE (%):

	2, 40–42	4, 118–120	5, 0–2
Carbonate	59.54	61.5	59.5

SITE 546 HOLE CORE 10 CORED INTERVAL 78.0–87.5 m sub-bottom

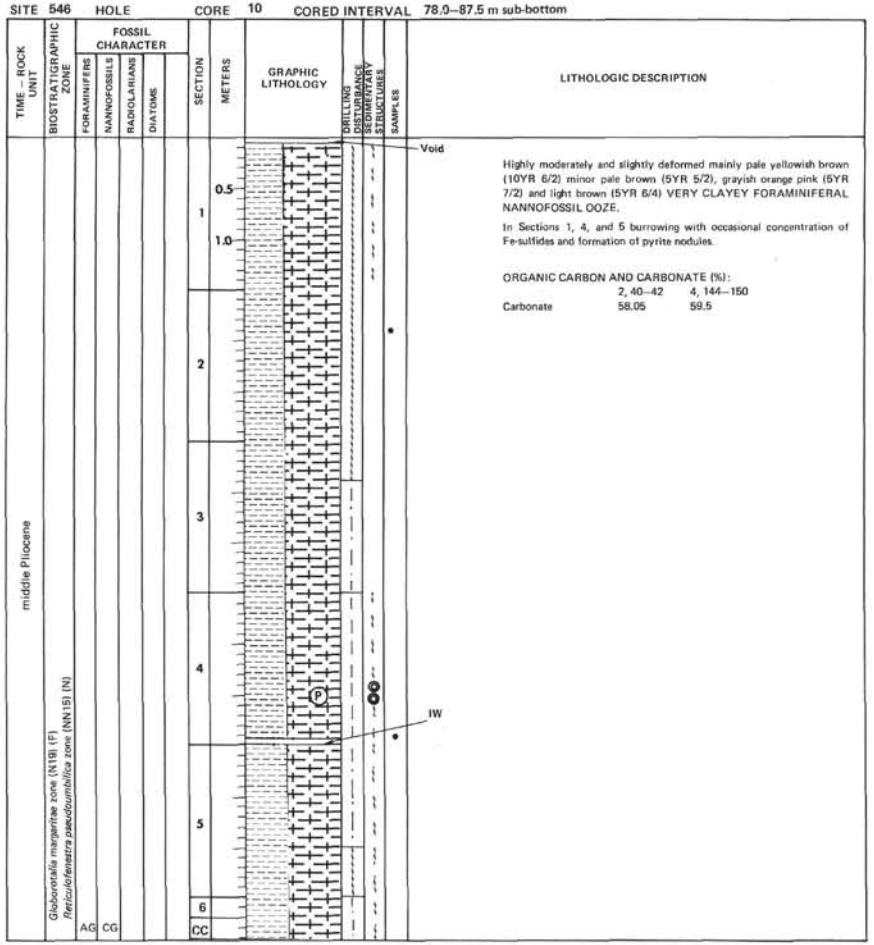

Highly moderately and slightly deformed mainly pale yellowish brown (10YR 6/2) minor pale brown (5YR 5/2), grayish orange pink (5YR 7/2) and light brown (5YR 6/4) VERY CLAYEY FORAMINIFERAL NANNOFOSSIL OOZE.

In Sections 1, 4, and 5 burrowing with occasional concentration of Fe-sulfides and formation of pyrite nodules.

ORGANIC CARBON AND CARBONATE (%):

	2, 40–42	4, 144–150
Carbonate	58.05	59.5

SITE 546 HOLE CORE 11 CORED INTERVAL 87.5–97.0 m sub-bottom

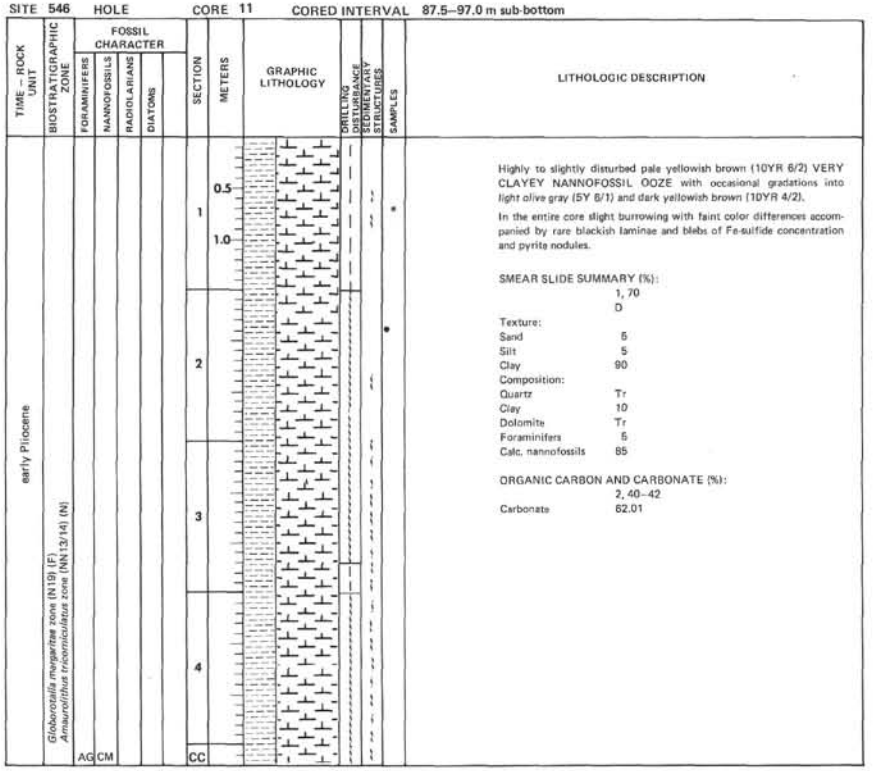

Highly to slightly disturbed pale yellowish brown (10YR 6/2) VERY CLAYEY NANNOFOSSIL OOZE with occasional gradations into light olive gray (5Y 6/1) and dark yellowish brown (10YR 4/2).

In the entire core slight burrowing with faint color differences accompanied by rare blackish laminae and blebs of Fe-sulfide concentration and pyrite nodules.

SMEAR SLIDE SUMMARY (%):

	1, 70 D
Texture:	
Sand	5
Silt	5
Clay	90
Composition:	
Quartz	Tr
Clay	10
Dolomite	Tr
Foraminifers	5
Calc. nannofossils	85

ORGANIC CARBON AND CARBONATE (%):

	2, 40–42
Carbonate	62.01

SITE 546 HOLE CORE 12 CORED INTERVAL 97.0–106.5 m sub-bottom

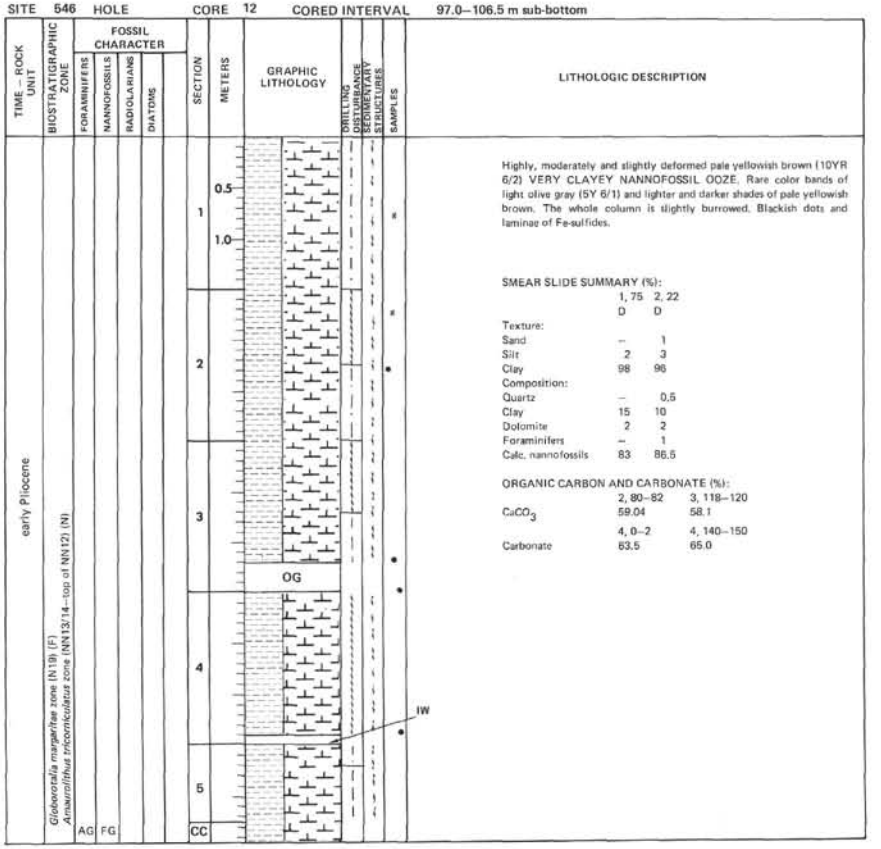

Highly, moderately and slightly deformed pale yellowish brown (10YR 6/2) VERY CLAYEY NANNOFOSSIL OOZE. Rare color bands of light olive gray (5Y 6/1) and lighter and darker shades of pale yellowish brown. The whole column is slightly burrowed. Blackish dots and laminae of Fe-sulfides.

SMEAR SLIDE SUMMARY (%):

	1, 75 D	2, 22 D
Texture:		
Sand	–	1
Silt	2	3
Clay	98	96
Composition:		
Quartz	–	0.5
Clay	15	10
Dolomite	2	2
Foraminifers	–	1
Calc. nannofossils	83	86.5

ORGANIC CARBON AND CARBONATE (%):

	2, 80–82	3, 118–120
$CaCO_3$	59.04	58.1
	4, 0–2	4, 140–150
Carbonate	63.5	65.0

SITE 546 HOLE CORE 13 CORED INTERVAL 106.5–116.0 m sub-bottom

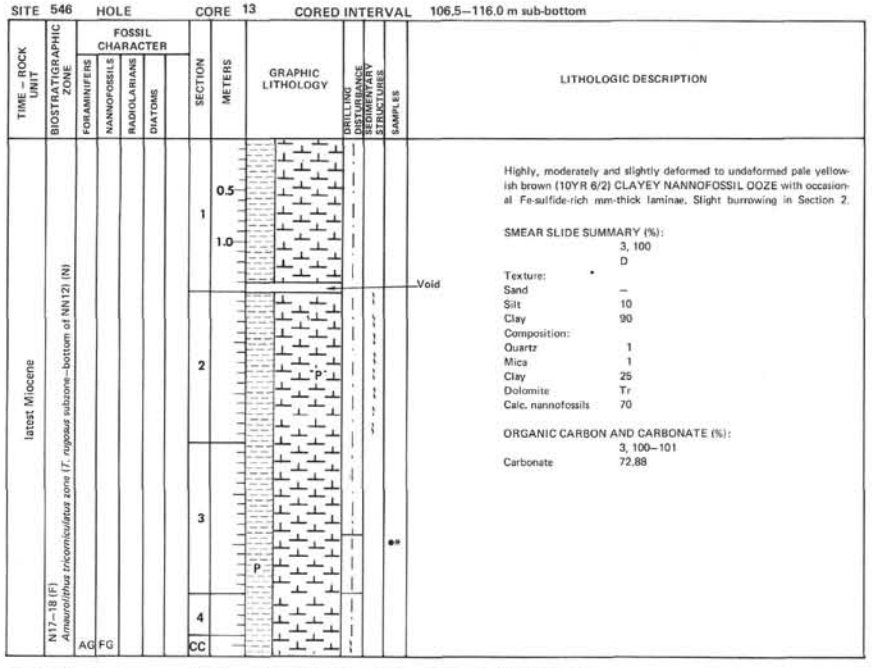

LITHOLOGIC DESCRIPTION

Highly, moderately and slightly deformed to undeformed pale yellowish brown (10YR 6/2) CLAYEY NANNOFOSSIL OOZE with occasional Fe-sulfide-rich mm-thick laminae. Slight burrowing in Section 2.

SMEAR SLIDE SUMMARY (%):

	3, 100 D
Texture:	
Sand	–
Silt	10
Clay	90
Composition:	
Quartz	1
Mica	1
Clay	25
Dolomite	Tr
Calc. nannofossils	70

ORGANIC CARBON AND CARBONATE (%):

	3, 100–101
Carbonate	72.88

SITE 546 HOLE CORE 14 CORED INTERVAL 116.0–125.5 m sub-bottom

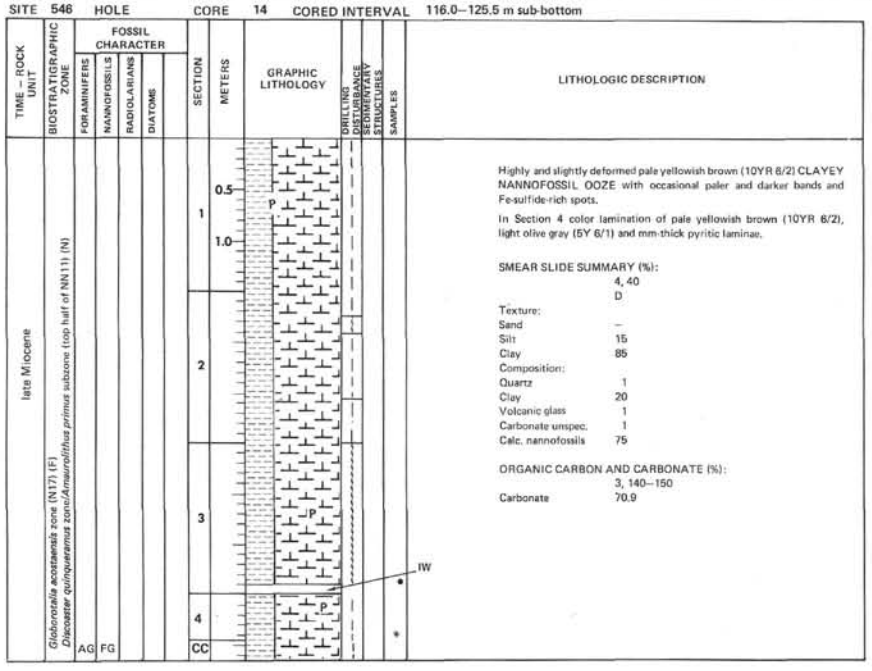

LITHOLOGIC DESCRIPTION

Highly and slightly deformed pale yellowish brown (10YR 8/2) CLAYEY NANNOFOSSIL OOZE with occasional paler and darker bands and Fe-sulfide-rich spots.

In Section 4 color lamination of pale yellowish brown (10YR 6/2), light olive gray (5Y 6/1) and mm-thick pyritic laminae.

SMEAR SLIDE SUMMARY (%):

	4, 40 D
Texture:	
Sand	–
Silt	15
Clay	85
Composition:	
Quartz	1
Clay	20
Volcanic glass	1
Carbonate unspec.	1
Calc. nannofossils	75

ORGANIC CARBON AND CARBONATE (%):

	3, 140–150
Carbonate	70.9

SITE 546 HOLE CORE 15 CORED INTERVAL 125.5–135.0 m sub-bottom

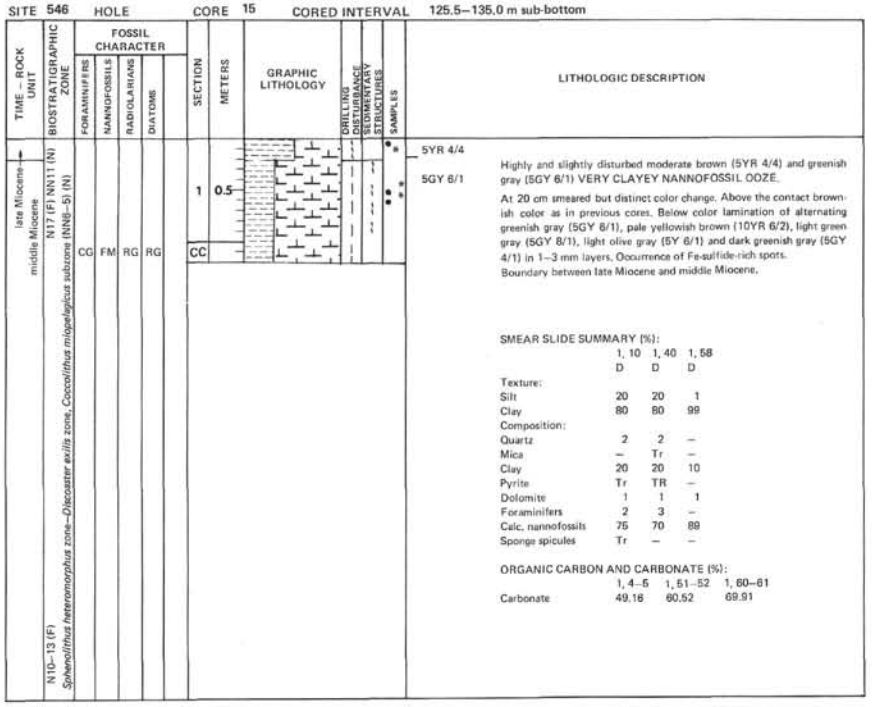

LITHOLOGIC DESCRIPTION

5YR 4/4

5GY 8/1

Highly and slightly disturbed moderate brown (5YR 4/4) and greenish gray (5GY 6/1) VERY CLAYEY NANNOFOSSIL OOZE.

At 20 cm smeared but distinct color change. Above the contact brownish color as in previous cores. Below color lamination of alternating greenish gray (5GY 6/1), pale yellowish brown (10YR 6/2), light green gray (5GY 8/1), light olive gray (5Y 6/1) and dark greenish gray (5GY 4/1) in 1–3 mm layers. Occurrence of Fe-sulfide-rich spots.

Boundary between late Miocene and middle Miocene.

SMEAR SLIDE SUMMARY (%):

	1, 10 D	1, 40 D	1, 58 D
Texture:			
Silt	20	20	1
Clay	80	80	99
Composition:			
Quartz	2	2	–
Mica	–	Tr	–
Clay	20	20	10
Pyrite	Tr	TR	–
Dolomite	1	1	1
Foraminifers	2	3	–
Calc. nannofossils	75	70	89
Sponge spicules	Tr	–	–

ORGANIC CARBON AND CARBONATE (%):

	1, 4–5	1, 51–52	1, 60–61
Carbonate	49.16	60.52	69.91

SITE 546 HOLE CORE 16 CORED INTERVAL 135.0–144.5 m sub-bottom

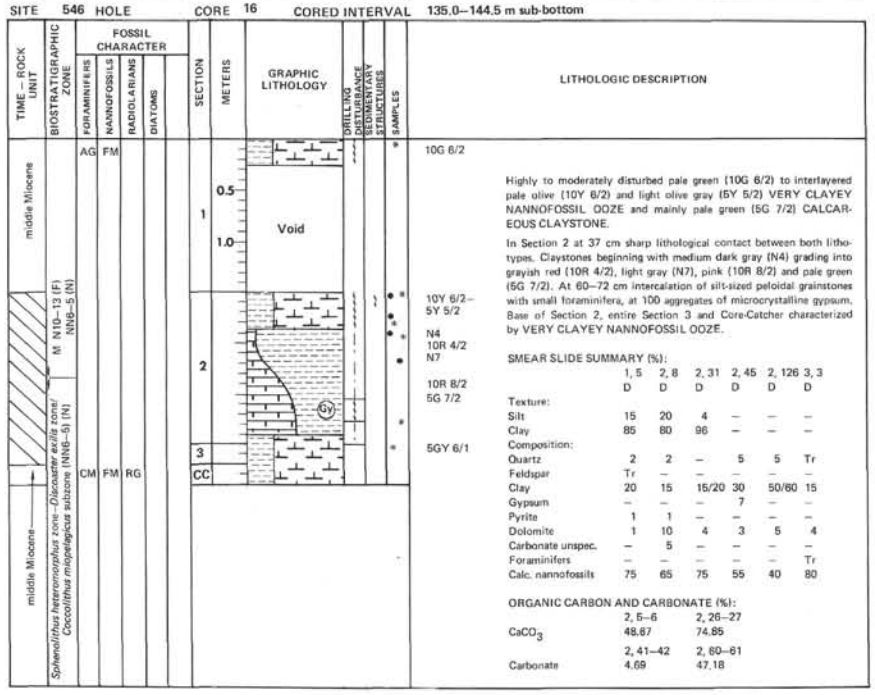

LITHOLOGIC DESCRIPTION

10G 6/2

10Y 6/2–5Y 5/2

N4

10R 4/2

N7

10R 8/2

5G 7/2

5GY 6/1

Highly to moderately disturbed pale green (10G 6/2) to interlayered pale olive (10Y 6/2) and light olive gray (5Y 5/2) VERY CLAYEY NANNOFOSSIL OOZE and mainly pale green (5G 7/2) CALCAREOUS CLAYSTONE.

In Section 2 at 37 cm sharp lithological contact between both lithotypes. Claystones beginning with medium dark gray (N4) grading into grayish red (10R 4/2), light gray (N7), pink (10R 8/2) and pale green (5G 7/2). At 60–72 cm intercalation of silt-sized peloidal grainstones with small foraminifera, at 100 aggregates of microcrystalline gypsum. Base of Section 2, entire Section 3 and Core-Catcher characterized by VERY CLAYEY NANNOFOSSIL OOZE.

SMEAR SLIDE SUMMARY (%):

	1, 5 D	2, 8 D	2, 31 D	2, 45 D	2, 126 D	3, 3 D
Texture:						
Silt	15	20	4	–	–	–
Clay	85	80	96	–	–	–
Composition:						
Quartz	2	2	–	5	5	Tr
Feldspar	Tr	–	–	–	–	–
Clay	20	15	15/20	30	50/60	15
Gypsum	–	–	–	7	–	–
Pyrite	1	1	–	–	–	–
Dolomite	1	10	4	3	5	4
Carbonate unspec.	–	5	–	–	–	–
Foraminifers	–	–	–	–	–	Tr
Calc. nannofossils	75	65	75	55	40	80

ORGANIC CARBON AND CARBONATE (%):

	2, 5–6	2, 26–27
$CaCO_3$	48.67	74.85
	2, 41–42	2, 60–61
Carbonate	4.69	47.18

SITE 546 HOLE CORE 17 CORED INTERVAL 144.5–154.0 m sub-bottom

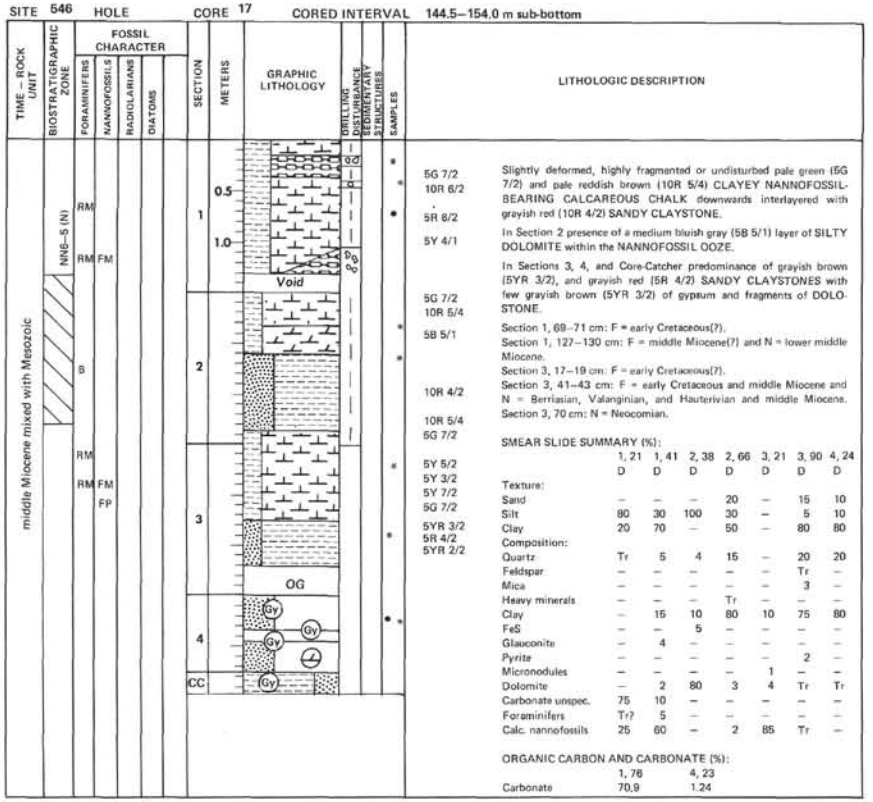

LITHOLOGIC DESCRIPTION

Slightly deformed, highly fragmented or undisturbed pale green (5G 7/2) and pale reddish brown (10R 5/4) CLAYEY NANNOFOSSIL-BEARING CALCAREOUS CHALK downwards interlayered with grayish red (10R 4/2) SANDY CLAYSTONE.

In Section 2 presence of a medium bluish gray (5B 5/1) layer of SILTY DOLOMITE within the NANNOFOSSIL OOZE.

In Sections 3, 4, and Core-Catcher predominance of grayish brown (5YR 3/2), and grayish red (5R 4/2) SANDY CLAYSTONES with few grayish brown (5YR 3/2) of gypsum and fragments of DOLOSTONE.

Section 1, 69–71 cm: F = early Cretaceous(?).
Section 1, 127–130 cm: F = middle Miocene(?) and N = lower middle Miocene.
Section 3, 17–19 cm: F = early Cretaceous(?).
Section 3, 41–43 cm: F = early Cretaceous and middle Miocene and N = Berriasian, Valanginian, and Hauterivian and middle Miocene.
Section 3, 70 cm: N = Neocomian.

SMEAR SLIDE SUMMARY (%):

	1, 21 D	1, 41 D	2, 38 D	2, 66 D	3, 21 D	3, 90 D	4, 24 D
Texture:							
Sand	–	–	–	20	–	15	10
Silt	80	30	100	30	–	5	10
Clay	20	70	–	50	–	80	80
Composition:							
Quartz	Tr	5	4	15	–	20	20
Feldspar	–	–	–	–	–	Tr	–
Mica	–	–	–	–	–	3	–
Heavy minerals	–	–	–	Tr	–	–	–
Clay	–	15	10	80	10	75	80
FeS	–	–	5	–	–	–	–
Glauconite	–	4	–	–	–	–	–
Pyrite	–	–	–	–	–	2	–
Micronodules	–	–	–	–	1	–	–
Dolomite	–	2	80	3	4	Tr	Tr
Carbonate unspec.	75	10	–	–	–	–	–
Foraminifers	Tr?	5	–	–	–	–	–
Calc. nannofossils	25	60	–	2	85	Tr	–

ORGANIC CARBON AND CARBONATE (%):

	1, 76	4, 23
Carbonate	70.9	1.24

SITE 546 HOLE CORE 18 CORED INTERVAL 154.0–163.5 m sub-bottom

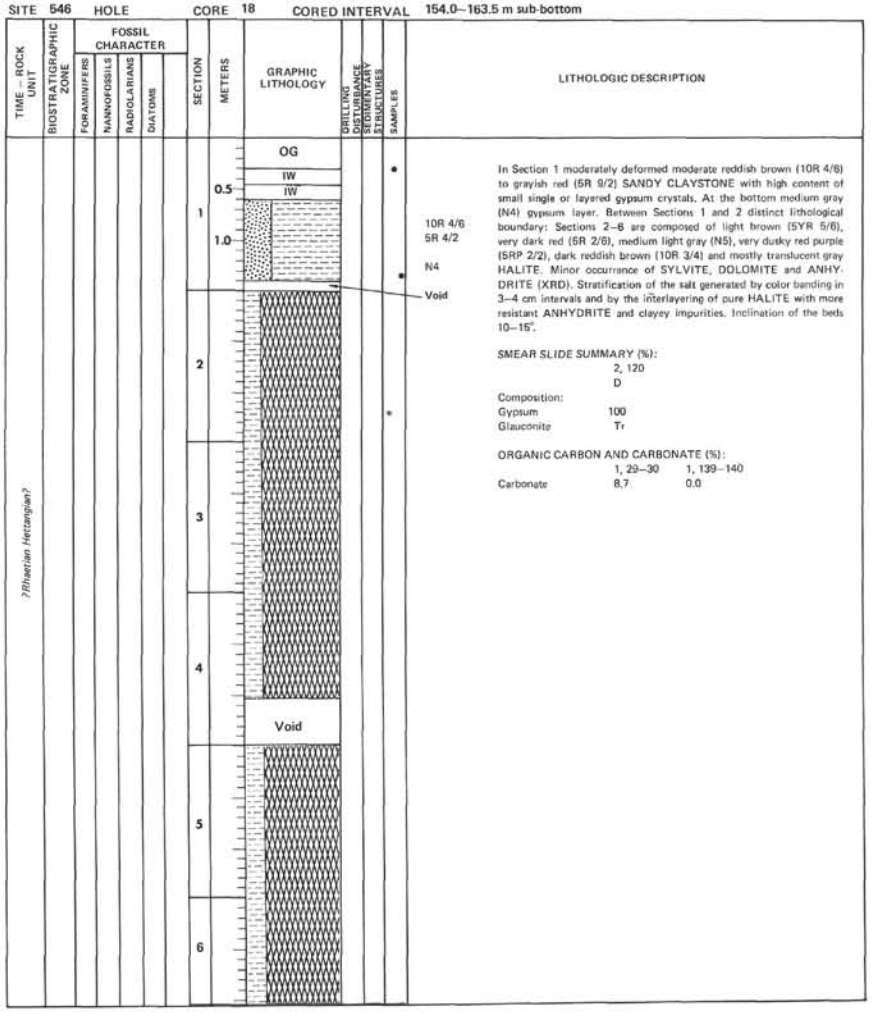

LITHOLOGIC DESCRIPTION

In Section 1 moderately deformed moderate reddish brown (10R 4/6) to grayish red (5R 9/2) SANDY CLAYSTONE with high content of small single or layered gypsum crystals. At the bottom medium gray (N4) gypsum layer. Between Sections 1 and 2 distinct lithological boundary: Sections 2–6 are composed of light brown (5YR 5/6), very dark red (5R 2/6), medium light gray (N5), very dusky red purple (5RP 2/2), dark reddish brown (10R 3/4) and mostly translucent gray HALITE. Minor occurrence of SYLVITE, DOLOMITE and ANHYDRITE (XRD). Stratification of the salt generated by color banding in 3–4 cm intervals and by the interlayering of pure HALITE with more resistant ANHYDRITE and clayey impurities. Inclination of the beds 10–15°.

SMEAR SLIDE SUMMARY (%):

	2, 120 D
Composition:	
Gypsum	100
Glauconite	Tr

ORGANIC CARBON AND CARBONATE (%):

	1, 29–30	1, 139–140
Carbonate	8.7	0.0

SITE 546 HOLE CORE 19 CORED INTERVAL 163.5–173.0 m sub-bottom

TIME – ROCK UNIT	BIOSTRATIGRAPHIC ZONE	FOSSIL CHARACTER: FORAMINIFERS	NANNOFOSSILS	RADIOLARIANS	DIATOMS	SECTION	METERS	GRAPHIC LITHOLOGY	DRILLING DISTURBANCE	SEDIMENTARY STRUCTURES	SAMPLES	LITHOLOGIC DESCRIPTION
?Rhaetian Hettangian?						1	0.5					Void Pale brown (5YR 5/2) to gray brown (5YR 3/2) and translucent white and gray HALITE. Stratification in 1–3 cm layers of pure and impure halite and intercalations of anhydrite.
						1	1.0					
						2						
						3						

SITE 546 HOLE CORE 20 CORED INTERVAL 173.0–182.5 m sub-bottom

TIME – ROCK UNIT	BIOSTRATIGRAPHIC ZONE	FOSSIL CHARACTER: FORAMINIFERS	NANNOFOSSILS	RADIOLARIANS	DIATOMS	SECTION	METERS	GRAPHIC LITHOLOGY	DRILLING DISTURBANCE	SEDIMENTARY STRUCTURES	SAMPLES	LITHOLOGIC DESCRIPTION
?Rhaetian Hettangian?						1	0.5					Pale brown (5Y 5/2) to dark yellowish brown (10YR 4/2) and olive gray (5Y 4/1) thinly layered HALITE. In the upperpart of the core content of impurities like anhydrite and clays 20–30% increasing to the bottom up to 50%. Color change downwards from grayish browns to reddish browns.
						1	1.0					
						2						
						3						
						4						
						5						

SITE 546 HOLE CORE 21 CORED INTERVAL 182.5–192.0 m sub-bottom

TIME – ROCK UNIT	BIOSTRATIGRAPHIC ZONE	FOSSIL CHARACTER: FORAMINIFERS	FOSSIL CHARACTER: NANNOFOSSILS	FOSSIL CHARACTER: RADIOLARIANS	FOSSIL CHARACTER: DIATOMS	SECTION	METERS	GRAPHIC LITHOLOGY	DRILLING DISTURBANCE	SEDIMENTARY STRUCTURES	SAMPLES	LITHOLOGIC DESCRIPTION
?Rhaetian Hettangian?						1	0.5 1.0					Mostly moderate reddish brown (10R 4/6), partly light brown (5YR 6/4), moderate brown (5YR 3/4) and olive gray (5Y 4/1) HALITE. Thin layering with bed-thicknesses of 0.5–3 cm emphasized by layers and aggregates of anhydrite and clay. Occurrence of angular discordances.
						2						
						3						
						4						
						5						


0 cm
1-1
1-2
1,CC
2-1
2-2
2-3
3,CC
3-1
3-2
3-3
3-4
3-5
25
50
75
100
125
150

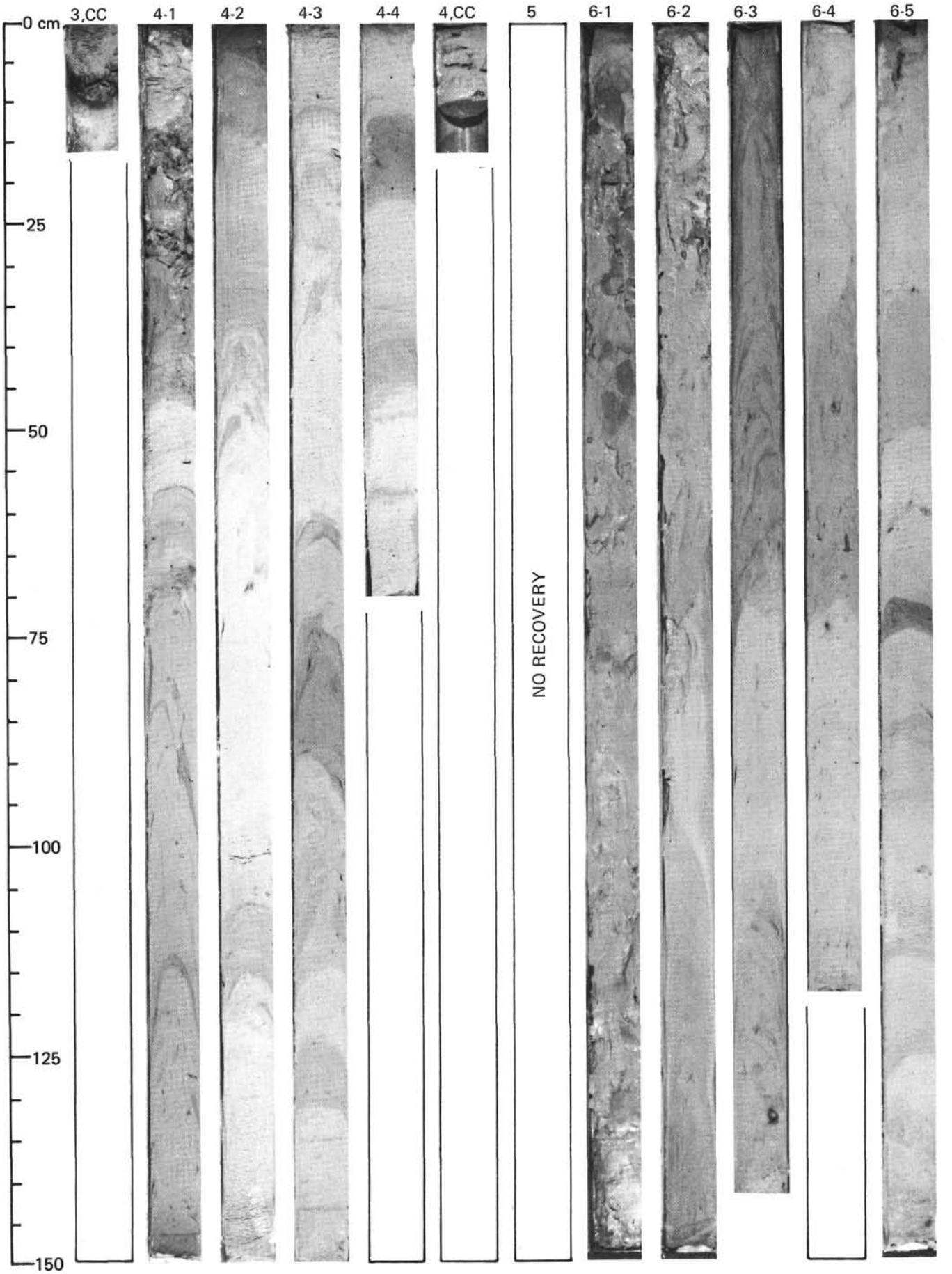
0 cm
25
50
75
100
125
150
3,CC
4-1
4-2
4-3
4-4
4,CC
5
NO RECOVERY
6-1
6-2
6-3
6-4
6-5

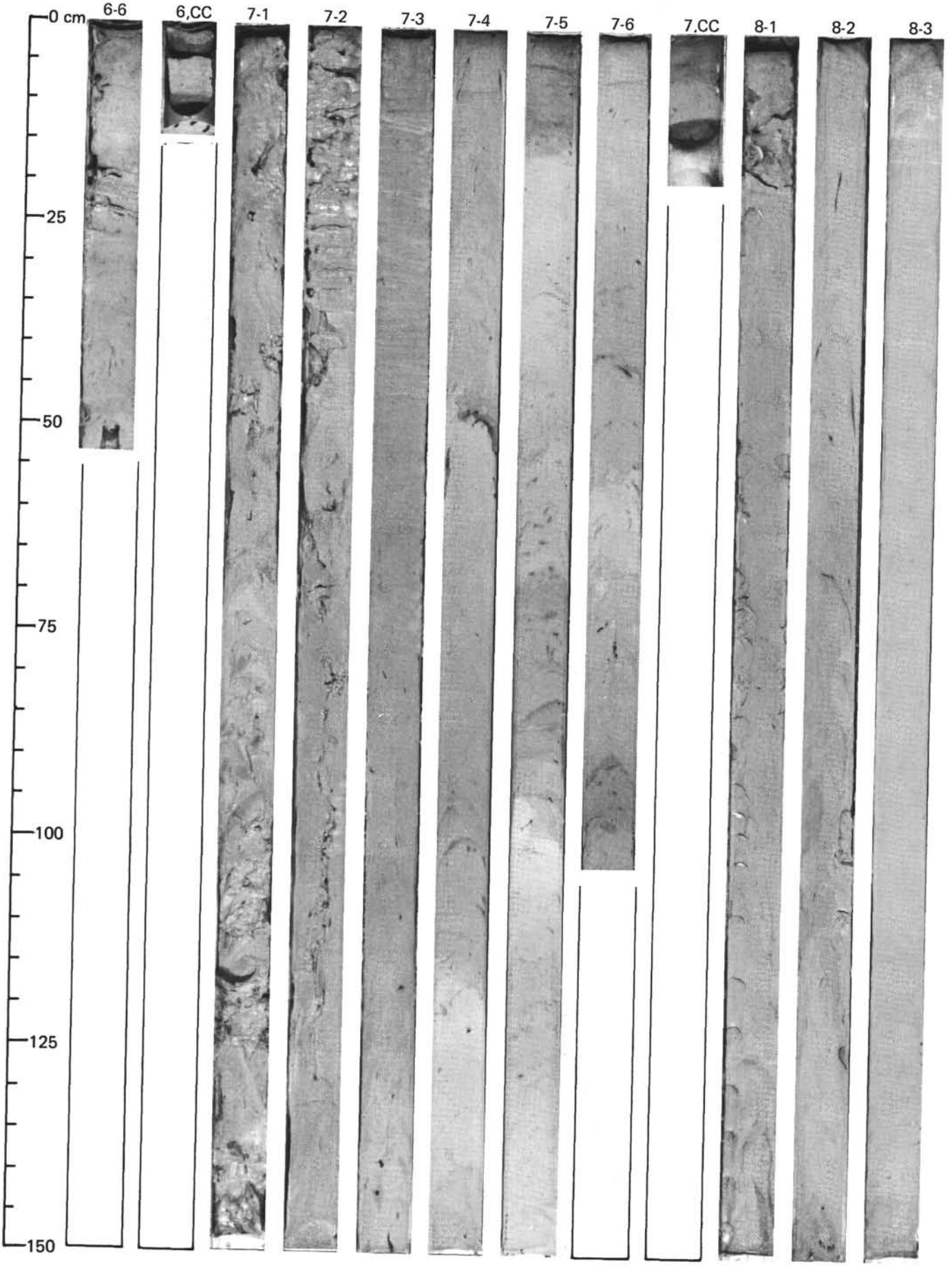
0 cm
6-6
6,CC
7-1
7-2
7-3
7-4
7-5
7-6
7,CC
8-1
8-2
8-3
25
50
75
100
125
150

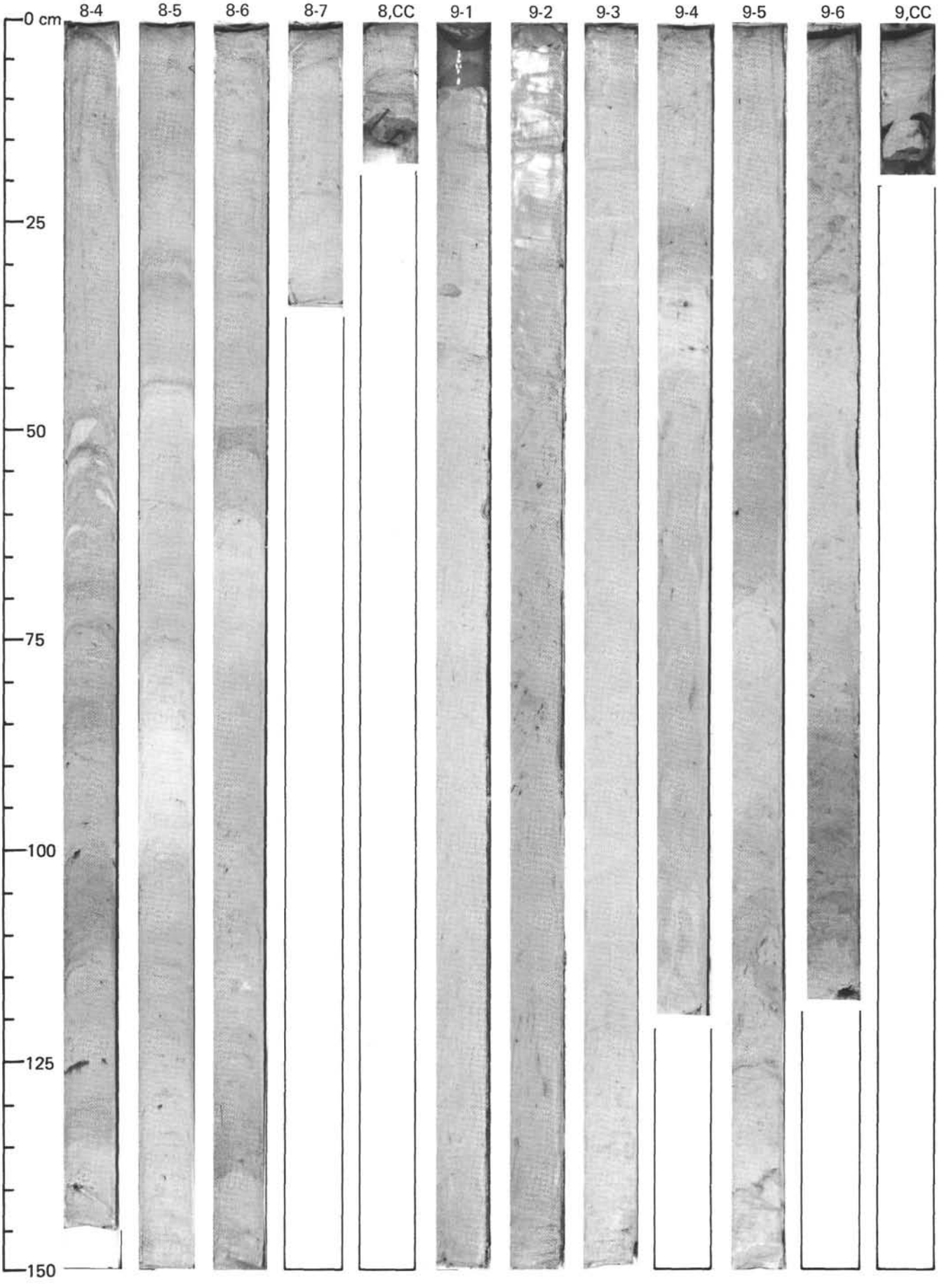
8-4
8-5
8-6
8-7
8,CC
9-1
9-2
9-3
9-4
9-5
9-6
9,CC
0 cm
25
50
75
100
125
150

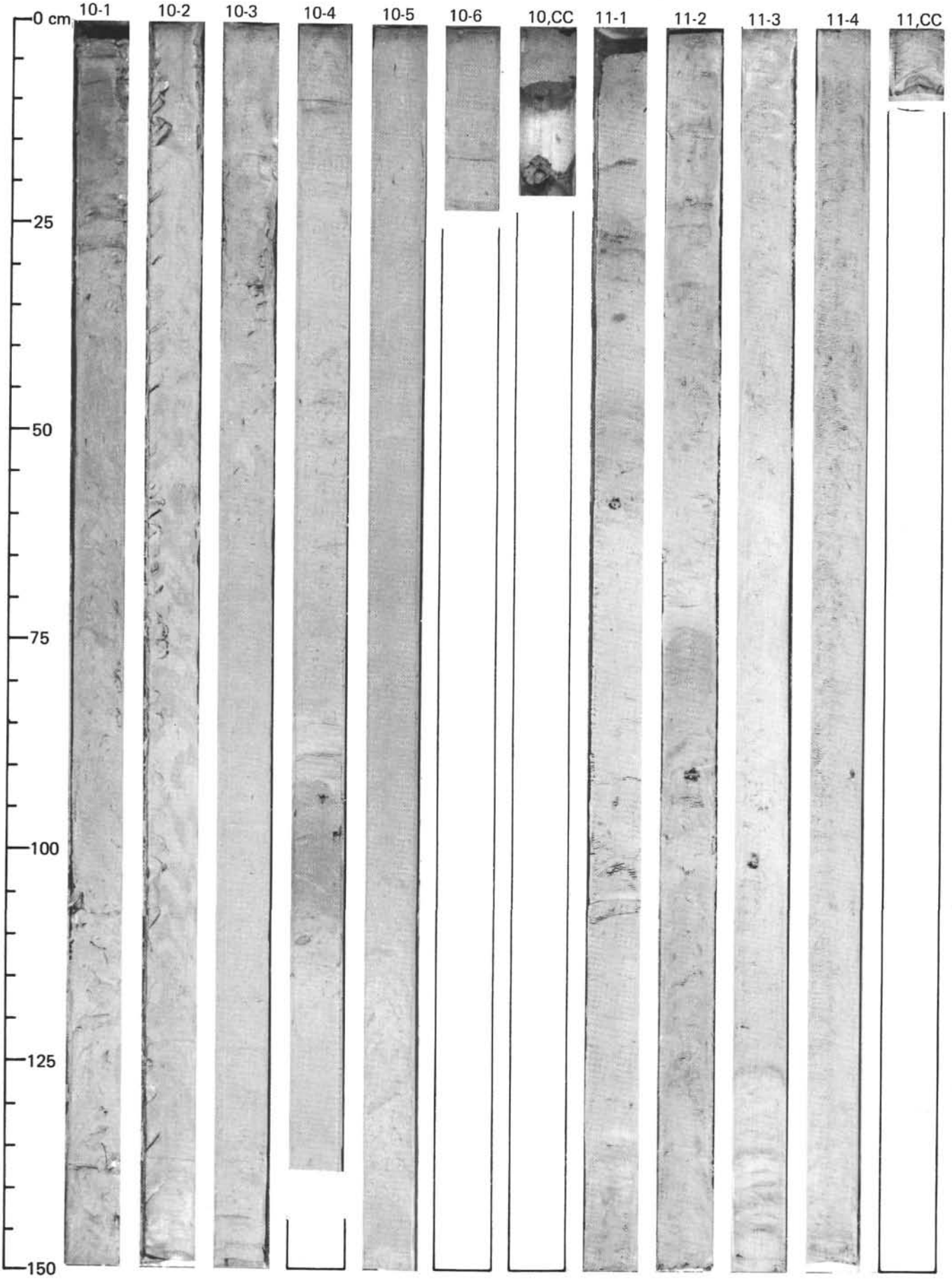
0 cm
10-1
10-2
10-3
10-4
10-5
10-6
10,CC
11-1
11-2
11-3
11-4
11,CC
25
50
75
100
125
150

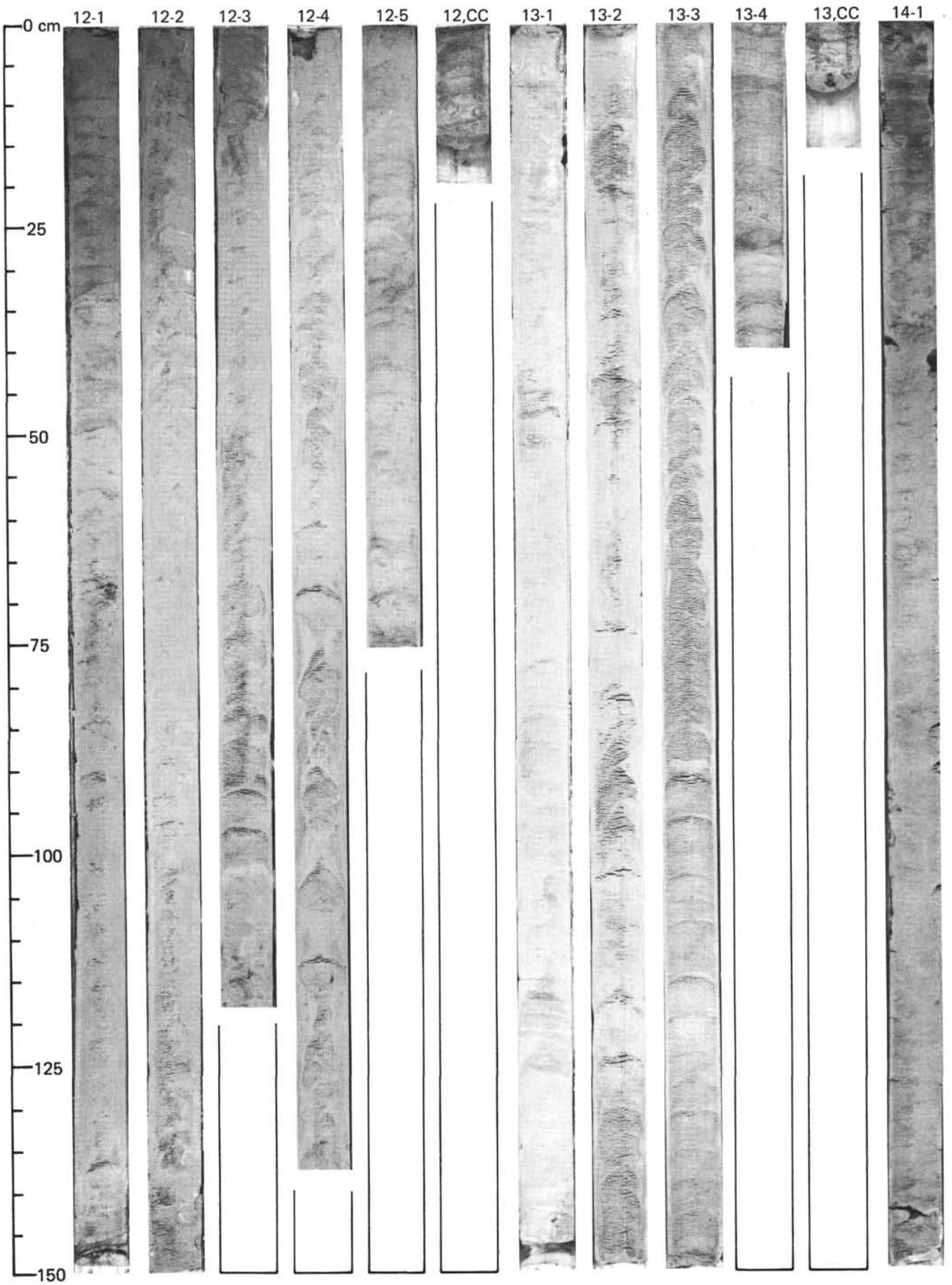
0 cm
25
50
75
100
125
150
12-1
12-2
12-3
12-4
12-5
12,CC
13-1
13-2
13-3
13-4
13,CC
14-1

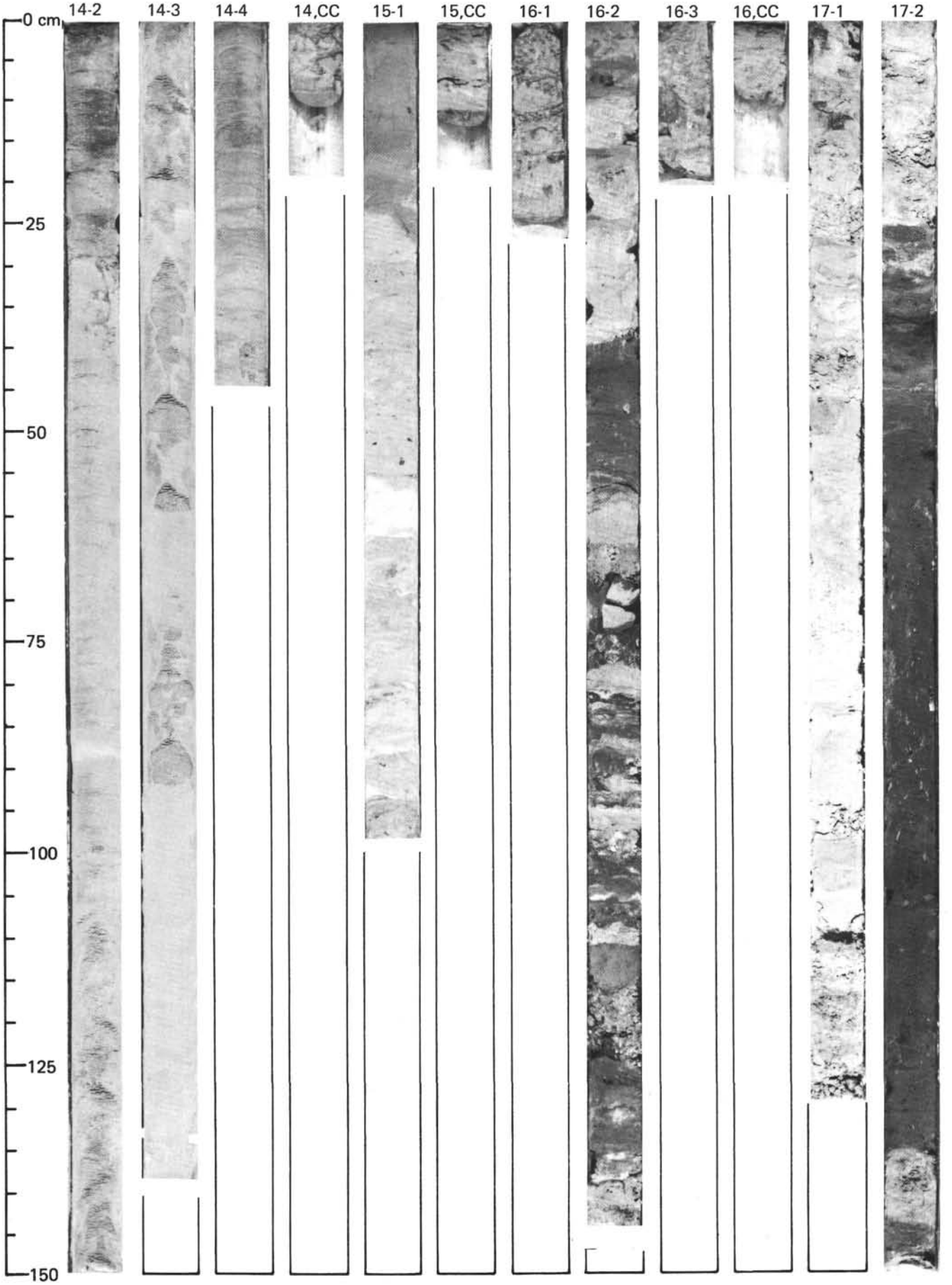
0 cm
25
50
75
100
125
150
14-2
14-3
14-4
14,CC
15-1
15,CC
16-1
16-2
16-3
16,CC
17-1
17-2

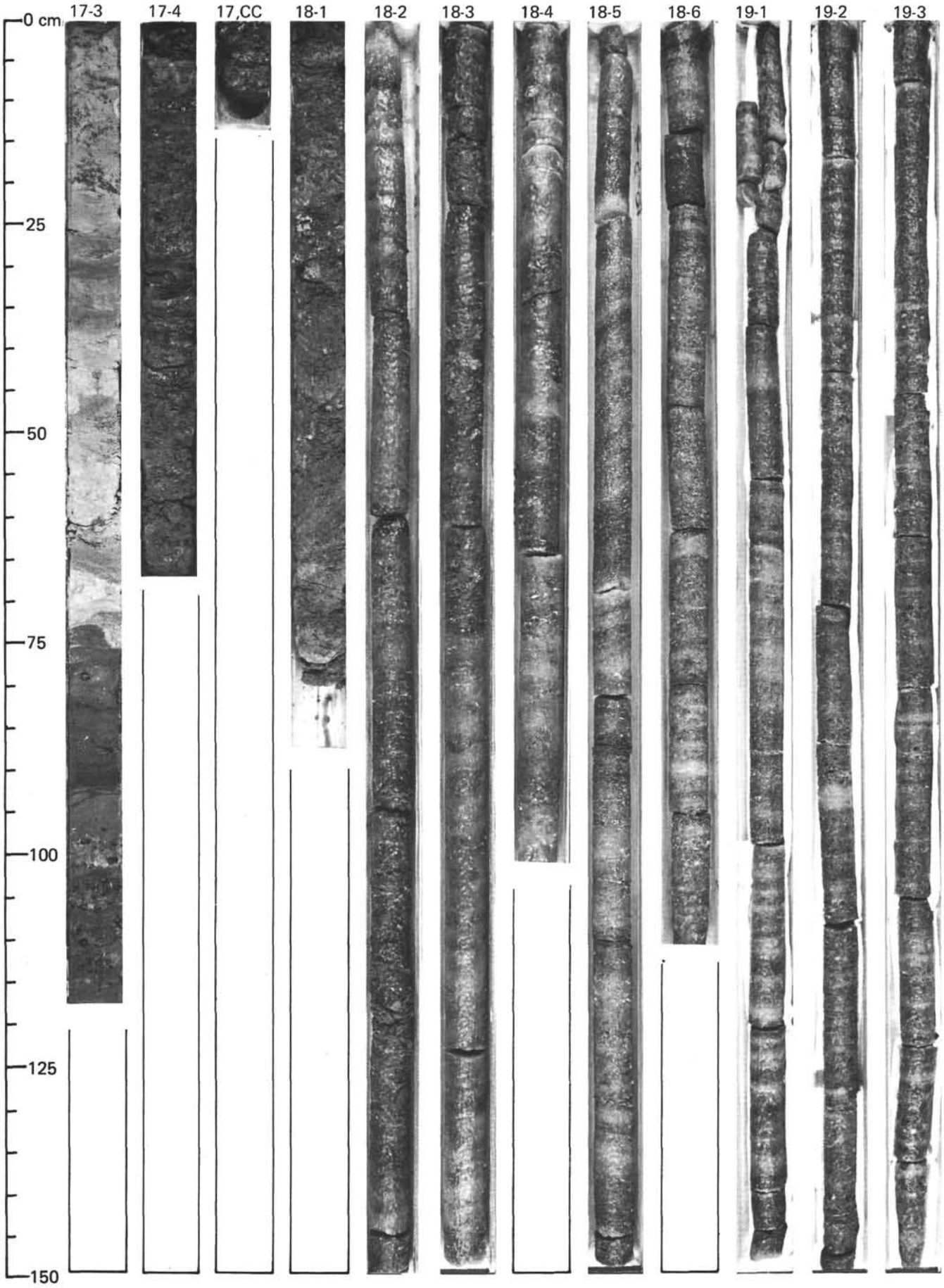
17-3
17-4
17,CC
18-1
18-2
18-3
18-4
18-5
18-6
19-1
19-2
19-3
0 cm
25
50
75
100
125
150

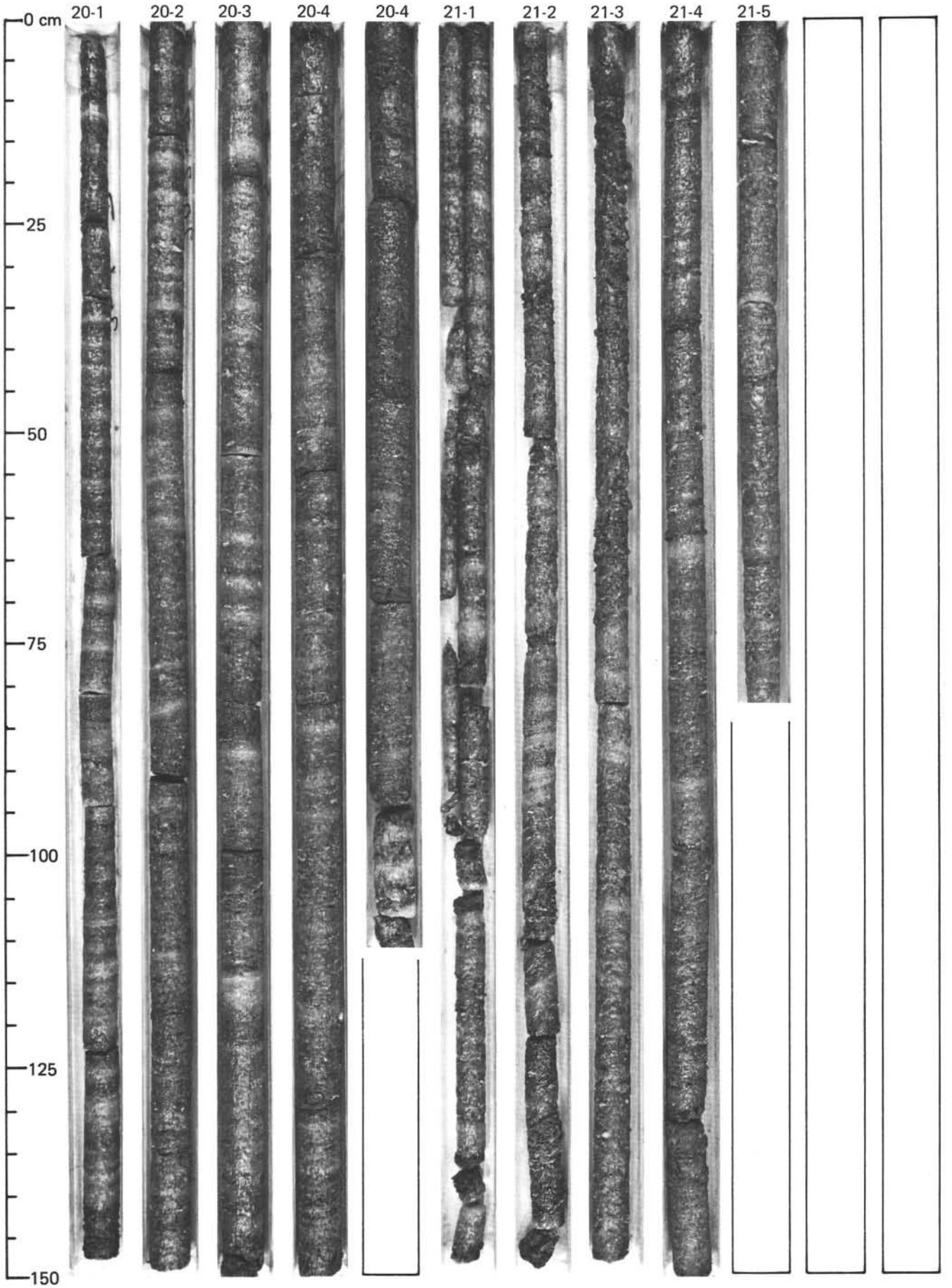
0 cm
25
50
75
100
125
150
20-1
20-2
20-3
20-4
20-4
21-1
21-2
21-3
21-4
21-5